Alma Mater Studiorum – Università di Bologna

DOTTORATO DI RICERCA IN
MODELLISTICA FISICA PER LA PROTEZIONE DELL'AMBIENTE

Ciclo XXIII

Settore Concorsuale di afferenza: 02/C1
Settore Scientifico disciplinare: FIS/05 - FIS/06

TITOLO TESI

The role of the West African Monsoon in the tropical to mid-latitudes climate

Presentata da: Massimiliano Pasqui

Coordinatore Dottorato

Prof. Rolando Rizzi

Relatore

Prof. Rolando Rizzi

Co - Relatore
Dr. Vincenzo Levizzani

Esame finale anno 2012

A mio figlio Francesco,
a mia moglie Pierangela,
ai miei genitori Alberto e Roberta.

"*Bear in mind that the wonderful things that you learn in your schools are the work of many generations, produced by enthusiastic effort and infinite labour in every country of the world. All this is put into your hands as your inheritance in order that you may receive it, honour it, and add to it, and one day faithfully hand it on to your children. Thus do we mortals achieve immortality in the permanent things which we create in common. If you always keep that in mind you will find meaning in life and work and acquire the right attitude towards other nations and ages*"
(Albert Einstein talking to a group of school children. 1934)

"*La ragione e il torto non si dividon mai con un taglio così netto,*
che ogni parte abbia soltanto dell'uno o dell'altro".
A. Manzoni, I promessi sposi, *I.*

"*The scientist does not study nature because it is useful;*
he studies it because he delights in it,
and he delights in it because it is beautiful."
H. Poincare

Abstract

The interaction between atmosphere – land – ocean – biosphere systems plays a prominent role on the atmospheric dynamics and on the convective rainfall distribution over the West Africa monsoon area during the boreal summer. This prominent role has been highlighted in many studies and recently has received a new emphasis due to the release of specialised datasets, both numerical and observational. In particular, the initialization of convective systems in the Sub – Sahelian region has been directly linked to soil moisture heterogeneities identified as the major triggering factors and responsible for the destabilization of the atmospheric boundary layer. Such low level conditions are favourable for convection development and propagation during the extended boreal summer (May to November). These evidences are now supported by modelling and observation study, but a "*unified description*" of the link between small scale and large scale dynamic behaviour still lacks. A gap thus exists between the dynamics of the single convective systems and the monsoon behaviour at sub - continental scale.

The present study aims at providing a contribution to fill this gap by investigating African monsoon large scale convective dynamics and, in particular, some characteristics of the rainfall diurnal cycle through an exploration of the hypothesis behind the mechanisms of a monsoon phenomenon as an emergence of a collective dynamics of many propagating convective systems. Such hypothesis is based on the existence of an internal self – regulation mechanism among the various components.

To achieve these results a multiple analysis was performed based on remotely sensed rainfall dataset, and global and regional modelling data for a period of 5 June-July-August seasons: 2004 - 2008. Satellite rainfall data and convective occurrence variability were studied for assessing typical spatio – temporal signatures and characteristics with an emphasis to the diurnal cycle footprint over West Africa.

Numerical modelling reanalysis datasets were studied in order to extract evidence of mutual interactions between the different components: soil dynamics, atmospheric variability, and convective occurrence footprint. Two completely different numerical representations of the physical mechanisms are analysed in order to reduce possible purely numerical effects: a global model and regional model simulations specifically developed for this analysis and based on Regional Atmospheric Modelling System – RAMS.

Results from numerical model datasets highlight the evidence of a synchronization between the destabilization of the convective boundary layer and rainfall occurrence due to the solar radiation forcing through the latent heat release. This fact can be considered as a basis of the spatio – temporal coherence, which, in turn, could be associated to the rainfall diurnal cycle. Thus, moisture provision, due to large scale and local latent heat flux, driven by solar radiation, synchronize with the convective rainfall occurrence footprint. This supports the conclusion that the studied interacting systems are associated with a process of mutual adjustment of rhythms.

Furthermore, this rainfall internal coherence was studied in relation to the West African Heat Low pressure system, which has a prominent role in the large scale summer variability over the Mediterranean area since it is acting as one of dynamic link between sub tropical and mid latitudes variability.

ACKNOWLEDGMENTS

This Phd research has been carried out at the Institute of Biometeorology – National Research Council (www.ibimet.cnr.it) and at LaMMA Consortium (www.rete.toscana.it) that I would like to acknowledge for support.

MSG-1 imagery is copyright of EUMETSAT and was made available by EUMETSAT's Unified Meteorological Archive and Retrieval Facility (UMARF). DMSP SSM/I data were obtained from the Comprehensive Large Array-data Stewardship System (CLASS) at NOAA's National Environmental Satellite, Data and Information Service (NESDIS), http://www.class.ngdc.noaa.gov. NCEP/DOE AMIP-II Reanalysis data were provided by the NOAA/OAR/ESRL PSD, Boulder, Colorado, USA, from their Web site at http://www.esrl.noaa.gov/psd/.

MERRA data (http://gmao.gsfc.nasa.gov/research/merra/intro.php) where downloaded from the Modeling and Assimilation Data and Information Services Center (MDISC) (http://disc.sci.gsfc.nasa.gov/mdisc/overview).

I'm grateful to the CDO – Climate data Operators Project (https://code.zmaw.de/projects/cdo) and to Grid Analysis and Display System – GrADS (http://grads.iges.org/grads/grads.html) for providing excellent analysis and displaying tools.

I would like to acknowledge Prof. Rolando Rizzi, for his help during this period as Tutor and Doctoral Coordinator.

Special thanks and grateful go to Vincenzo Levizzani, Samantha Melani and Francesca Guarnieri for their help along this long period and in particular for sharing with me the beauty of this research. Their efforts and work were fundamental for this research.

ABOUT THE AUTHOR

Massimiliano Pasqui è nato a Roma il 5 luglio 1971. Si è laureato in Fisica nel 1996 con votazione finale 110/110 discutendo la tesi dal titolo "Effetti viscosi nella turbolenza sviluppata", presso il Dipartimento di Fisica dell'Università degli Studi di Roma, Tor Vergata.
Dal 1998 al 2002 ha collaborato con la Fondazione per la Meteorologia Applicata (FMA) e con il Laboratorio per la Meteorologia e la Modellistica Ambientale (LaMMA) a Firenze.
Nel 2002 è diventato ricercatore a contratto all'Istituto di Biometeorologia (IBIMET) del Consiglio Nazionale delle Ricerche (CNR).
Dall'aprile 2008 è diventato ricercatore a tempo indeterminato presso lo stesso istituto.
Si occupa di meteorologia, climatologia e modellistica ambientale. Ha partecipato a numerosi progetti di ricerca Nazionali ed internazionali, tra i quali: RAMSES (E.U., 5th F.P.); DECIDE (Agenzia Spaziale Europea, ESA); EURAINSAT (E.U., 5th F.P.); STORM/ARTU (Autorità di Bacino del fiume Arno); CLIMAGRI (MIPAAF, UCEA); WINDUST (Ministero dell'Ambiente); TEMPIO (MIPAAF), C_FORSAT (MIUR – Futuro in ricerca), AGROSCENARI - Scenari di adattamento dell'agricoltura italiana ai cambiamenti climatici (MIPAAF).

Massimiliano Pasqui was born in Rome on 5 July 1971. He graduated in Physics in 1996 with a final vote 110/110, with a dissertation title: "Viscous effects in fully developed turbulence", at the Department of Physics, University of Rome Tor Vergata.
From 1998 to 2002 he collaborated with the Foundation for Applied Meteorology (FMA) and the Laboratory for Meteorology and Environmental Modelling (LAMMA) in Florence.
In 2002 he became a contract researcher at the Institute of Biometeorology (IBIMET) of the National Research Council (CNR).
Since April 2008 he became permanent researcher at the same institute.
His main research interests are dealing with: eteorology, climatology and environmental modelling. He has participated in numerous national and international research projects, including: RAMSES (EU, 5th FP); DECIDED European Space Agency (ESA); EURAINSAT (EU, 5th FP) STORM / ARTHUR (Arno River Basin Authority); CLIMAGRI (MIPAAF, UCEA); WINDUST (Ministry of Environment); TEMPLE (MIPAAF), C_FORSAT (MIUR – Futuro in Ricerca), AGROSCENARI - Scenarios of adaptation of Italian agriculture to climate change (MIPAAF).

INDEX OF FIGURES

Table of Contents

1 INTRODUCTION

1.1 West Africa Monsoon: a physical background

The summer African monsoon is one of the major climatic large-scale phenomena that is thought to impact on atmospheric dynamics at great distances. To date the monsoon complex phenomenology is far from being fully understood in its driving multiple mechanisms, and consequently its spatial and temporal precipitation distribution remains a key research topic. Many general circulation models (GCM) have been tuned for reproducing the African monsoon dynamics but their capability to correctly represent deep convection is still very limited. The synergic use of satellite observations and limited area models (LAM), based on the analysis of systematic satellite rainfall estimates at a very high spatial resolution and regional scale simulations, has a potential for the reconstruction of the monsoon fine dynamics.

The African climate has been recognised as one of the "hot spots" in the Earth climate system (Solomon et al., 2007; Kirtman and Pirani, 2008). A reliable and detailed space/time representation of the rainfall distribution covering a wide range of dynamic scales in Northern Tropical Africa during the monsoon season is thus of primary importance. The main reason is that a better appraisal of the overall mechanisms could notably increase our level of understanding of the physics of the climate system not only in the area, but also at the global scale. In addition an improved capability of modelling and thus predicting the physical behaviour of the system could help managing operational issues, such as the agricultural activities in areas in which the productivity necessarily impacts large segments of the population.

Reproducing the rainfall dynamics through numerical models involves specific challenges in conceiving the right parameterization that are necessary to described the complex precipitation mechanisms, with their load of numerical and physical approximations. In particular, in Africa the diurnal forcing effects have a strong impact on the boundary layer determining its transition between stable and unstable conditions favourable for the onset of convection (Wang et al., 1994; Leroux, 2001; Parker et al., 2005b; Kikuchi and Wang, 2008; Taylor et al. 2011a; Taylor et al., 2011b).

Precipitating systems over Africa have been extensively studied from a variety of points of view over the past two decades. They are mostly associated to large scale convective events such as Mesoscale Convective Systems (MCS) (Laing et al., 1993, 2008; Hodges and Thorncroft, 1997;

Mathon et al., 2002; Jackson et al., 2009), squall lines (Rowell and Milford, 1993), and deep convective systems in general (e.g., Futyan and Del Genio, 2007). The West African Monsoon (WAM) dynamics (Sultan and Janicot, 2003a,b) and the role of synoptic wave perturbations on convective systems (Nguyen and Duvel, 2008) have also been explored though leaving considerable ground for further investigations. These systems result from a strong interaction between the large scale flow and the small scale dynamics, and are thus difficult to be correctly represented by numerical models.

The intraseasonal time – scale monsoon variability during the boreal summer is a result of many different superimposed physical mechanisms, both atmospheric and oceanic. They are characterized by modulating conditions from daily up to 60 days period for developing and maintaining organized convective systems over Africa. The faster rainfall modulation is associated with the synoptic variability of the African Easterly Wave (AEW) (Thorncroft and Hoskins, 1994a,b; Pytharoulis and Thorncroft, 1999; Thorncroft and Hodges, 2001; Mohr and Thorncroft, 2006). These atmospheric transients are characterized by low–mid level wind shear maxima and high convective available potential energy (CAPE) in the vicinity of elevated terrain producing a high probability of generating intense and propagating convective systems in the area (Mohr and Thorncroft, 2006). For this reason AEWs are identified as one of the main factors in modulating the rainfall space–time distribution at regional scale, both of weak and intense convective systems at the daily time scale. Recently, this association between AEWs and rainfall maxima location and occurrence has been revised by Kiladis et al. (2006) and Hall et al. (2006) who have argued that AEWs are better described as a response to coherent and organized convection, revealing that this relationship is far to be purely atmospheric. A second identified high frequency convective modulating mechanism is the soil moisture pattern as noted by Parker et al. (2005b). The soil moisture pattern plays a strong role in sustaining daytime favourable conditions in the convective boundary layer (CBL) to maintain the convection diurnal cycle and in modulating the low level moisture horizontal advection.

Longer time scale rainfall variability was studied by several authors. Seo et al. (2008) have modelled precipitation from AEWs finding that heavy rainfall events, occurring on the 2–6-day time scales associated with the easterly waves, account for a significant fraction (> 60% – 70%) of the simulated variance of precipitation, which implies a considerable alteration of the larger-scale annual mean rainfall due to these heavy rainfall events. Janicot and Sultan (2001) have pointed out large and coherent fluctuations in the rainfall and wind fields at intra-seasonal time scale over West Africa. These enhanced (weakened) phases of the WAM last in average 9 days and are included in a dominant quasi-periodic signal of about 15 days.

A 25 – 90 days modulation, primarily forced by Rossby cyclonic circulation moving westward off the Indian ocean was found by Janicot et al. (2009) and produced by the Madden Julian Oscillation (MJO) anomaly as identified by Lavender and Matthews (2009).

At monthly to seasonal time scale the atmospheric dynamic characterisation of the African Monsoon can be analysed with the African Easterly Jet (AEJ), which is the primarily jet flow developed in response to the inverse latitudinal surface temperature gradient during boreal spring in the sub – Sahelian region (Cook, 1999; Hsieh and Cook, 2005; Parker et al., 2005a; Leroux and Hall, 2009; Wu et al., 2009).

West African Monsoon variability is strongly forced by the sea surface temperatures standardised anomaly (SSTAs) of the Gulf of Guinea. Warm Gulf of Guinea SSTAs generates a rainfall increases along the Guinean coast while the precipitation decreases over the Congo Basin. These features can be understood through the dynamical response of a Kelvin wave along the equator and a Rossby wave to the west of the SSTA. The first is associated with a weakening of the Walker circulation, while the latter tends to strength the West African Monsoon and the upward vertical velocity. The effects of Cold SSTAs are opposite, but weaker (Vizy and Cook, 2001). The monsoon circulation influences the precipitation over the Sahel, in particular southern Sahel (10N-15N), in two main ways. The moisture is transported by the low-level southerly flow. The proximity of the monsoon circulation and circulation over Sahara generates a strong low-level convergence to force air parcels to rise vertically until the level of free convection (Vizy and Cook, 2002). Positive SST anomalies in the Eastern Pacific and in the Indian Ocean, negative in the northern Atlantic and in the Gulf of Guinea are related with droughts conditions over all the West Africa (Fontaine and Janicot, 1996; Eltahir and Gong, 1996).

Droughts limited to Sahel are due to a positive SST anomaly northward in the southern Atlantic and a negative pattern in the northern Atlantic. Floods along the West Africa are associated with positive anomalies in the northern Atlantic, while the floods limited to Sahel are related to different forcing: northward expansion of negative SST anomalies in the southern Atlantic, positive SST departures in the northern Atlantic, and development of negative SST anomalies in the eastern Pacific (Fontaine and Janicot, 1996).

The Principal Components Analysis (PCA) performed on the summer precipitation in the Sahel region, demonstrates that the two leading principal components (PCs) explain almost the half of the variability of the precipitation. Moreover two main patterns are present: the first along the Gulf of Guinea coast, between the equator and 10°N, dominated the interannual variability, the second associated with the continental convergence in the Sahel (between 10°N and 20°N) affected by the interdecadal variability. The decomposition of these two leading PCs into high and low-frequency

components shows the role of the SST of the Southern Atlantic and Indian Ocean for driving the long-term variability, while the interannual variations are driven by the ENSO (Giannini et al. 2003).

The presented analysis is an extended version of Melani et al., (2010) study which started from the findings of Melani et al. (2008) presenting a more detailed analysis of precipitation and of the associated atmospheric dynamics. Satellite rainfall fields are used to investigate the dynamic mechanisms driving the precipitation episodes, their distribution and propagation characteristics for the WAM and more generally for the northern African monsoon, during the core of the rainy season. A five-year climatology (2004 - 2008) of satellite precipitation estimations is presented, as derived from a multi-sensor approach involving geostationary (Meteosat Second Generation, MSG) and polar orbiting (Special Sensor Microwave Imager, SSM/I, onboard the Defense Meteorological Satellite Program, DMSP, spacecrafts) satellite observations. The precipitation fields show precise features and zonal propagation properties as well as the nature of the diurnal cycle by means of statistical analyses of the seasonal Hovmöller diagrams. Even if satellite rainfall estimations are generally affected by large uncertainties (see Chapter 2), the information contained in the precipitation fields in terms of spatial and temporal distribution of the precipitating systems leads to results that are somewhat different with respect to those stemming from similar analyses based on thermal infrared brightness temperature (TB) data (Laing et al., 2008). Recent studies over Northern Tropical African continent (Laing et al., 2004; 2008) and East Asia (Wang et al., 2004, 2005), based on satellite-measured cloud top TBs using thermal infrared imagery, investigated the dynamical monsoonal characteristics through deep cloud system formation. Over the Northern African area there are no radar nor rain gauge networks providing reliable measurements to explore the warm season rainfall variability. Satellite estimations, with their good spatio-temporal sampling, are thus the only viable source of data for characterizing these precipitation phenomena presenting a "phase-locked" behaviour.

Note that other studies were conducted over the area using data from the Tropical Rainfall Measuring Mission (TRMM) Precipitation Radar (PR) such as those by Geerts and Dejene (2005) on the regional and diurnal variability of the vertical structure of precipitation systems, and those by Sealy et al. (2003) on the comparison of the products from various satellite precipitation datasets over West Africa. TRMM data were used also by Schumacher and Houze (2006) to study the stratiform component of precipitation over sub-Saharan Africa and tropical East Atlantic.

Such studies require the appropriate knowledge of the vertical structure, but TRMM data do not ensure the necessary space-time repetition to address problems such as that examined in the present

paper. Precipitation estimations from passive sensors using the geostationary orbits as the necessary backbone maintain a high value for these studies as already pointed out by Levizzani et al. (2001).

1.2 Outline of the Thesis

In order to highlight the presence of an internal dynamical coherence of WAM a series of three data analysis and interpretation phases have been provided: 1) a rainfall distribution analysis by means of satellite remote sensed data; 2) a reanalysis strategy, developed for this study and base on a regional numerical model; 3) a synchronization data analysis of modelled simulation datasets available.

A detailed description of remote sensed satellite data used for describing the rainfall diurnal cycle in West Africa Monsoon area is shown in Chapter 2. Phase locking footprint is analyzed and related to large scale atmospheric forcing acting on that region along with a coherent rainfall episodes study, an estimation of rainfall diurnal cycle and an harmonic analysis. Other modelling datasets used within this work, but not computed directly, are described as well.

A full description of the complex reanalysis strategy, base on a regional modelling system and originally developed for this study, is described in Chapter 3. An evaluation procedure for regional model reliability has been proposed as well. In particular, in order to measure capability to numerically represent rainfall diurnal cycle model and observed rainfall data were analyzed and studied.

Synchronization analysis and its interpretation are then provided in Chapter 4. A brief overview of sync theory is shown at the beginning in order to provide a specific introduction of conceptual framework along with results and discussion.

The final Chapter 5 is a summary of principal results presented in the thesis with conclusion remarks and some perspectives for a future development of this study.

2 Datasets and Methods

2.1 Satellite rainfall estimates data

The study domain is centred over Central Africa and extends from 3° to 20°N and 18° to 48°E. The area and the orography of the region are shown in Fig. 2.1. The western boundary of the area is chosen on the basis of the prevailing south-easterly low-level flow insisting on the gulf of Guinea, which is an intense source of heat and humidity, while to the east the limit is dictated by the fact that the Arabic peninsula acts as additional trigger for convective activity. The northern boundary is fixed in order to exclude the Atlantic fronts, thus mainly focusing on the atmospheric features only induced by the African monsoon itself. Cross sections of the maximum surface elevation within each latitude band are shown in Fig. 2.2. Complex orography spans the whole area west to east with a maximum elevation of ~ 5 km in correspondence of the Ethiopian Highlands (east of 34°E) and an average terrain height below 2 km.

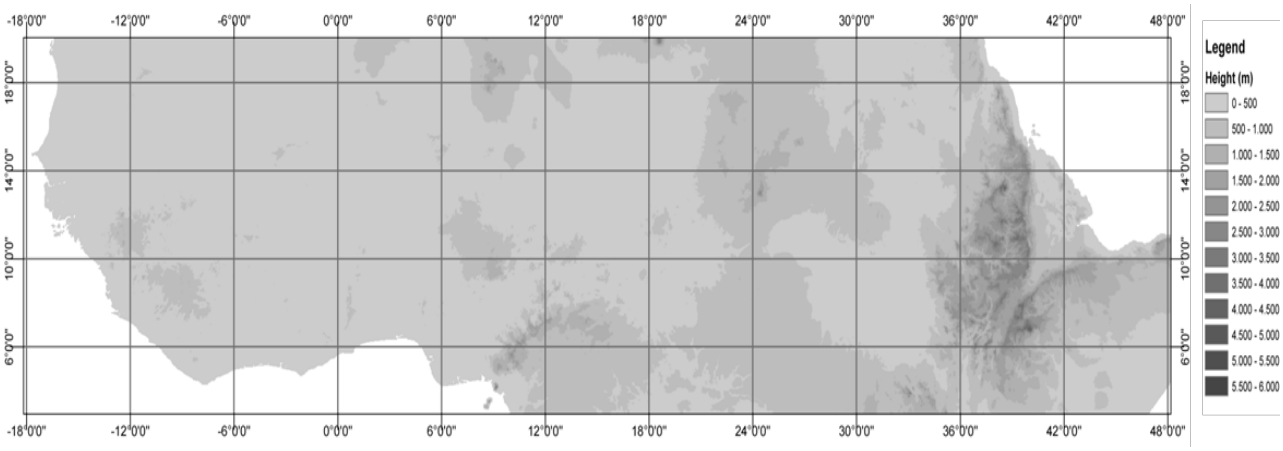

Fig. 2.1: Computational domain for rainfall estimates Hovmöller diagrams, also showing main topographic features.

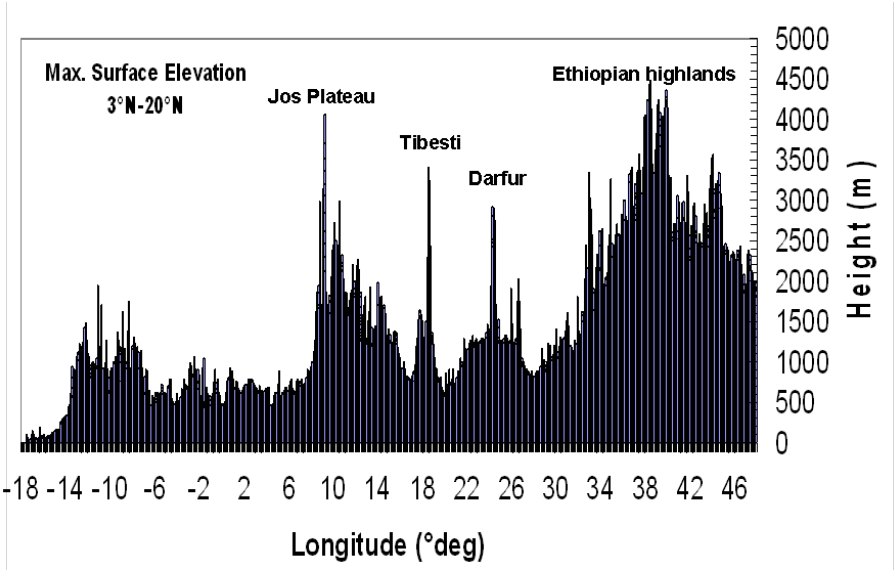

Fig. 2.2: Maximum surface elevation (m) inside the domain along each zonal strip (0.04°) between 18°W and 48°E.

The study period, hereinafter defined as the "warm season", is June-August over five-years (2004-2008). Precipitation patterns are used as a proxy for inferring the principal dynamic characteristics of the African monsoon.

The rainfall estimates consist of instantaneous rainfall maps produced every 15 minutes at the LAMMA Consortium (Laboratory of Monitoring and Environmental Modelling for the sustainable development, http://www.lamma.rete.toscana.it) with a spatial resolution of 3 × 3 km^2 at nadir; no off-line procedure was implemented for backward integration of the passive microwave (PMW) data. The precipitation estimations are derived from an infrared (IR) and PMW "blended" technique (Turk et al., 2000a,b) that dynamically correlates IR TBs as measured by geostationary sensors and instantaneous rain rates as computed from PMW radiometer data (NOAA-NESDIS algorithm; Ferraro and Marks, 1995; Ferraro, 1997). The procedure merges the high refresh time and space resolution of the data of the Spinning Enhanced Visible and InfraRed Imager (SEVIRI) (Schmetz et al., 2002) on board the MSG geostationary satellite, with the sensitivity to the microphysics of precipitating clouds of the SSM/I PMW instrument on board the DMSP polar orbiting spacecrafts (Hollinger et al., 1990).

The LAMMA laboratory is equipped with a receiving station that acquires MSG real time High Rate Information Transmission (HRIT) data every 15 minutes. Data are supplied already rectified in digital format and contain also geolocation and calibration parameters. PMW data are downloaded via ftp connection from the CLASS (Comprehensive Large Array-data Stewardship System) archive (http://www.class.noaa.gov); data are available about 1 hour after the satellite acquisition and are supplied in Sensor Data Record (SDR) format. A calibration procedure is

applied to transform sensor counts in TB, as required by the input procedure of the precipitation estimation algorithm.

Note that satellite rainfall estimations need to be associated with an estimation of the quality of the retrieval. However, not much work has been devoted to date to this crucial task and only recently validation campaigns were started to explore the error characteristics of the available products. In particular, the International Precipitation Working Group (IPWG, http://www.isac.cnr.it/~ipwg/) has launched a program for in situ continental-scale validation of daily rainfall estimates from the operational satellite algorithms providing near-real-time global rainfall products against rain gauges and radars where high-quality networks exist, such as in the United States, Western Europe, Australia, Japan, South America (Ebert et al., 2007). Among others, fundamental work on the evaluation of operational products was conducted by McCollum et al. (2002) over the continental United States and Hossain and Huffman (2008) on the error metrics at relevant hydrological scales. Sapiano and Arkin (2009) have recently evaluated and intercompared datasets at a variety of spatial and temporal resolutions within the IPWG Program to Evaluate High Resolution Precipitation Products (PEHRPP) with the intent of guiding dataset developers and informing the user community regarding the error characteristics of the products. Finally, Turk et al. (2009) have examined over-land validation statistics for the algorithm used in the present study using a high-resolution, nearly-homogeneous, 1-min reporting gauge dataset over Korea across telescoping space and time scales.

The assessment of the uncertainty associated with the estimation in Africa poses additional difficulties due to the data sparsity and quality. Lebel and Amani (1999) propose a procedure for the Sahelian area whose products are charts giving the standard estimation error as a function of the network density, the area, and the rainfall depth in the region. An extension is proposed for larger timescales (decade, month, and season).

2.1.1 Analysis of Hovmöller diagrams

Propagation characteristics of rainfall systems are determined using a methodology similar to that of Carbone et al. (2002), Wang et al. (2004), Laing et al. (2008), Levizzani et al. (2010), and described in detail by Ahijevych et al. (2001); some modifications (described below) have been introduced on the mechanism for the identification of the convective precipitating episodes.

The instantaneous rainfall maps are projected onto a regular lat/lon grid (~ 0.04° × 0.04°) and constitute the database for generating the Hovmöller diagrams. Only half of the precipitation dataset is used (i.e., a map every 30 minutes) in order to reduce the computational time without critically affecting the information content. The domain of interest (Fig. 2.1), centred on the

prevailing African monsoon flow area (~ 1900 × 7200 km2), is first divided into 1650 zonal narrow strips, each 0.04° wide (~ 4 km), running from 3° to 20° in the N-S direction.

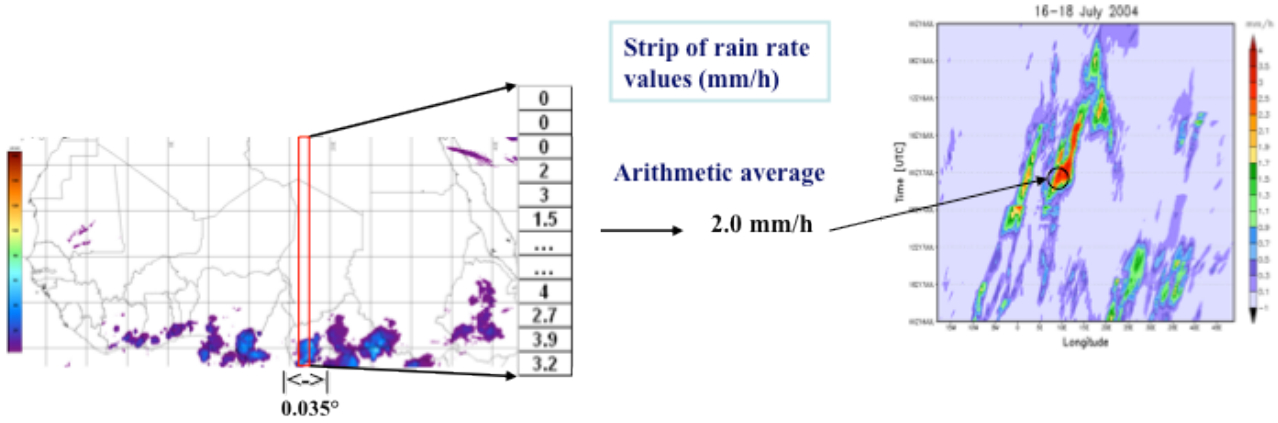

Fig. 2.3: Overall scheme for Hovmöller diagram computation.

Then, for each longitudinal strip, all the convective precipitating sequences are identified along all latitudes and the average values are calculated (Fig. 2.3). A sequence is identified when found at least longer than 15 pixels (~ 60 km) and with a rain rate higher than a given threshold (that will be defined later). Finally, the longitude-time Hovmöller diagrams are produced considering only the highest rain rate sequences.

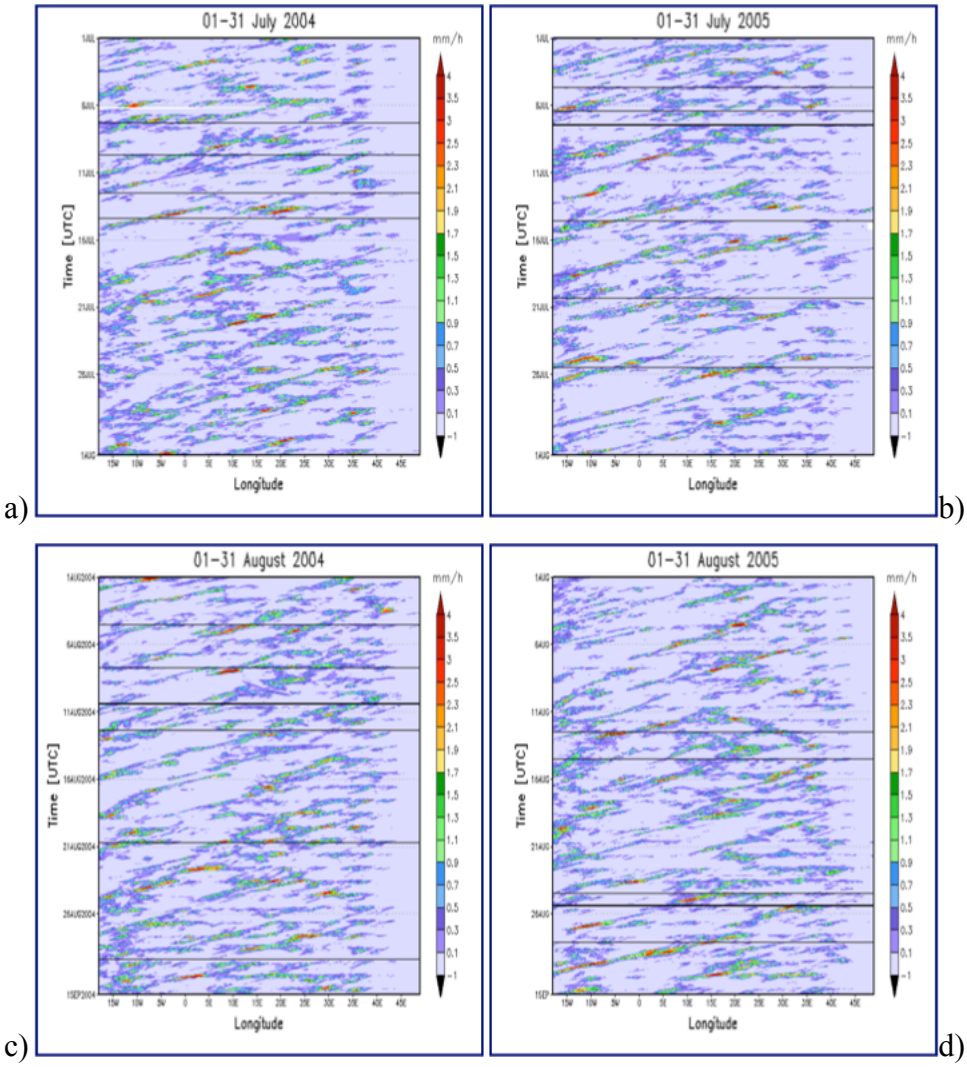

Fig. 2.4: As an example streaks events identified by the methodology described above for 4 different months: a) July 2004, b) July 2005, c) August 2004 and d) August 2005.

A quantitative analysis on the longitude-time rainfall streaks is then conducted to quantify their coherence, longevity and span. A two-dimensional (2D) autocorrelation function (see Carbone and Tuttle, 2002), uniform in one direction and cosine weighted in the other, is superimposed to the instantaneous rainfall estimate strips in the Hovmöller space to find their angle, duration and span. The 2D function is stepped through all longitude-time coordinates (0.04°/30 min) and rotated (at 1° angular increments) until the correlation coefficient is maximised (> 0.35). Sequences of contiguous fits in the Hovmöller space define the coherent cloud patterns (rainfall streaks). For computing a span/duration statistics, the cosine weighting dimension of the 2D autocorrelation function is matched to 6 h (12 grid points) rainfall duration at a given longitude, and the rectangular pulse set to 3.2° (80 grid points), i.e. the span/duration characteristics of the African MCSs (Mathon and Laurent, 2001). A deeper analysis on rainfall streaks on variability and characteristics is

presented in Melani et al., 2010, and it is not described here since this study is focused on the precipitation diurnal cycle.

2.1.2 Large scale atmospheric analysis

The analysed 5 year period is characterised by a large variability in terms of monsoon dynamic behaviour and thus rainfall intensity and spatio/temporal distribution over West Africa. The large scale WAM atmospheric dynamics can be summarised through the analysis of the zonal wind characteristics using the identification of its fast and slow variability modes. Fast transients, such as AEWs, can be highlighted through coherent streaks of westward propagating maxima at 600 hPa in a longitude-time Hovmöller diagram by averaging the zonal wind in latitude between 0° – 20°N. These disturbances are present during the whole season with important intraseasonal fluctuation (Sultan and Janicot, 2003; Sultan et. al., 2003). A slow variability at the monthly time scale can be shown through zonal wind latitudinal cross section where AEJ jet stream, along with Tropical Easterly Jet (TEJ) and Subtropical Westerly Jet location and intensity, summarising the main features of the tropical circulation in the area (Chen and Van Loon, 1987; Cook, 1999; Diedhiou et al., 1999; Thorncroft and Blackburn, 1999; Grist and Nicholson, 2001).

The five years study period (2004 – 2008) is analysed using the NCEP/DOE AMIP-II Reanalysis atmospheric dataset (Kanamitsu et al., 2002). In particular, the monthly zonal wind cross sections, averaged between 0° and 10°W, are computed (Fig. 2.5). The month of June 2004 (not shown) presents a very intense AEJ with a core speed > 15 m s^{-1} instead of the typical values of about 12 m s^{-1} observed in the following years. This high value is generally associated with a strong latitudinal surface temperature gradient. August 2005 shows a stronger and north – shifted AEJ along with a period of intense westward propagating AEWs (Fig. 2.5.a) over the continent.

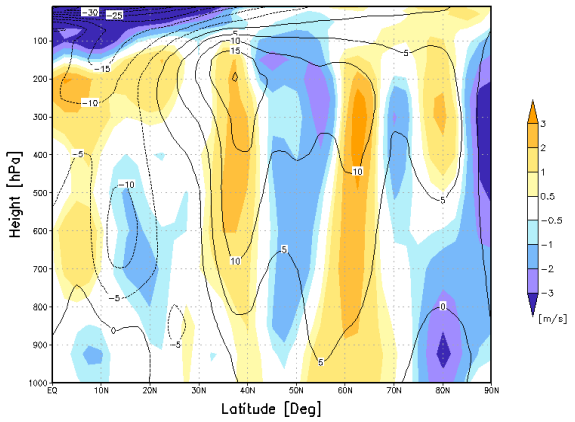

a)

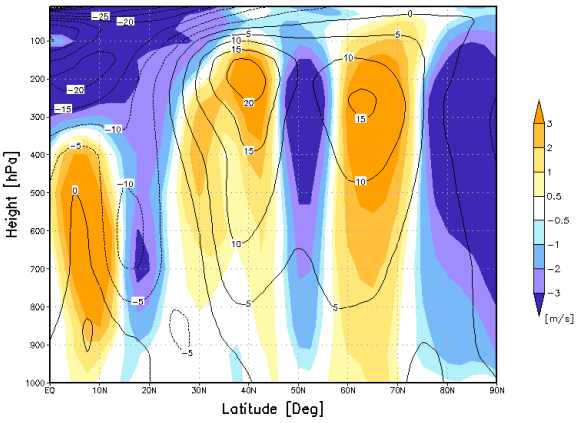

b)

Fig. 2.5: Monthly zonal wind (contour) and anomaly (shaded) cross section [m s^{-1}] for August: a) 2005 and b) 2007. The data are averaged between 0° and 10°W; contouring are every 3 m s^{-1}. Anomaly are computed with respect the 1979-2009 climatology.

During July 2007 (not shown) a strong low level westerly flow is present with wind speed values > 3 m s^{-1} and reinforcing in August (Fig. 2.6). This flow pattern is associated with the northernmost location of the AEJ among the analysed years. This latter circulation pattern in July – August 2007 determines an intense moist air advection from the Gulf of Guinea feeding convection inland far from the coast in the sub – Sahelian belt. Streaks of zonal wind (see Fig. 2.6) are associated with the westward intensification of AEJ between 20 and 40°E. Among the analysed four boreal summers, summer 2007 was characterised by strong and long lasting streaks in June (not shown), which were drastically reduced and shifted eastward in August (Fig. 2.5).

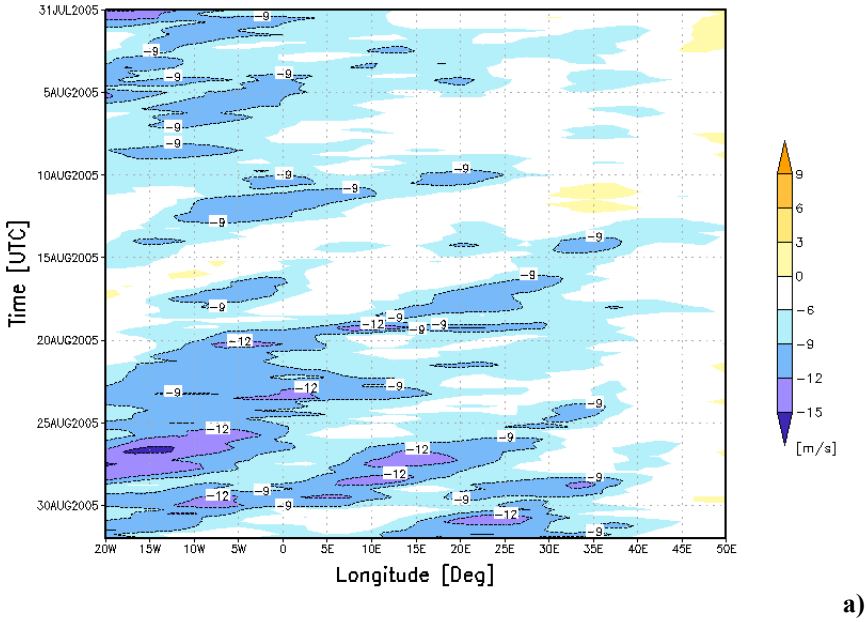

a)

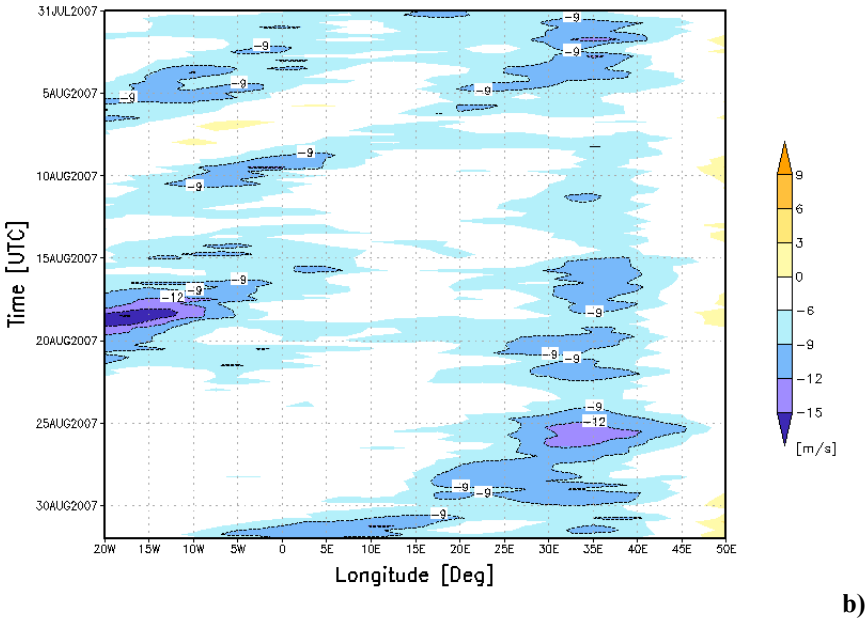

b)

Fig. 2.6: Hovmöller diagrams (longitude-time) for zonal wind [m s^{-1}] at 600 hPa for August: a) 2005 and b) 2007. Data are averaged between 0° and 20°N. Intense westward propagating streaks are clearly visible.

A similar behaviour is registered for the wind shear maxima (Fig. 2.7). This suggests a weak AEJ streak with a few synoptic disturbances moving westward, while the surface latent heat longitude - time plot (Fig. 2.7) shows over the continent (between 45°E and 15°W) a synchronous diurnal variability, which plays a fundamental role in sustaining and regenerating convection in propagating systems (Trenberth, 1999; Parker et al., 2005b; Douville et al., 2007).

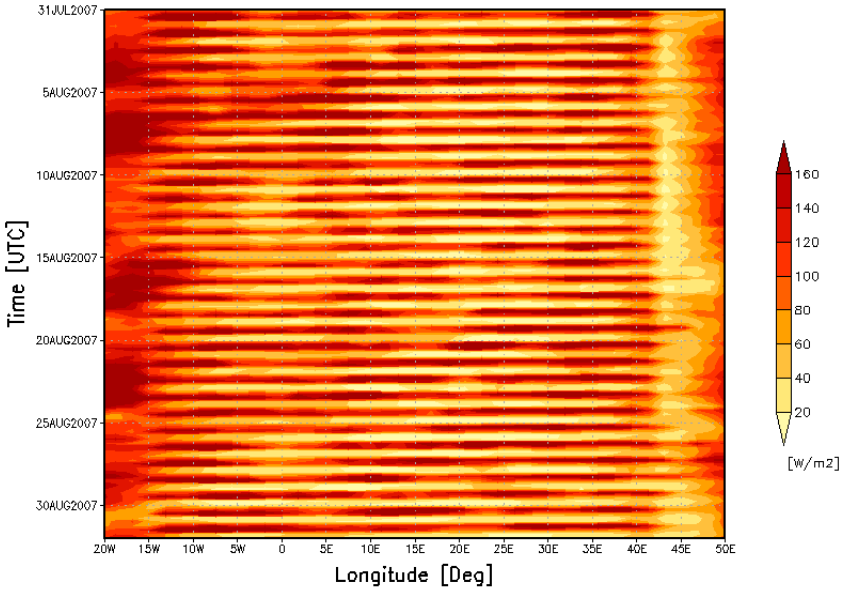

a)

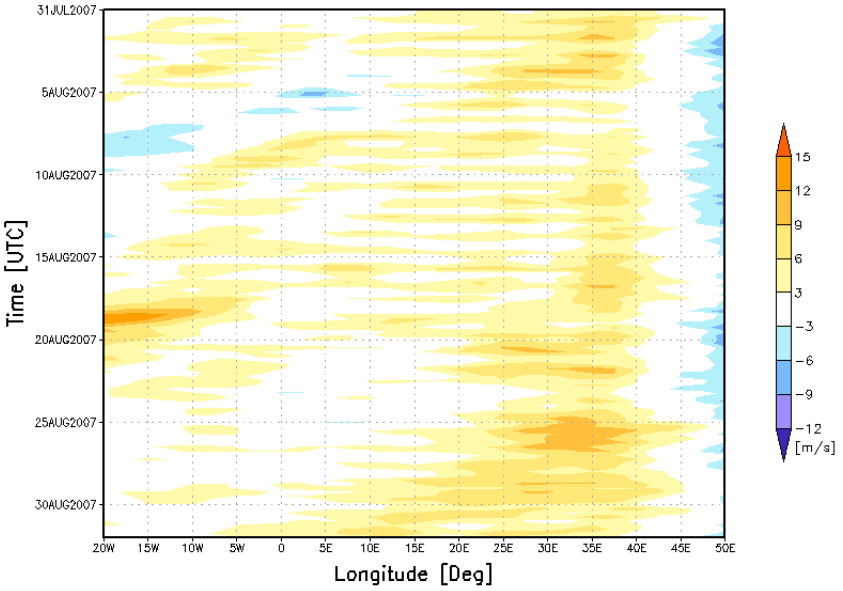

b)

Fig. 2.7: Hovmöller diagrams (longitude-time) for: a) surface latent heat flux [W m^{-2}] and b) wind shear [m s^{-1}] between 600 hPa and 925 hPa for August 2007. Data are averaged between 0° and 20°N.

The MJO index computed at 20°E (from CPC www.cpc.ncep.noaa.gov, using an Extended Empirical Orthogonal Function analysis applied to pentad velocity potential at 200-hPa, http://www.cpc.ncep.noaa.gov/products/precip/CWlink/daily_mjo_index/details.shtml) reveals a long period of enhanced convection, the blue shading between 20°E and 70°E in June and in the second half both of July and August 2007 (Fig. 2.8).

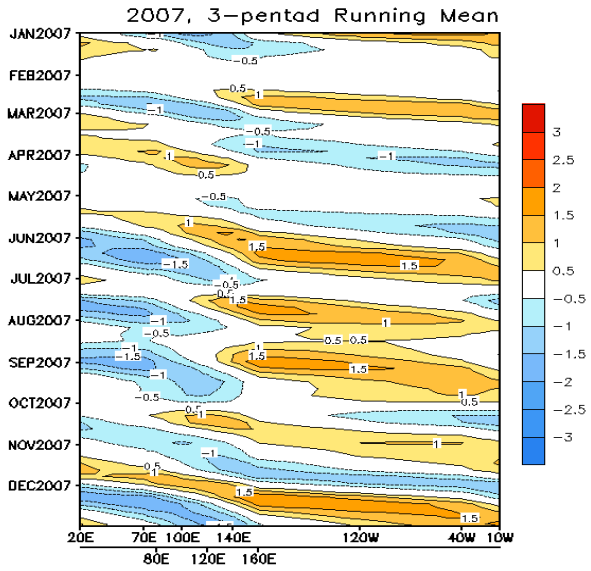

Fig. 2.8: Extended Empirical Orthogonal Function (EEOF) analysis is applied to pentad 200-hPa velocity potential (CHI200) anomalies equatorward of 30°N during ENSO-neutral and weak ENSO winters (November-April) in 1979-2000. Anomalies are based on the 1979-1995 period, and each index is normalized by its standard deviation during ENSO-neutral and weak ENSO winters (November-April) in 1979-2000.

2.1.3 Analysis of coherent rainfall episodes

The investigation of the inherent coherence of precipitation episodes showing a well-defined phase-locked behaviour is carried out using satellite-based rain rate longitude – time Hovmöller diagrams for the 2004-2008 period of record. This section focuses on the propagation characteristics of the "organized" rainfall episodes and the corresponding statistics of the rainfall streaks.

A few examples of coherent rainfall episodes are presented hereafter with emphasis on a qualitative inspection of intraseasonal and interannual variations of precipitation patterns.

The colour scale of the plates in Fig. 2.6 and Fig. 2.7 represents the latitude-averaged (3 - 20°N) rainfall estimates with a rain rate value higher than a selected threshold. In this domain the well-organized precipitating systems appear as streaks of estimated rainfall rate showing coherent westward propagation characteristics. A number of tests (not shown) were conducted on various rain rate threshold values, to find the most appropriate for capturing the most relevant features. A rain intensity value of 1 and 5 mm h^{-1} were chosen to reduce spurious signals not due to convective precipitating cells in the first case, and to highlight the core and the strength of the precipitating systems in the second case.

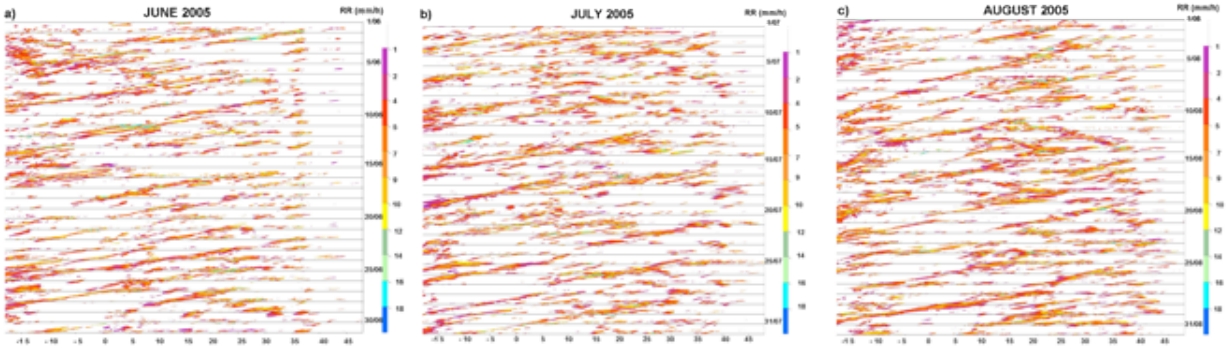

Fig. 2.9: Hovmöller diagrams (longitude-time) of instantaneous rainfall estimates with a threshold higher than 1 mm h-1 for: a) June 2005, b) July 2005, and c) August 2005. The white horizontal strips are due to missing data.

In the first two weeks of June 2005 (Fig. 2.9a) a more widespread distribution of precipitation is noted with respect to the end of the month with a non propagating convection across narrow spans of longitude in the eastern part of domain. Genesis zones are evident in the eastern (west of 30°) and in the western (west of 10°E, 0°, 10°W) parts of the domain, with precipitation episodes that span on the average more than 460 km and last about 10 h. In the last two weeks, a rainfall distribution is detected more representative of the approaching midsummer conditions. The non propagating diurnal convection, in phase with the solar heating, is more pronounced in the eastern part of the domain and spans a larger longitude strip. Convective activity strongly propagates westward and occurs more or less daily while rainfall streaks retain their coherence from the Ethiopian highlands to the Jos Plateu, especially in the second half of June. Several cloud systems span large distances (1000-3000 km) with a propagation speed between 10 and 20 m s^{-1}. Suppression of convection appears in the eastern (3-5; 26-28 June) and in the western (17-19; 27-30 June) part of the domain.

Midsummer conditions are well represented by July 2005 (Fig. 2.9b). The propagating convection occurs daily and frequently originates west of the Ethiopian highlands (west of 35°E). Secondary maxima are also evident influenced by the Darfur mountains (west of 20°E), the Jos Plateau and the Cameroon mountains (west of 10°E), and also from elevated terrain along the western coast of the Sahel (see Fig. 2.2). The non-propagating convection mainly occurs east of 30°E, in phase with the diurnal heating and representing the dominant mode of convection east of the Ethiopian highlands. The development of convection is also linked to the lower levels of the AEJ, which becomes more stable when progressing into the rainy season. The variability of the precipitation patterns is associated with the amount of convection east of 30°E, with the suppression of the precipitating systems in the eastern (e.g., 11-13; 23-25 July) and western (e.g., 11-13; 26-29 July) part of domain. It is also linked to the rate of occurrence of the higher rain intensities west of the Darfur mountains (e.g., 15-30 July).

The first half of August (Fig. 2.9c) presents similarities with July, including the non-propagating convection in the eastern domain, coupled with the diurnal heating. However, while further progressing into the rainy season the westward propagating precipitation structures, although of greater intensity with respect to July, are less coherent and highly intermittent, indicating a regime of more chaotic and less predictable convection as we approach the end of the monsoon season. Moreover, note the suppression of convection west of 0° for the 12-15 August period. The second half of August 2005 exhibits frequent convective events along all the longitudinal domain. However, the coherent rainfall patterns are less organized, with a shorter duration and span with respect to the first part of the month. The suppression of convection in the western and eastern part of the domain becomes more and more evident, approaching the monsoon season end.

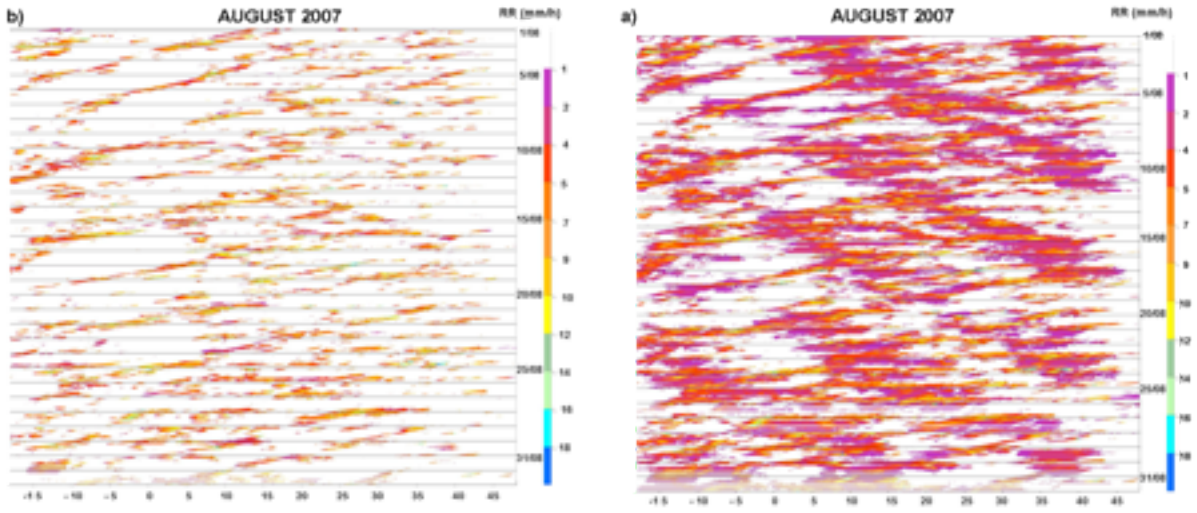

Fig. 2.10: Same as in Fig. 2.9, but for August 2007 with a rain rate threshold value higher than a) 1 mm h-1, b) 5 mm h^{-1}.

Fig. 2.10 shows the rainfall streaks for August 2007, this year being chosen for its particular long-lived and strong monsoon characteristics with a rain rate threshold value > 1 mm h^{-1} (see Fig. 2.10a) and 5 mm h^{-1} (see Fig. 2.10b). A widespread distribution of rainfall is evident across all the longitudinal domain with a more marked strength of the monsoon in terms of both a higher propagation speed and span of the rainfall streaks, which in the second half of August reach the values of 16.7 m s^{-1} and 560 km, respectively. When a higher rain rate threshold value (Fig. 2.10b) is used, the cloud structures retain their coherence, especially on the first and last days of August, while in the middle part of the month rainfall events become more intermittent and less coherent.

2.1.4 Rainfall estimate diurnal signal

The mean diurnal cycle of satellite-retrieved rainfall patterns during the warm season (JJA) for the entire period of record (2004-2008) coupled with the zonal displacement of precipitation is

examined to investigate periodicities at time scales of 1 day or less. The number of days during which precipitation intensity was higher than 1 mm h^{-1} constitutes an event, for each longitude-time coordinate, with a temporal sampling of 30 min and spatial resolution of 0.04°. Fig. 2.11 shows the mean diurnal cycle for the June, July and August averages over the five-years (2004-2008) at a given longitude-time (UTC) coordinate pair. In these diagrams the diurnal cycle is repeated twice for clarity sake.

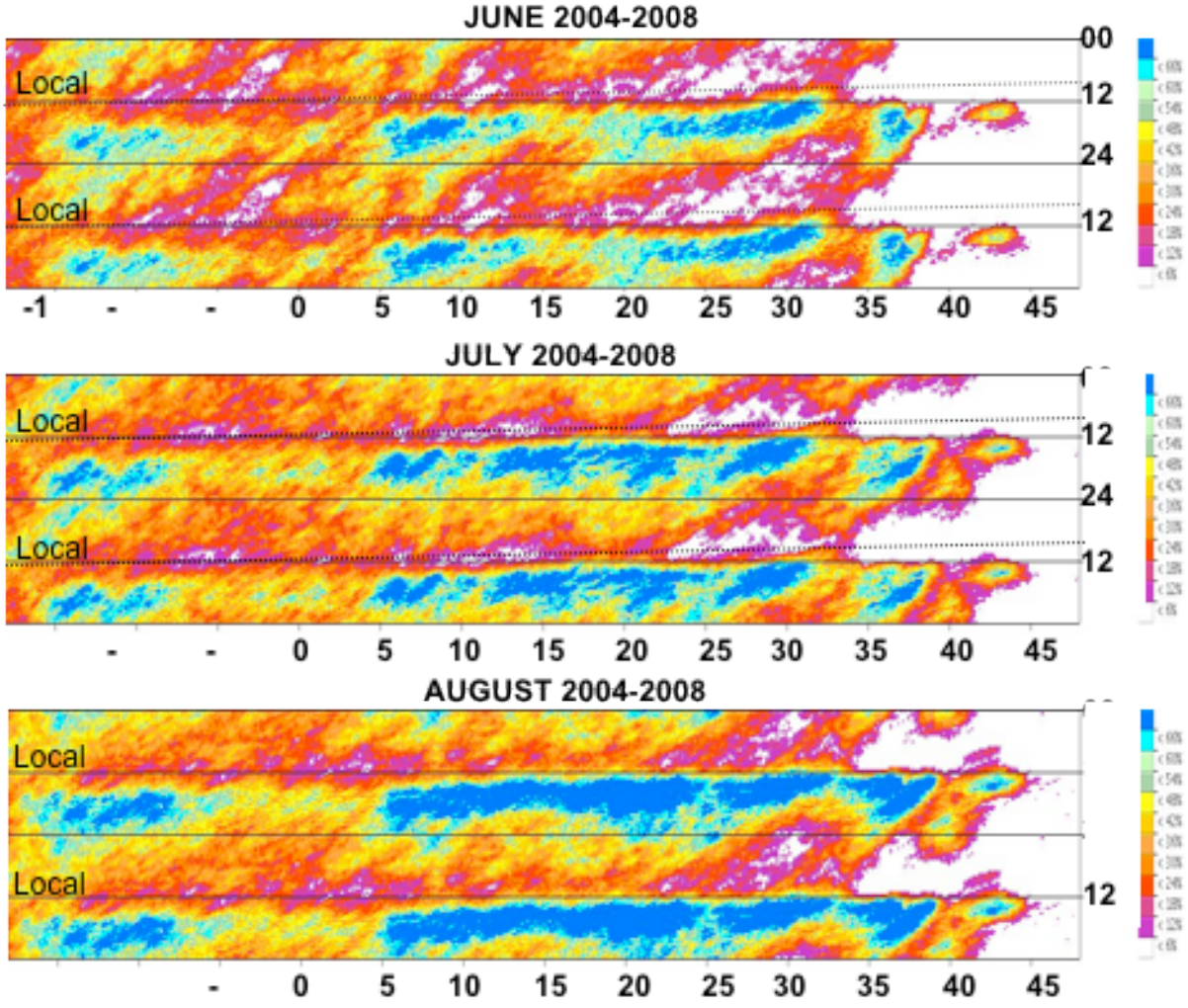

Fig. 2.11: Mean diurnal cycle of pixels with an instantaneous rainfall rate > 1 mm h-1 in the Hovmöller (longitude-time) space for June, July and August 2004-2008. The diagrams are repeated twice on top of each other for more clarity.

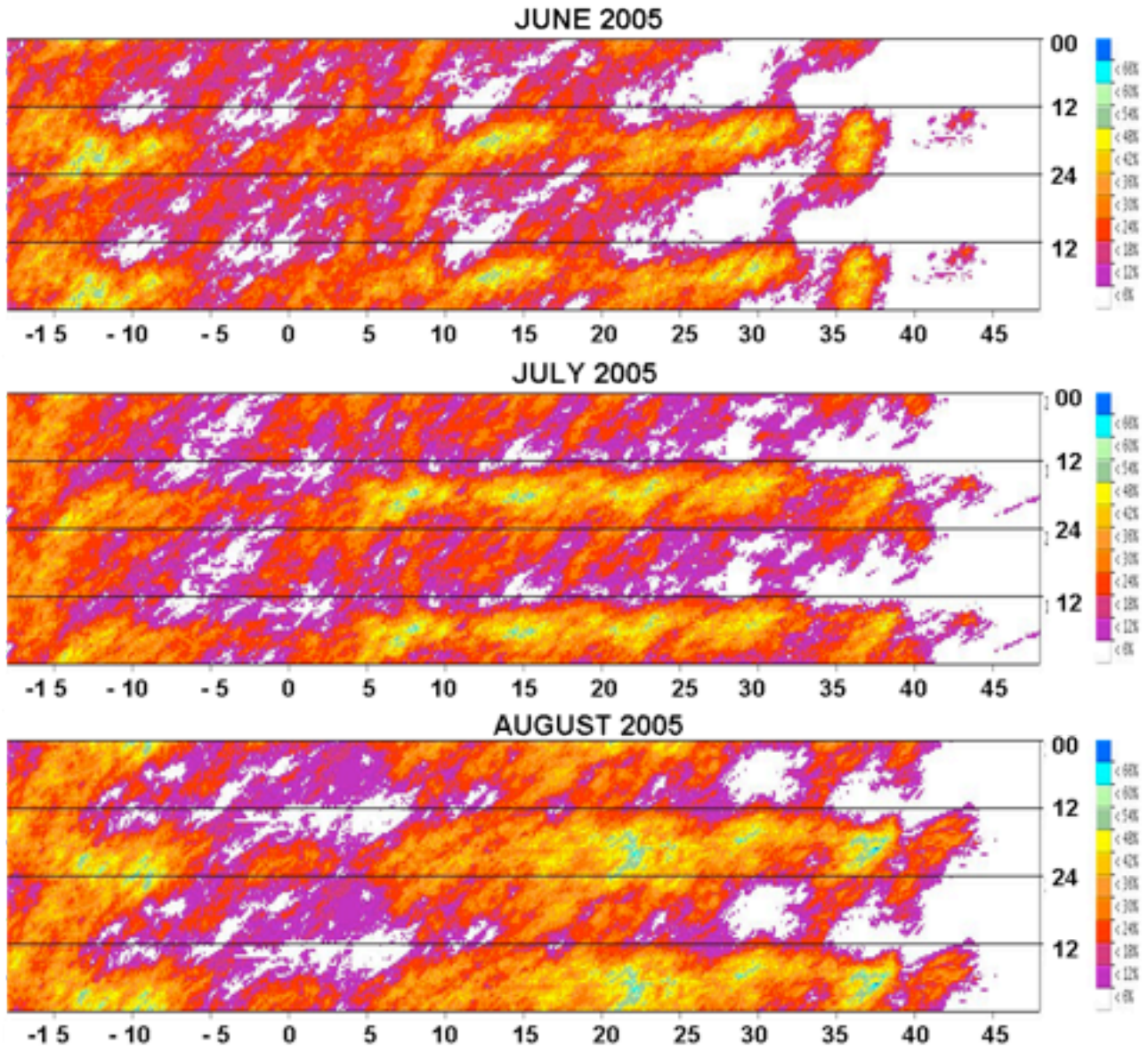

Fig. 2.12: Same as in Fig. 2.11, but for June, July, and August 2005.

Over the African continent the interaction between the elevated topography (see Fig. 2.1 and Fig. 2.2) and the strong heating during the day creates the right conditions for the formation of intense convection, as previously evidenced in Fig. 2.6 and Fig. 2.7, forming a highly unstable boundary layer (McGarry and Reed, 1978). Heavy rainfall is more pronounced in the late afternoon and early evening over most of the study domain.

The convection in the eastern part of the domain (west of 30°E) shows a daily oscillation across the continent (maxima near 1300-1600 UTC) and mainly initiates in the lee of steep topography (maxima in correspondence of the Ethiopian highlands), consistently with the thermal heating in close match with the elevated terrain (Tetzlaff and Peters, 1988; Laing and Fritsch, 1993). This

orographycally induced convection propagates westward to a certain extent and contributes to the occurrence of the maxima located east of 25°E.

The Darfur mountains and the Tondou Massif (20-25°E) originate other frequency maxima between 1400 and 1600 UTC in the 5°-15°E longitudinal band where convection is triggered by the Air Mountains, the Jos Plateau and the Cameroon Highlands; the timing of peak convection is between 1500 and 1900 UTC. A frequency minimum occurs in the region 5°E-5°W where the flat terrain provides little trigger for the convection initiation. Farther west, maxima can be found in proximity of late evening or night time, essentially due to the elevated lands near the west coast.

The frequency of the overall convective activity clearly increases as the summer progresses and near the time of maximum solar heating a distinct impact of terrain elevation on the development of convection is noted. By local midnight, land-based convection enters a dissipation phase, which on average ends in the (late) morning. The diurnal cycle climatological mean is shown in Fig. 2.11 where the diurnal signal is averaged over the whole analysed period 2004 – 2008.

The intraseasonal rainfall variability is also analysed and presented hereafter for 2005 (Fig. 2.12), chosen for its particular long-lived and strong monsoon characteristics. June (Fig. 2.12a) shows a diminished diurnal amplitude compared to the seasonal average and the quasi-suppression of diurnal maxima in the 5°-2.5°W longitudinal belt. The convection exhibits diurnal maxima in the afternoon (1400-1800 UTC) with a well-defined propagation from the eastern source of convection inducing the nocturnal/morning maxima in the western part of the domain (15°W-10°W). July (Fig. 2.12b) retains similar major features with a strengthening of the diurnal cycle and a more widespread distribution of precipitation. The convective activity is suppressed at night time, especially around 3°W, 30°E ad 38°E. In August (Fig. 2.12c) the occurrence of precipitation further increases with an evident westward streak frequency; the streaks are longer lived, faster and longer. A sharp diurnal signal linked to topographic features is evident across all longitudes. In correspondence with the maximum solar heating strong convection develops that enters a dissipation phase around midnight to the end of the morning.

2.1.5 Harmonic decomposition

Time series of the diurnal precipitation occurrence, as described in section 2.1.1 and shown in Fig. 2.11, are analysed using Discrete Fourier Transforms (DFT) and the results are presented in Fig. 2.13.

Three strong diurnal maxima located downwind of the Jos Plateau, the Darfur and the Ethiopian Highlands (17°W-10°W; 5°E-10°E; 15°E-25°E) are evident with a diurnal minimum east of 35°E. These findings consistently match the thermal forcing principles in presence of elevated terrain and diurnal frictional variation. In the lee of the principal plateaus the signals at both diurnal and synoptic ranges increase significantly from June to August (Fig. 2.13), showing a more longitudinal widespread distribution of convection along all longitudinal strips. The two weaker semidiurnal signals are located in the eastern part of the domain (25°E-30°E; west of 35°E), where the land-sea contrast may lead to the formation of sea-land breezes, mainly local in nature. The 4 longitudinal bands, where the power spectrum maxima are located, are shown in Fig. 2.14.

The phase and amplitude of the diurnal and semidiurnal signals shown in Fig. 2.13 are illustrated in Fig. 2.15, Fig. 2.17. A harmonic decomposition of wave numbers 0-2 is performed for the four longitudinal bands 5° in width (16°W-11°W; 5°E-10°E; 19°E-24°E; 33°E-38°E), which present maxima in the power spectra described in Fig. 2.13. These harmonics explain more than 90% of the total variance observed within all longitudinal bands. A further analysis has been computed increasing the number of harmonic component in the synthetic signal and compared to the remote sensing data. Increasing the wave number component in the June period increases the explained variance of several units and the synthetic signal is closer to the remote sensed signal.

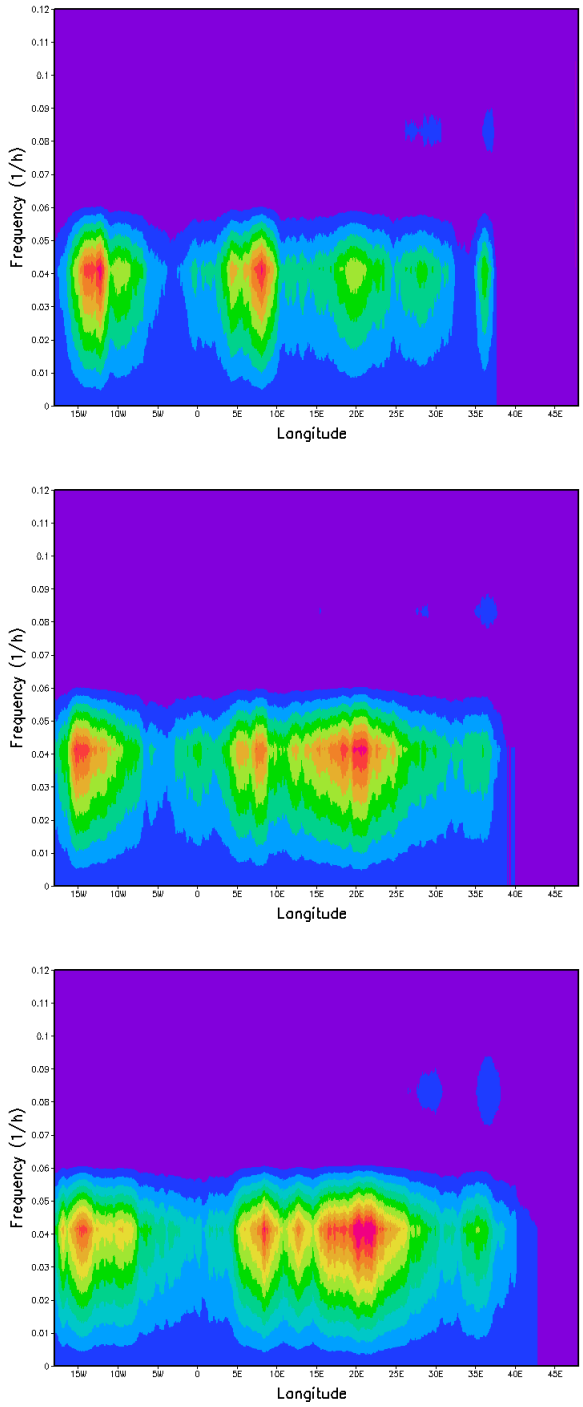

Fig. 2.13: Power spectrum of the mean diurnal cycle of the instantaneous rainfall rate greater than 1 mm h-1 in the Hovmöller space (Fig. 2.11) for: June (top), July (middle), and August (bottom) 2004-2008, plotted as a function of frequency (h-1) and longitude (degree).

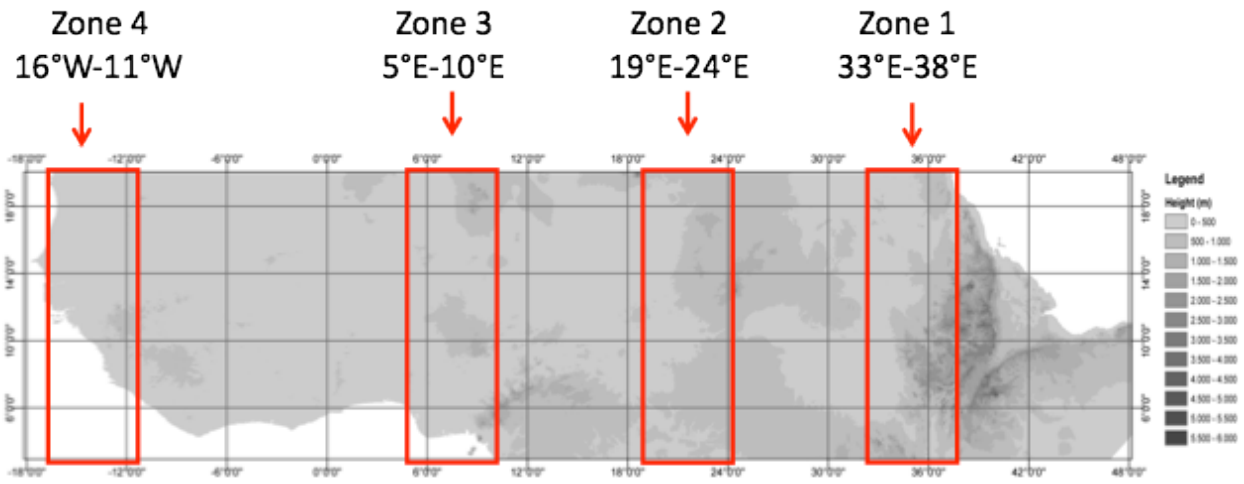

Fig. 2.14: Geagraphical areas identified from the power spectrum distribution where maxima are located.

The diurnal signal is strengthened in amplitude generally more significantly in the central parts of the domain (zones 2 and 3) and its peak time is shifted earlier in the day passing from east to west, according to the preferential zonal direction of propagation of the rainfall episodes, with maxima near 2200 and 1700 UTC and minima near 1000 and 0500 UTC in zone 4 and 1, respectively.

On the contrary, semidiurnal signals were shifted relatively little in their timing across the four zonal bands, peaking near 0300-0600 UTC and 1400-1800 UTC, with a minimum in the lee of the Ethiopian Highlands. With the progress of midsummer conditions, the peaking time in the different longitudinal zones remains almost unchanged, while the amplitude of both the diurnal and semidiurnal signals are strengthened, reaching a value of percentage of precipitation occurrence of 80% and 64% in August for the zone 3, respectively.

Note that the original data trend differs more significantly from the sum of the harmonics in correspondence of the morning peak for all the analysed zones, where on average the original data present a delay of a couple of hours in the time peaking with respect to the harmonics summation (see Fig. 2.15, Fig. 2.16 and Fig. 2.17). The reason is because the time of the first harmonic peak in the diurnal variation can be different from the actual maximum from a few to several hours, due to its essentially non-sinusoidal behaviour.

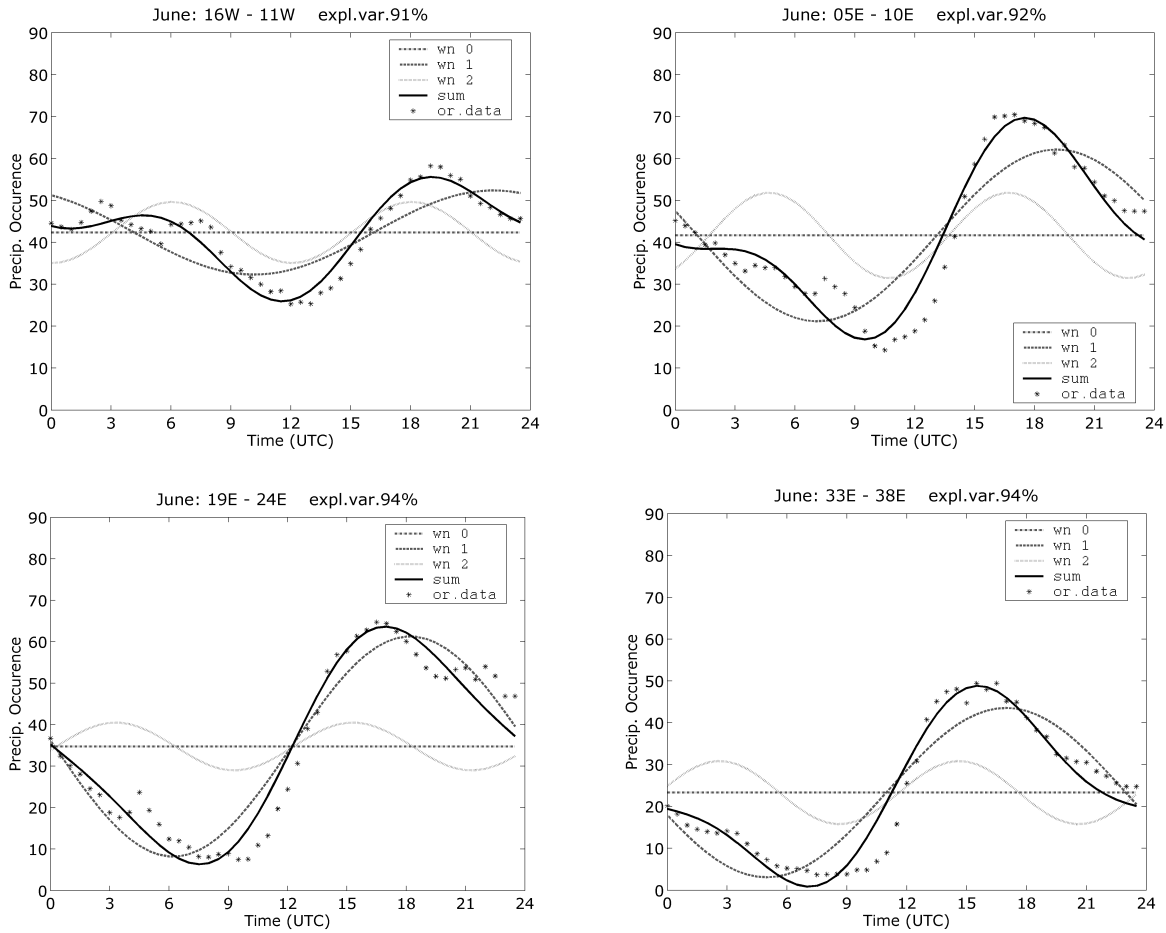

Fig. 2.15: Harmonic decomposition (wave numbers 0-2) of mean diurnal cycle of instantaneous rainfall intensities greater than 1 mm h-1 in Hovmöller space in Fig. 10, for the four longitudinal bands 5° width: a) 16°W-11°W; b) 5°E-10°E; c) 19°E-24°E; d) 33°E-38°E, for June 2004-2008. Dotted, grey dashed, long dashed and thick solid lines represent wave numbers 0, 1, 2 and their summation, respectively, while stars depict original data before decomposition.

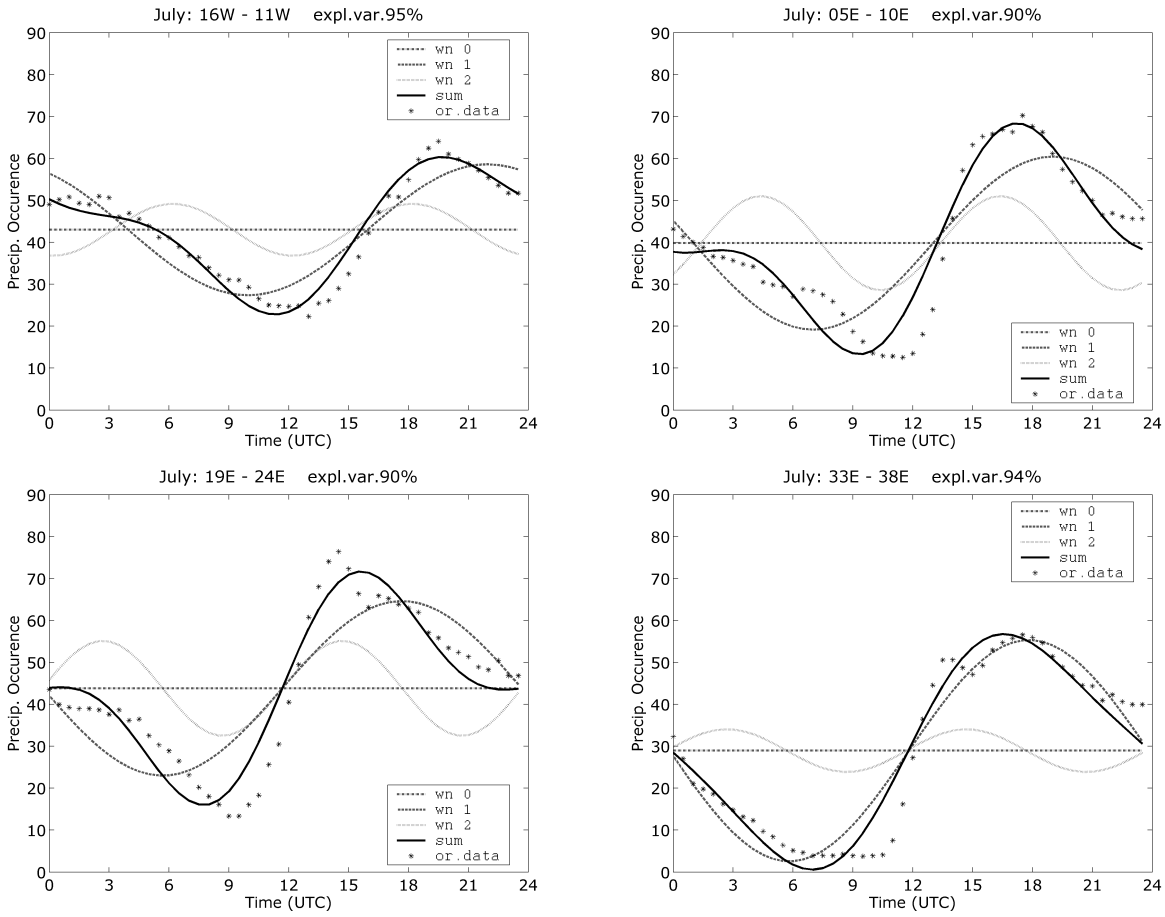

Fig. 2.16: Same as in Fig. 2.15, but for July 2004-2008.

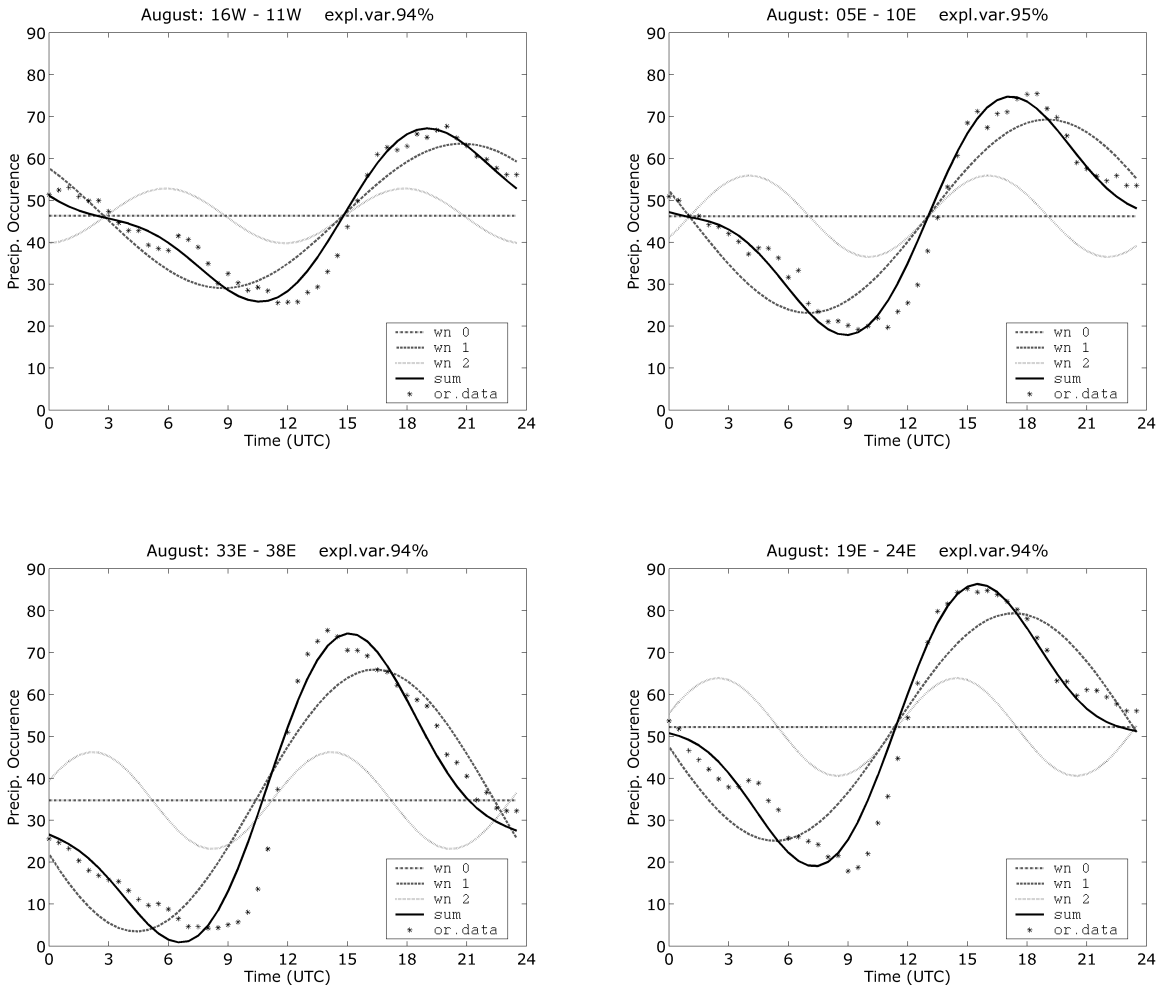

Fig. 2.17: Same as in Fig. 2.15, but for July 2004-2008.

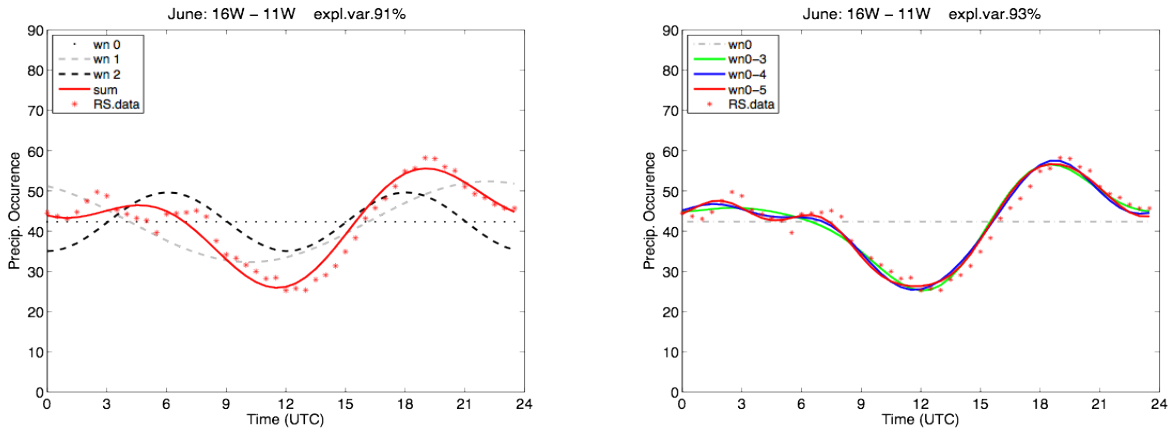

Fig. 2.18: Harmonic decomposition (wave numbers 0-2) of mean diurnal cycle of instantaneous rainfall intensities greater than 1 mm h-1 in Hovmöller space, for the longitudinal band 5° width 16°W-11°W, for June 2004-2008 (left). Dotted, grey dashed, long dashed and thick solid red lines represent wave numbers 0, 1, 2 and their summation, respectively, while stars depict original data. Green, blue and red thick solid lines represent wave numbers 0, 1, 2, 3 summation, respectively (right).

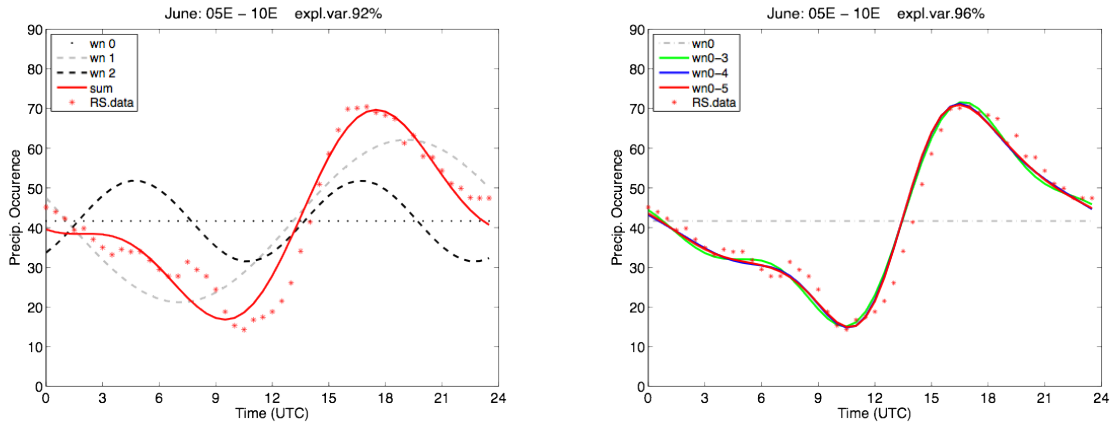

Fig. 2.19: Same as in Fig. 2.18, but for 5°E-10°E band.

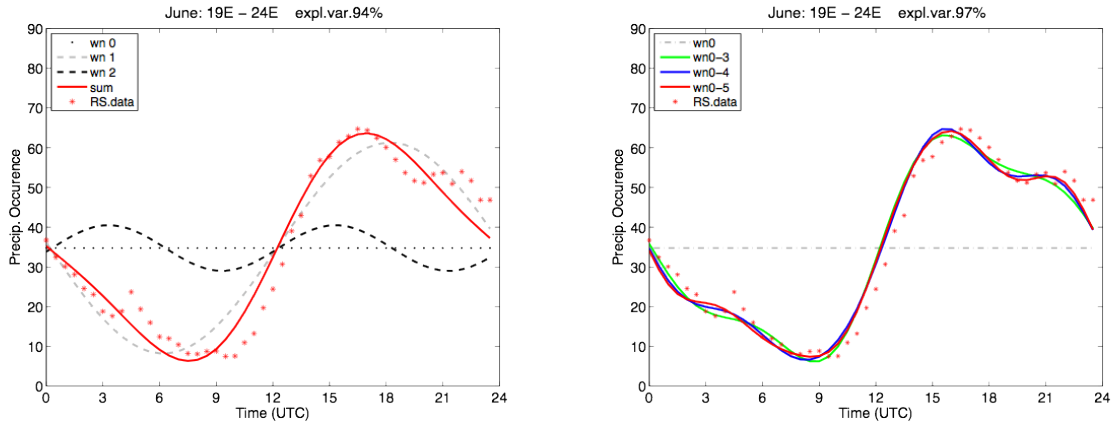

Fig. 2.20: Same as in Fig. 2.18, but for 19°E-24°E band.

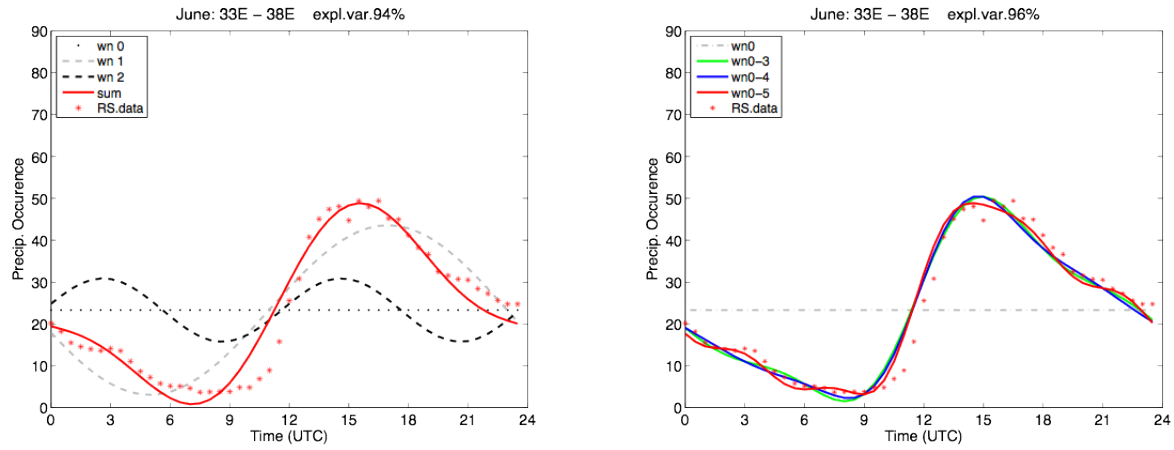

Fig. 2.21: Same as in Fig. 2.18, but for 33°E-38°E band.

2.2 Summary of remote sensed rainfall data

A climatology of 5-year (2004-2008) warm season (June-August) precipitating convection in Central Africa was shown in order to highlight structure and characteristics of convective rainfall systems. A blended IR-PMW satellite rainfall estimation method (Turk et al., 2000a,b) was used to characterise the convective precipitation patterns, inferring their zonal propagation characteristics, coupled with the diurnal displacement of precipitation.

Specifically, convection is found to initiate in the lee of steep topography, consistently with the thermal heating forcing from elevated terrain sources; it occurs more or less daily, showing coherent westward propagation characteristics.

The zonal propagation of convection across the domain shifts the diurnal maxima of convection. The interaction between the elevated topography and the strong diurnal heating creates favourable conditions for forming a highly unstable boundary layer, promoting the long lasting episodes. Maxima of precipitation frequency are more pronounced in the late afternoon and early evening, over most of the study domain. Instantaneous satellite rainfall rate were thus analysed to investigate the dynamical monsoonal characteristics and consequently to improve the space-time characterisation of the convective precipitation phase.

Differences with previous studies (Laing et al., 2008) that used IR TBs from geostationary satellites support the use of satellite rainfall estimates for this type of studies since they contribute to eliminate some of the artefacts of the IR imagery in detecting convective precipitation, such as cold cirrus shields and dissipating convection stages.

2.3 Vertical Integrated Moisture Transport - VIMT

In order to evaluate the dynamical structure of convection of the WAM it is useful to identify prognosis indices, which have the following characteristics:

a) they should be representative of small scale dynamics, since convective systems are the individual components of the monsoon and involve strong local scale features such as initialisation, moisture feeding and rainfall variability;
b) they should be representative of large scale atmospheric dynamics, since occurrence and location of a convective system within the framework of the monsoon system are the result of large scale wind patterns, soil moisture heterogeneity, atmospheric high and low frequency variability such as African easterly waves;
c) they should have a sub diurnal temporal variability linked to the occurrence of convective systems in the monsoon active phase.

For this purpose the Moist Static Energy (MSE) equation can be chosen (Dalu et al., 2009). In particular defining MSE as:

$$MSE = gz + C_pT + Lq \qquad (eq.\ 1)$$

where *gz* represent the energy contribution to the parcel from the geopotential field, by means of its potential energy due to its height with respect to the surface, the C_pT term represents the entropy, due to its temperature, and the *Lq* term measure the latent heat contribution for the presence of water in the air parcel.

Fontaine and Philippon (2000) have shown that the analysis of the MSE gradient can stratify areas of different monsoon dynamics and separate the monsoonal air from the desert air.

Dalu et al. (2009) analysed the behaviour of each term of MSE equation x and y component. They found that, during the active phase of WAM, ∂y(MSE) in the PBL is almost entirely made of $\partial y(Lq)$, while the contribution of [$\partial y(gz) + \partial y(C_pT)$] is almost negligible. From such evidence they developed an hydrological index for the onset and the withdrawal of monsoon activity based on the transported MSE by the wind. Once more, on the annual cycle of MSE·$\boldsymbol{V}$ only the Vertical Integrated Moisture Transport (VIMT) term $Lq\cdot\boldsymbol{V}$ is relevant during the WAM active phase. Using these findings Dalu et al. (2009) the onset and withdrawal index for the WAM area similar to those proposed in Fasullo and Webster (2003) for the Indian Monsoon.

The VIMT is thus a relevant parameter for characterising the active phase of convection of WAM as identified from the points a), b) and c) before. The VIMT vertical extent of integration is limited from the surface to the 850 hPa or mathematically defined as follows:

$$VIMT = \int_{Surface}^{850\,hPa} (q \cdot \vec{V})dp \qquad (eq.\ 2)$$

Different analysis used potential energy divergence (Polcher 1995) where the role of convection could be considered as the transformation of enthalpy and latent energy available in the lower atmosphere into potential energy that is uplifted in the upper troposphere. Thus a fundamental property of convective events should be considered as a footprint of potential energy divergence in the lower troposphere at daily time scale. Using the VIMT vector instead of potential energy divergence is mainly due to the possibility of analysing single components of transport instead of areal effects.

In the present study VIMT, as an integral quantity, is considered as one of the principal parameters in order to detect possible synchronisation between latent heat release and convective systems occurrence and dynamics.

2.4 Modern Era Retrospective-analysis for Research and Application - MERRA Reanalysis

Since the first release of the long term global analysis product in 1996 by the NCEP/NCAR 40 - years Reanalysis Projects (Kalnay and Coauthors, 1996) and more during the following 15 years it was clear the importance of a coherent datasets representing the all the interconnected component of the Earth climate variability. More efforts have been done during this period incrementing data availability and reliability: Reanalysis - 2 NCEP/DEO (Kanamitsu et al., 2002) , ECMWF ERA-40 Reanalysis (Uppala et al., 2006), ECMWF ERA - Interim (Dee et al., 2011), Japanese Reanalysis (JRA) (Onogi et al., 2007). These datasets cover different time periods from 1948 to present. Recently a new effort has been done by NASA with the Modern Era Retrospective - analysis for Research and Application (MERRA) Project funded by NASA Modeling Analysis and Prediction (MAP) program and released in 2011. The MERRA project main objective, as declared by NASA are: *"a) Utilizing the NASA global data assimilation system to produce a long-term (1979-present) synthesis that places the current suite of research satellite observations in a climate data context. b) Providing the science and applications communities with state-of-the-art global analyses, with emphasis on improved estimates of the hydrological cycle on a broad range of weather and climate time scales.*" MERRA WebSite.

This new global dataset covers the 1979 – present, a period when remote sensing data assimilation in numerical models provides a broader and deeper knowledge of the Earth climate system representation and dynamics. A the state of the art of data assimilation system in GMAO, namely the Goddard Earth Observing System Atmospheric Data Assimilation System, version 5 (GEOS-5), was applied with the target of obtaining an improved atmospheric data assimilation for a better representation of the hydrological cycle. Main goals of the MERRA dataset are the implementation of Incremental Analysis Updates (IAU) to slowly adjust model evolution towards observed states; high frequencies of output data to 1 hour for surface fluxes, soil states, columnar integral fields, while a 3 hours of time frequency for atmospheric diagnostic 3D fields; data availability at full model resolution (*1/2* degrees Latitude × *2/3* degrees Longitude) for all the 3 - hourly fields and a large number three dimensional 3 hourly atmospheric diagnostics on 42 pressure levels will also be

available, but at the coarse (1.25 degree) resolution; 72 model levels from surface deep inside in the stratosphere (Rienecker and Coauthors, 2011).

3 Regional Modelling

3.1 Regional reanalysis configuration

Since the NCEP/NCAR Reanalysis Project released the atmospheric global datasets a new strategy to increase our understanding of the atmospheric dynamics has become accessible (Kalnay et al., 1996; Kanamitsu et al., 2002). However, a space-time dynamical scale gap still remains and should be filled in order to catch the details of the regional atmospheric circulation. Low-cost parallel computing power is now a reality and, thus, dynamic downscaling using regional models is an opportunity at hands (e.g., Soderman et al., 2003; Miguez-Macho et al., 2005; Castro et al., 2005). Low-resolution dataset produced by global models cannot resolve many dynamical characteristics of atmospheric physical mechanisms at regional scale in the tropics. In particular, the interaction between the large scale easterly flow with both the Ethiopian highlands and the sub–Sahelian mountain ridges are not fully represented at such resolution. The topographic uplift mechanism, acting as convective triggering, is, in general, underestimated due to the smoothed topography used by global models. Furthermore, at such large spatial scale, the complex interaction between soil moisture and the convective boundary layer is not satisfactory represented thus reducing the possibility of reproducing the strong coupling between soil and atmosphere as revealed by observed data analysis (Kohler et al., 2009; Taylor and Ellis, 2006; Taylor et al., 2007; Taylor et al., 2011a) and numerical model experiments (Mathon et al., 2002; Alonge et al., 2006; Gantner and Kalthoff, 2009; Vivoni et al., 2009). Thus, in order to better model the local interactions and increase the quality of the description of the atmospheric evolution it is important to define a "downscaling technique" using a regional modelling approach. In recent years several modelling experiments have been proposed to describe the behaviour of the West African Monsoon (Sijikumar et al., 2006; Cook and Vizy, 2006; Druyan et al., 2006, 2007). Following these approaches the modelling study presented in this work is based on the Regional Atmospheric Modelling System (RAMS).

RAMS is an atmospheric regional model and its dynamical core is constructed around the full set of non-hydrostatic, compressible equations both for atmospheric dynamics and thermodynamics, plus a large selection of parameterizations for physical mechanisms (see details at http://www.atmet.com and Pielke et al., 1992; Chen and Avissar, 1994; Golaz, 2001; Pielke, 2001; Walko et al., 2000) such as turbulent diffusion, solar and terrestrial radiation, moist processes, cumulus convection, and

energy exchange between the atmosphere and the surface through a vegetation layer (Avissar and Schmidt, 1998; Chen and Avissar, 1994; Golaz, 2001; Pielke, 2001). The physical "package" of the model describes a number of atmospheric effects: (i) an isentropic analysis package (ISAN) for computing initial and boundary conditions (Pielke et al., 1992); (ii) an atmospheric turbulent Mellor-Yamada diffusion scheme (Mellor and Yamada, 1982); (iii) a cloud microphysics parameterization scheme (Walko et al., 1995; Meyers et al., 1997); (iv) the modified Kain-Fritsch type cumulus parameterization scheme (Castro et al., 2002, 2005); (v) the Harrington radiative transfer parameterization scheme (both for short and long wave radiation) (Walko et al., 1995); and (vi) the Land Ecosystem Atmosphere Feedback scheme (LEAF-3) for the energy and moisture exchanges between soil, vegetation and atmosphere (Walko et al., 2000).

The vertical representation of the simulation domain is defined using a terrain–following σ_z vertical coordinate system (Pielke, 2002). Near the ground the vertical levels follow the silhouette profile of terrain topography transforming the original 1 km x 1 km resolution of the Global USGS GTOPO30 dataset (http://eros.usgs.gov/Find_Data/Products_and_Data_Available/gtopo30_info) to the horizontal resolution of RAMS domains. Above the atmospheric boundary layer, levels follow a smoother atmospheric pressure profile. Thus the horizontal resolution of a specific RAMS domain defines not only a length scale over which actual topography height is computed, but, more fundamentally, the way in which atmospheric flows are numerically represented both in the horizontal and in the vertical. In areas where the topography has a complex morphology, such as high mountain ridges or narrow valleys, the simultaneous adoption of a high horizontal resolution domain is needed in order to numerically resolve dynamic small scale features. Furthermore a non–hydrostatic formulation of the equations of motion in RAMS takes into account the evolution of these atmospheric small scale features. The capability of a detailed description of motion is achieved at the expense of an increase of computing resources needed for the regional simulation (Meneguzzo et al., 2001, Meneguzzo et al., 2003, Pasqui et al., 2005). This regional re-analysis strategy of nesting a regional model into a global model dataset, where only observed data were assimilated, represents the most reliable approach for the representation of the atmospheric behaviour.

The proposed dynamic downscaling strategy is based on nesting the RAMS model into the NCEP/DOE AMIP-II Reanalysis atmospheric fields (Kanamitsu et al., 2002) used as initial and boundary atmospheric conditions every 6 hours throughout the simulation period via a weak lateral nudging setting, acting on a 10° wide frame. Thus every 6 hours the RAMS model is forced at the boundary, using tendencies of the atmospheric fields: temperature, geopotential height, relative humidity and wind, both meridional and longitudinal components. The nudging technique provides

a smooth forcing in the lateral domain frame, leaving the interior part of the computational domain free to evolve. Since no model restarts were imposed, after a small period of 10 to 15 days, all the atmospheric fields are in the dynamical equilibrium with the soil and vegetation. Starting simulations at the end of the tropical dry season guarantees low values of systematic under estimation of soil moisture initialization. As the tropical wet season onset is reached, at the end of May in the Sahelian area (Sultan and Janicot, 2003), all the atmospheric fields and the soil state within the model domain are in dynamical equilibrium.

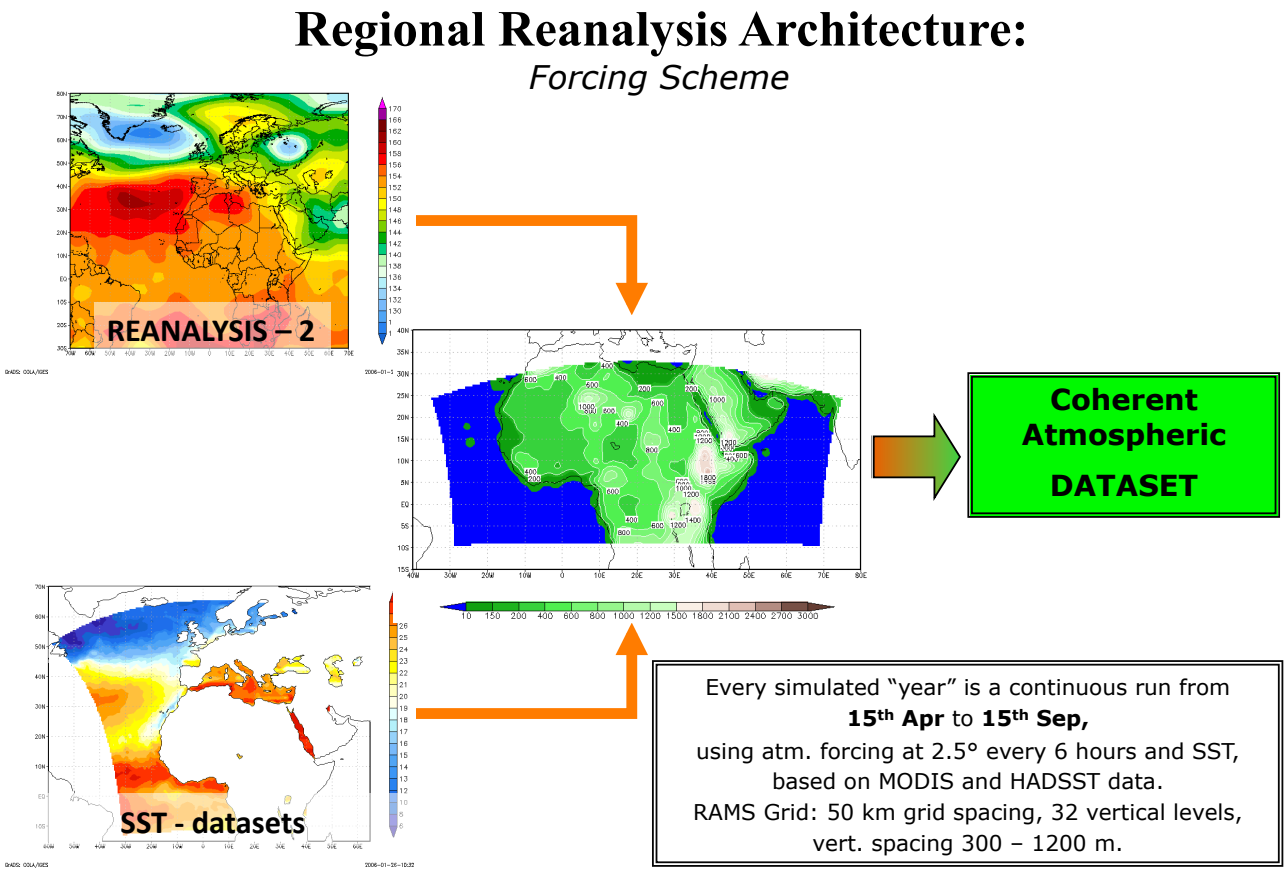

Fig. 3.1: Overall RAMS simulation scheme adopted for the regional reanalysis approach. The regional model RAMS is forced by atmospheric and sea surface temperature both at the initial time and during the simulation period.

RAMS is also forced by sea surface skin temperature providing the computational domain with the observed source of heat and moisture fluxes. Two different datasets were chosen as input for the RAMS simulations. The first dataset were the MODIS SST fields (http://podaac.jpl.nasa.gov, MODIS Terra Global Level 3 Mapped Thermal IR SST) from PODAAC - NASA. This dataset has a 8 days of temporal resolution (Brown and Minnett, 1999) and it is linearly interpolated between two subsequent dates. It could be considered as a high resolution dataset able to represent high

frequency variability of the sea surface temperature during the simulation periods. A second forcing dataset was the SST and sea ice data from HadISST (Rayner et al., 2003). It was chosen as the reference dataset within the WAMME Initiative (http://wamme.geog.ucla.edu/initiative.html) and could be considered as a low resolution dataset both for space and time variability. The monthly to daily time interpolation removes every high frequency variability signature of the Atlantic Ocean dynamics. Furthermore the low spatial resolution, 1° × 1°, alters many specific patterns in the Guinea Gulf, which as a significant impact on the intraseasonal variability of precipitation in the Sahelian region (Vizy and Cook, 2002). Since the ocean surface variability is described only through the sea surface temperature in a "one – way" forcing from the ocean to the represented RAMS atmosphere, these two SST datasets provide a sensitivity analysis of the RAMS model to the ocean variability itself. This sensitivity analysis is performed for each simulated year for which a single long run is started on April up to September from 2004 to 2008, covering the full five-year climatology period.

A single domain is used, characterized as follows (see Fig. 3.2): 30 km and 60 km of grid spacing, covering a portion of the northern hemisphere ranging in latitude from 10°S to 33°N and in longitude from 35°W to 75°E, 36 vertical levels. The spatial resolution and the coverage of the RAMS domain is far larger than the study area in order to feed the reanalysis dataset at the boundary over flat and ocean areas in the east – west boundary, achieving a stable representation of the atmospheric forcing at the larger scale. The boundary layer has been described in the model with a high level of accuracy, as one of the acting physical mechanisms in this tropical area is the interaction of the easterly flow with the topography along with the surface energy exchanges between soil and atmosphere. The vertical layers were defined based on a stretched vertical coordinate algorithm and resulted to be more dense at lower elevations (the vertical spacing ranges form 300 m near the surface to 1200 m in the free troposphere). This vertical set-up was introduced as a balanced choice between a suitable representation of the atmosphere and the numerical stability of the simulation itself (Pasqui et al., 2005).

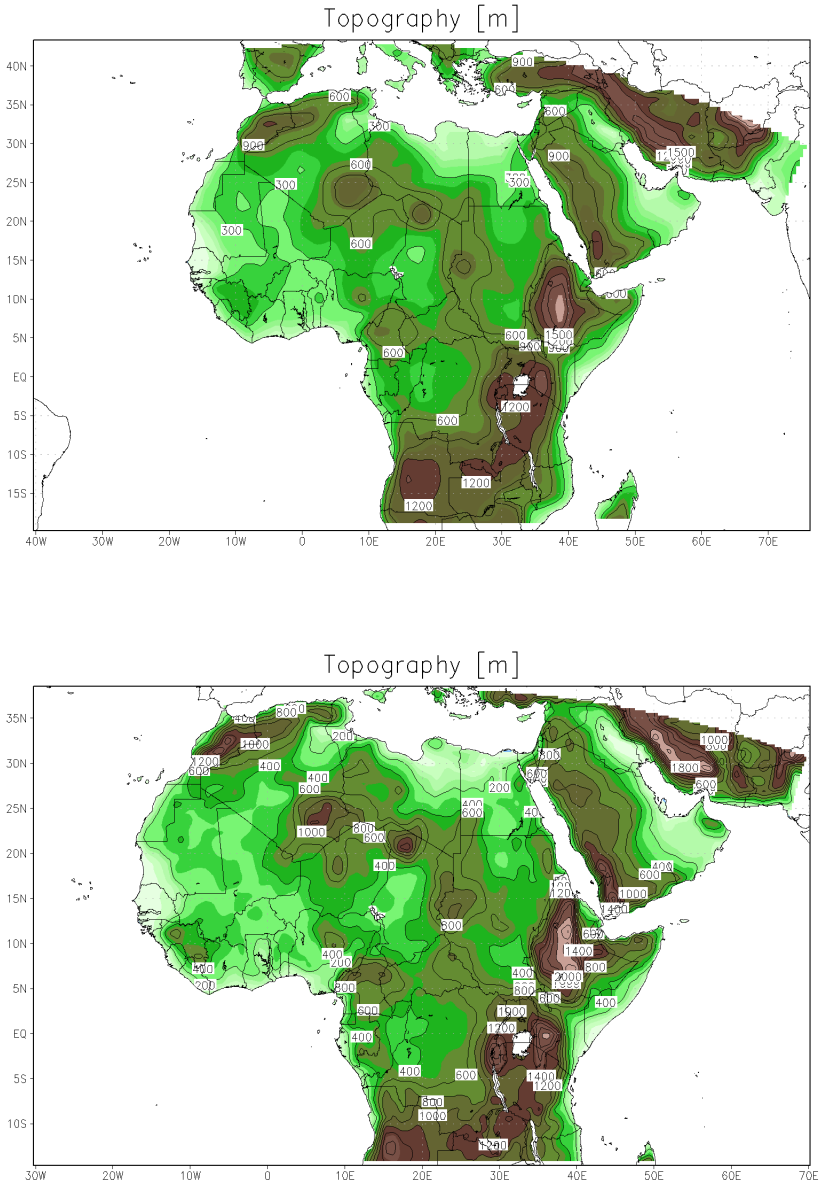

Fig. 3.2: RAMS model topography: the low-res configuration (upper panel) and high-res configuration (lower panel).

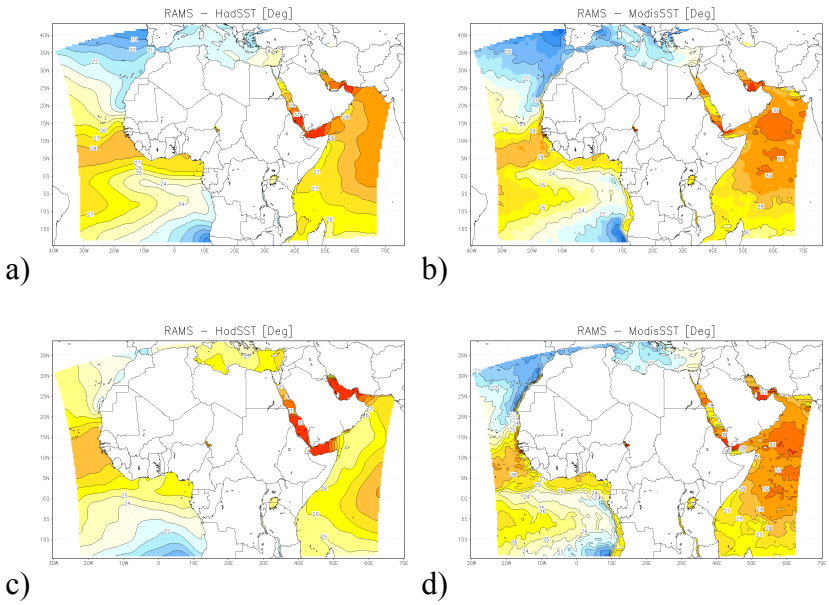

Fig. 3.3: Example of SST fields forcing the RAMS model: a) HadSST at 15th June 2005, b) ModSST at 15th June 2005, c) HadSST at 15th July 2005, b) ModSST at 15th July 2005. Different spatial resolution appears clearly through different SST smoothness patterns.

3.2 Model evaluation on the precipitation diurnal cycle

Satellite rainfall estimates, and in particular the MSG rainfall estimate described in the previous chapter, were used in the set up phase of the model configuration as a reference and guidelines. Rainfall occurrence and its spatio – temporal variability have been taken into account to properly represent the simulated large and local scale atmospheric behaviour and the resulting precipitation distribution and cycles.

Summary of domains and naming follows:

• The Low-resolution RAMS grid (hereafter L-RAMS), with 130 × 130 grid points at 60 km of horizontal spacing and 36 vertical levels, covers a large area ranging from 10°S to 33°N latitude and from 35°W to 75°E longitude Fig. 3.2). The spatial resolution and the coverage of the L-RAMS was chosen to integrate the NCEP/NCAR Reanalysis – 2 dataset (2.5° × 2.5°of spatial resolution), to achieve a stable representation of the atmospheric circulations at the synoptic scale, and to set the boundary conditions far from the study area. The simulation time step, which is the model nominal maximum time resolution, is chosen to be 120 sec. This choice guarantees a dynamical stability and an adequate representation of slow and fast moving systems described at that spatial resolution.

• The High-resolution or regional RAMS grid (hereafter H-RAMS), with 220 × 100 grid points at 30 km of horizontal spacing and 36 vertical levels, covers the study area on a domain similar to the L-RAMS, and provides a stable representation of the atmospheric circulation at regional scale with an increased horizontal resolution (Fig. 3.3). As the L-RAMS simulation set up, the H-RAMS has been forced with Reanalysis – 2 atmospheric dataset (2.5° × 2.5°of spatial resolution). In order to guarantee an adequate nudging a larger frame was chosen, 10 grid points wide. The simulation time step, for this configuration, is chosen to be 12 sec. This choice guarantees a dynamical stability and an adequate representation even of very fast moving systems described at that spatial resolution.

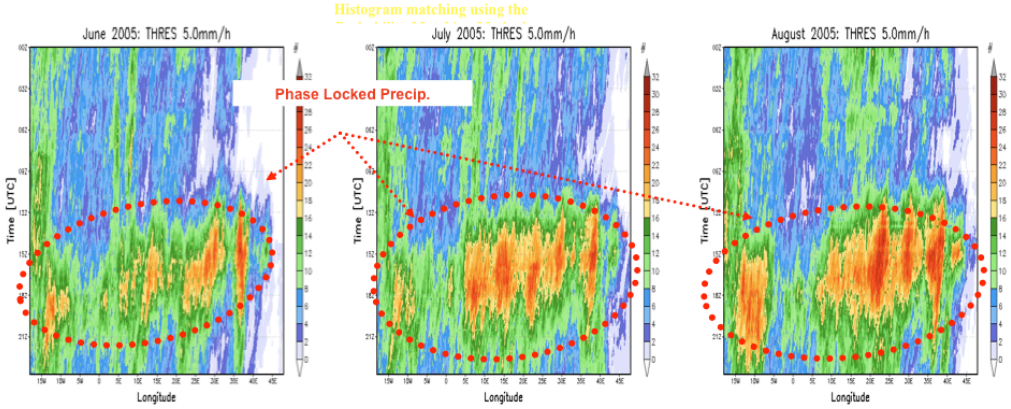

Fig. 3.4: Precipitation diurnal cycle (as in Melani et al., 2010) computed with satellite MSG rainfall estimates.

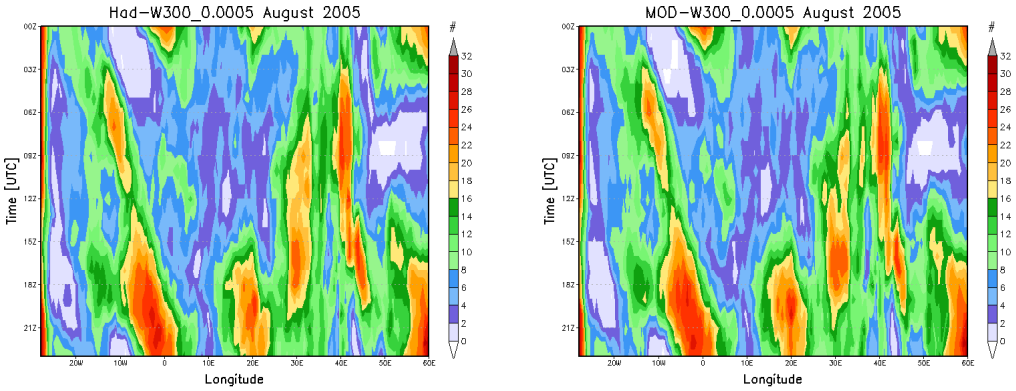

Fig. 3.5: Precipitation diurnal cycle computed using RAMS LowRes vertical velocity field at 300hPa as footprint of deep convection; HadSST forcing (left) and ModisSST forcing (right).

The footprint of the RAMS convection diurnal cycle has been compared with one computed by MSG satellite – based precipitation patterns as in Melani et al. (2010).

As a general comment, the persistency of precipitation systems decreases toward the west, while the signal due to the diurnal variations is generally evident across all longitudes between 0° and 40°E but becomes less evident westward. The convection in the eastern part of the domain shows a daily oscillation across the African continent (maxima near 1500-1600 UTC) and mainly initiates in the lee of steep topography (maxima in correspondence to the Ethiopian highlands, the Darfur mountains, the Jos Plateau and the mountains of Cameroon) and it is consistent with the thermal heating due to the terrain elevation and the results in literature (Tetzlaff and Peters, 1988; Laing and Fritsch, 1993; Laing et al., 2008; Melani et al., 2010). Farther west, maxima can be found in correspondence to the late evening or night-time hours. The westward propagation of precipitation patterns was even more evident in the average diurnal cycle when moving from June to August and signals could travel longer distances. In these diagrams, the coherent rainfall patterns represent a phase-locked occurrence of the precipitation events. Vertical velocity at 300 hPa is a "clear" tracer of convection and it was preferred in the comparison with the precipitation estimations at higher resolution retrieved from satellite observations. Fig. 3.4 and Fig. 3.5 show the mean diurnal cycle of RAMS modelled vertical velocity at 300 hPa for the months of August 2005, at a given longitude-UTC coordinate as an example for the HadSST and ModSST forcings, respectively. A stronger convective activity can be observed for the last two months, with precipitation peaks near 1600-1700 UTC and a maximum amplitude corresponding to the Ethiopian highlands (33°E-38°E). In 2005 a marked convective activity is observed with maximum amplitudes corresponding to the Ethiopian highlands (33°E-38°E) and the Darfur mountains (20°E). Unrealistic precipitation peaks are however visible during morning time in the easterly part of the domain, especially in July and August 2005. Probably this is due to the incorrect representation of the dynamical interactions between the African Easterly Jet (AEJ) and the Ethiopian orography by the regional model, producing a physically unrealistic dynamical signal.

The methodology has correctly detected and followed the evolution of the intense convection dynamics in terms of organised rainfall events with coherent propagation in the longitude-time space, characteristics of those tropical areas (Melani et al., 2010). In this sense, the coherence characteristics allowed to study the intraseasonal variability of the monsoon regime, the diurnal cycle and the zonal component of motion.

These results are relevant in the overall understanding of the dynamics of monsoon precipitation genesis and evolution, and their impacts on the long-term forecasting and climatic change studies:

- the higher the model resolution the better is the characterisation of maxima of rainfall diurnal cycle, both in time and in space;

- furthermore MODIS – SST dataset greatly improved the overall description of convection features during the season providing a better representation of rainfall amount variability, and thus it was selected as reference model configuration for the synchronization analysis, shown in Chapter 4.

3.3 Model evaluation on the seasonal time scale

The reconstruction of the monsoon dynamics with a regional model has shown good skills in the detection of some phase-locked behaviours, typical of those precipitation patterns, in the perspective of a better understanding and forecasting of the considered phenomenology. In order to represent the African climate variability at small scales we need regional high-resolution modelling. This is why we have to tune small scale dynamics simulated by the regional models: diurnal cycle analysis can highlight problems arising from the simulations and thus numerical modelling should be able to correctly represent such cycle.

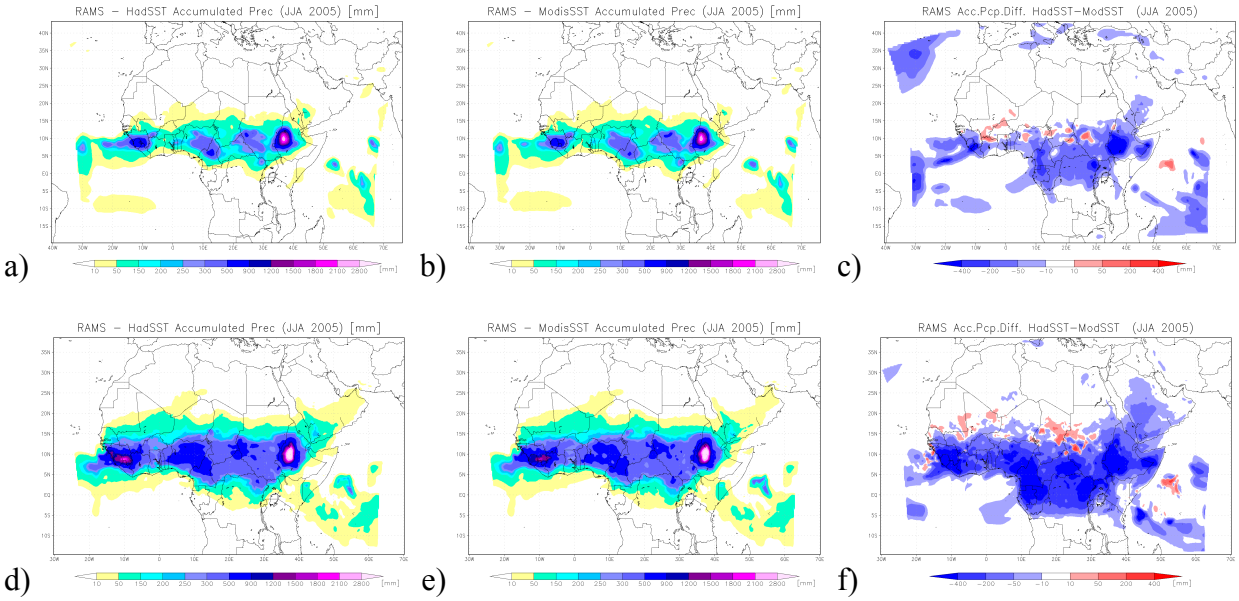

Fig. 3.6: Comparison among RAMS horizontal resolution and SST forcings for JJA – 2005: a) total cumulated precipitation for the L-RAMS forced by HadSST, b) L-RAMS forced by ModSST, c) difference between HadSST – ModSST cumulated precipitation for the L-RAMS set up. D) total cumulated precipitation for the H-RAMS forced by HadSST, e) H-RAMS forced by ModSST, f) difference between HadSST – ModSST cumulated precipitation for the H-RAMS set up.

The RAMS reliability in representing the West Africa monsoon dynamical system has been tested with respect to remote sensing dataset with an appropriate time resolution. In particular the TRMM Multi-Satellite Precipitation Analysis (TMPA; computed at fine intervals as 3B-42) intercalibrated (to 2B31) and combined 2A-12, SSMI, AMSR and AMSU precipitation estimates (referred to as High Quality – HQ) were used. The IR rainfall estimates from geostationary IR observations are retrieved by calibrating the IR brightness temperatures to the HQ estimates. The 3B-42 estimates consist of the HQ where available and IR otherwise, all scaled to match the monthly satellite/rain gauge analyses in 3B-43. The output is precipitation for 0.25 × 0.25 degree grid boxes on the latitude band 50° N-S every 3 hours (http://trmm.gsfc.nasa.gov/3b42.html). Several papers describe this global high-resolution rainfall product (Huffman et al., 2007), its algorithm (Huffman et al., 1995, 1997). Hereafter reference to the TRMM Multi-Satellite Precipitation Analysis will be simply indicated as the TRMM dataset.

Following the standard approach of a local evaluation of rainfall precipitation (Wilks, 1995) by using categorical skill scores. The first step to verify this kind of binary forecasts is to compile a 2 × 2 “contingency table” showing the frequency of "yes" and "no" reproduced and corresponding to observations:

contingency table		observation	
		YES	NO
forecast	YES	a) hits	b) false alarm
	NO	c) miss	d) correct rejectio

Fig. 3.7: Contingency table representation of "hits" and "miss" occurrence.

There are two cases when the modelled field is correct, either a "hit" or a "correct rejection" and two cases when the modelled event is incorrect, either a "false alarm" or a "miss". A perfect representation of the study event would have only hits and correct rejection, with the other cells equal to 0.

An event is defined as the cumulated precipitation, over a fixed threshold, simulated for a specific 3 hours time frame in a specific model grid point. To directly compare these datasets, the TRMM precipitation rainfall has been projected and up-scaled to the RAMS grid. The measure that examines by default the event by measuring the proportion of observed events that were correctly forecasted is Probability of Detection (POD):

$POD = \frac{a}{a+c}$ range of POD is zero to one, a perfect score = 1.

POD is sensitive to hits but takes no account of false alarms and it is thus required that POD be examined together with the False Alarm Rate (FAR).

$FAR = \frac{b}{a+b}$ range of FAR is zero to one, a perfect score = 0.

Variability of POD and FAR is shown according to different resolution configurations and both ModSST and HadSST forcing. All the following considerations are valid for all the rainfall seasons simulated: from 2004 to 2008 and thus they have a general validity.

There is a large variability of skill scores both in space and in time, but some comments can be highlighted. The higher values of POD are confined in regions downstream to the mountain chains. This is always true even if it reveals differences according to different resolution and sea surface temperature forcing. Increasing model resolution provides a wider portion of domain with high values of POD in every sub period of the monsoon season. These portions where precipitation is correctly simulated both in time and location extends far way from the mountain chain, highlighting the conclusion that H-RAMS provides a correct representation of propagation of rainfall systems far from the triggering location. The L-RAMS only provides a good representation of the initialization of convective systems, but it fails in the propagation description. The SST forcing does not highlight any prominent behaviour: both ModSST and HadSST are characterized by similar patterns of POD. Since the total amount of precipitation at seasonal scale is very different from ModSST and HadSST (Fig. 3.6) the analysis of marginal improvements, explained by POD, reveals different aspects of the regional modelling behaviour: the long term moisture provision is essentially linked to large scale supplies, and in particular to ocean sea surface temperature. Rainfall systems propagation is, on the other hand, strictly linked to local surface features and how good is the physical description provided by the numerical model. The analysis of the FAR skill score shows how the areas where RAMS is able to correctly represent propagating systems are embedded in the band where rainfall occurred. These high reliable areas are smaller than those where POD is high, but nevertheless represent a wide portion of geographical area characterized by convection. There is a broad area where POD is low and FAR is high. It extends north in the Sahelian area up to the southern border of the Saharan desert. It is the region where just a few rainfall systems are observed and only a very high model resolution could improve significantly their representation. Note that the so called Inter-tropical Convergent Front (ITF), where the southern large scale moist flow from the ocean encounters the northerly dry flow from the Saharan desert, is essentially

located at the same latitude no matter the SST forcing or resolution is adopted. This consideration should be studied deeply even if a direct explanation supports the fact that it is a large scale feature and thus both L-RAMS and H-RAMS are able to represent it.

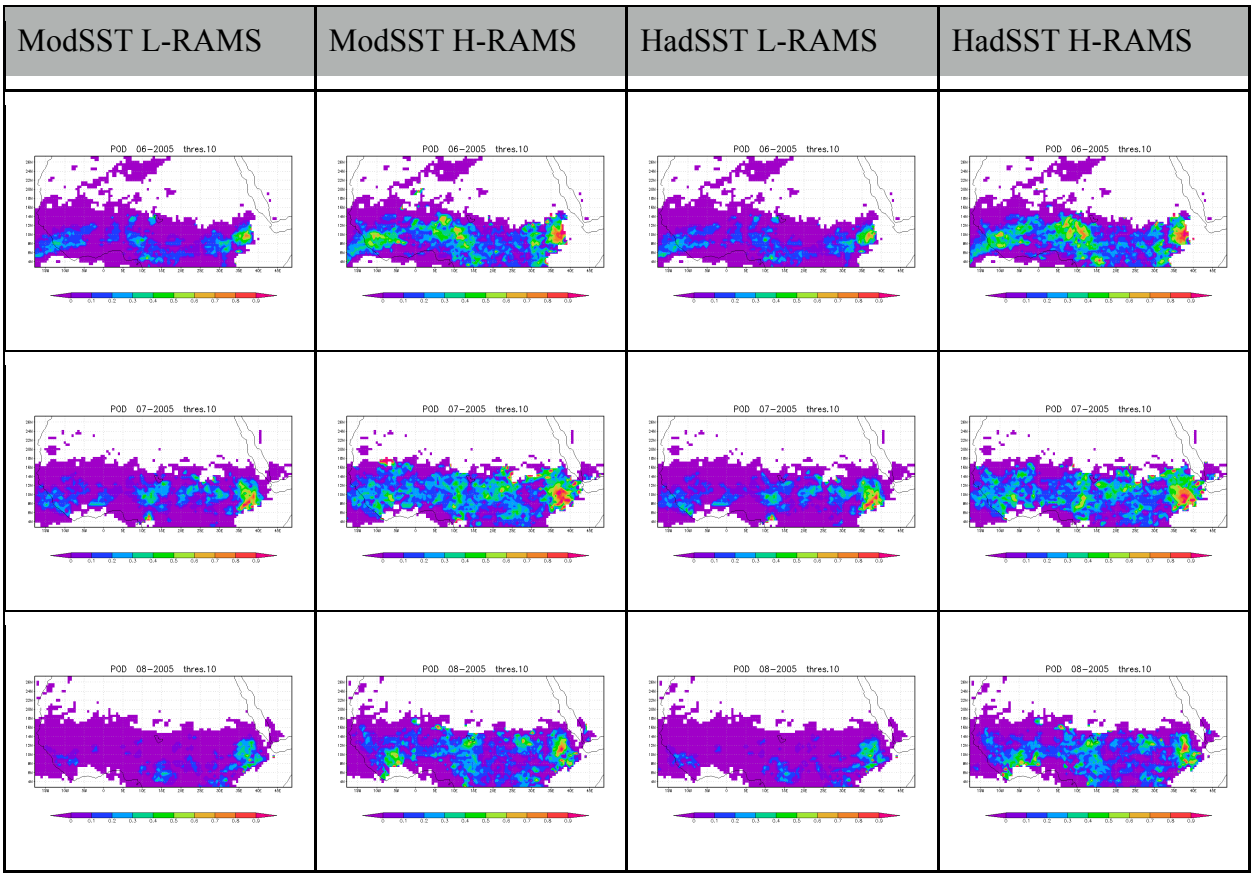

Fig. 3.8: A example of Probability of Detection maps for the JJA – 2005. By column different sea surface forcings: ModSST and HadSST and different RAMS configurations: L-RAMS, at 50km of horizontal resolution, and H-RAMS, at 30km of horizontal resolution. By rows different months of the JJA- 2005 season: June, July and August.

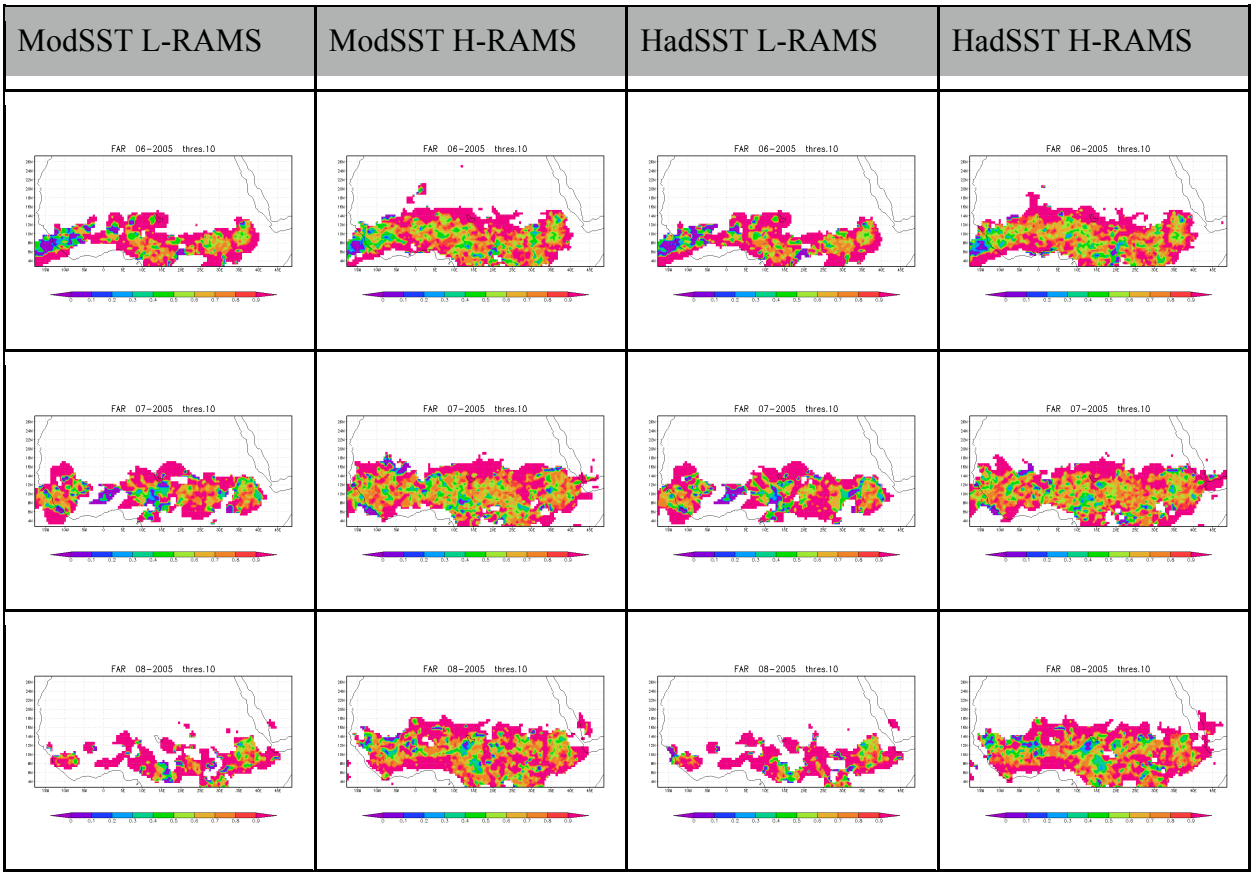

Fig. 3.9: A example of False Alarm Rate maps for the JJA – 2005. By column different sea surface forcings: ModSST and HadSST and different RAMS configurations: L-RAMS, at 50km of horizontal resolution, and H-RAMS, at 30 km of horizontal resolution. By rows different months of the JJA- 2005 season: June, July and August.

3.4 High frequency variability

One of the aims of this study is the characterization of the diurnal signature of convective rainfall and his link with the high frequency atmospheric and surface variability. Thus a further evaluation of simulated rainfall high frequency variability as a whole is needed. Following Wang et al. (2010) a Principal Component Analysis (PCA) has been performed. The highest temporal resolution rainfall field has been analyzed for regional modelling simulation, with RAMS, the global simulation MERRA and the estimated rainfall patterns from TRMM and MSG.

The following steps where performed for all the datasets:

- all the datasets were projected on the same latitude – longitude regular grid: from 3°N to 20° N and from 20°W to 60°E with an horizontal resolution of 0.5 × 0.5 degree.

- all data are projected with respect to the Local Time axis.
- a time average has been computed for each available time step: 1 hour for the RAMS model simulations and the MSG rainfall estimates, 3 hours for the MERRA and TRMM datasets. The average period was the JJA season for the 2004-2008 years.
- Once obtained the average signature, a PCA has been computed in the time mode.
- In order to compare more directly the footprint of diurnal cycle variability, the PCA loadings are normalized with respect to their respective maximum values.
- Three principal components are retained for each dataset.

At the end of such procedure for each dataset there are three patterns, by means of empirical orthogonal functions (EOFs), and three amplitude time series, by means of loadings (Navarra and Simoncini, 2010).

	TRMM [%]	MSG-RR [%]	MERRA [%]	RAMS-Had-LR [%]	RAMS-Mod-LR [%]	RAMS-Had-HR [%]	RAMS-Mod-HR [%]
1st EOF ExpVariance	*50.1*	*48.3*	*64.6*	*72.2*	*77.2*	*27.4*	*34.0*
2nd EOF ExpVariance	*24.8*	*25.3*	*48.5*	*58.4*	*55.3*	*18.7*	*21.8*
3rd EOF ExpVariance	*4.7*	*9.5*	*12.3*	*12.7*	*14.3*	*4.1*	*4.9*

Tab. 1: Explained variance for the first three EOFs modes for each datasets analyzed.

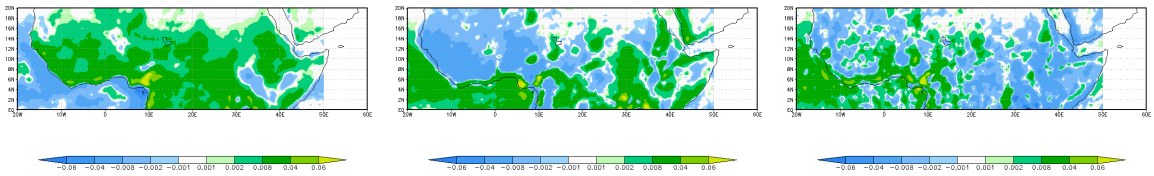

Fig. 3.10: First 3 EOFs for TRMM precipitation diurnal cycle for JJA, 2004-2008 period.

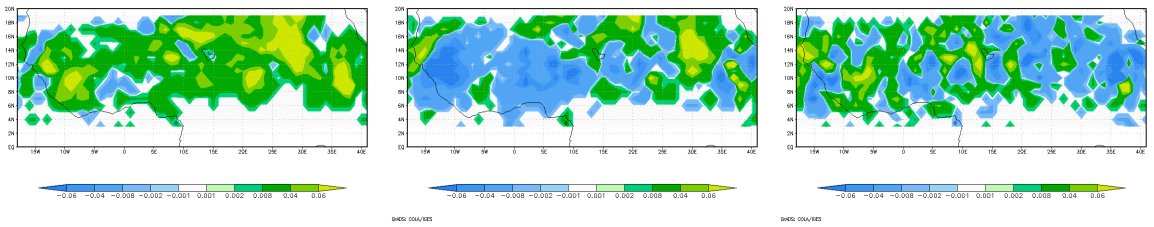

Fig. 3.11: First 3 EOFs for MSG rain rate estimates diurnal cycle for JJA, 2004-2008 period.

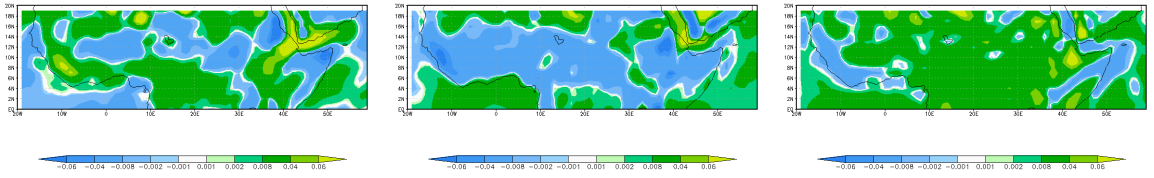

Fig. 3.12: First 3 EOFs for MERRA precipitation diurnal cycle for JJA, 2004-2008 period.

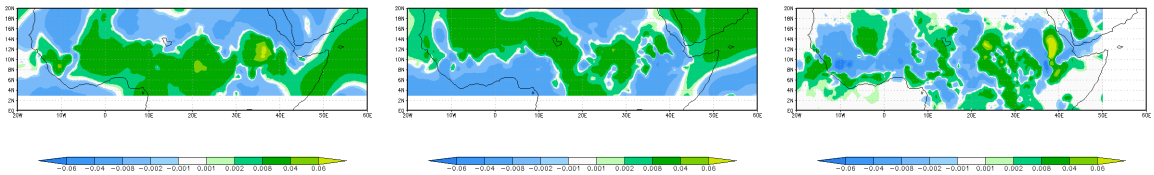

Fig. 3.13: First 3 EOFs for L-RAMS (ModSST) precipitation diurnal cycle for JJA, 2004-2008 period.

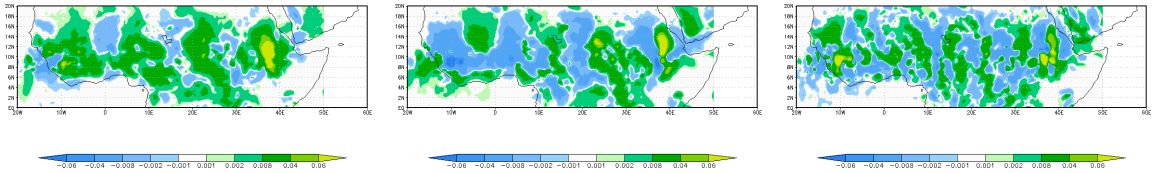

Fig. 3.14: First 3 EOFs for H-RAMS (ModSST) precipitation diurnal cycle for JJA, 2004-2008 period.

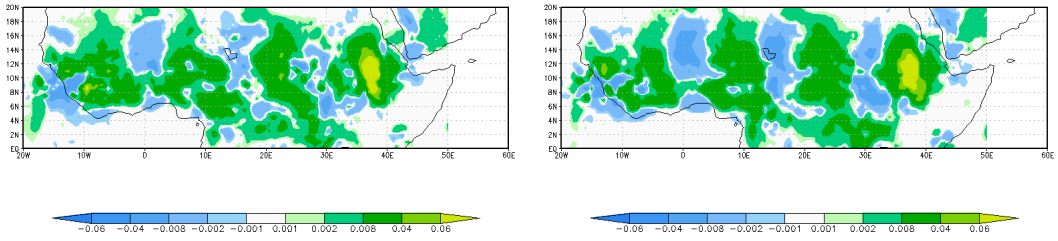

Fig. 3.15: First EOFs for H-RAMS precipitation: ModSST (left) and HadSST (right).

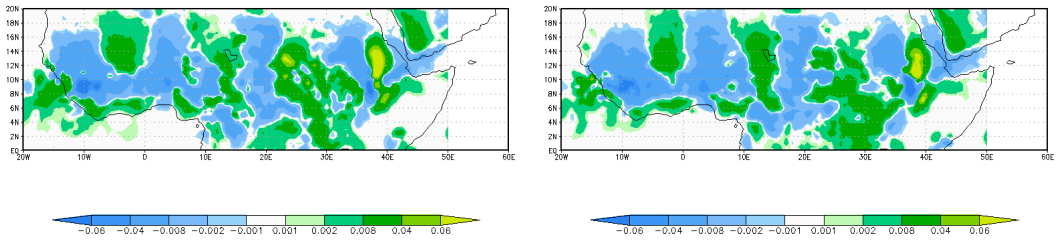

Fig. 3.16: Second EOFs for H-RAMS precipitation: ModSST (left) and HadSST (right).

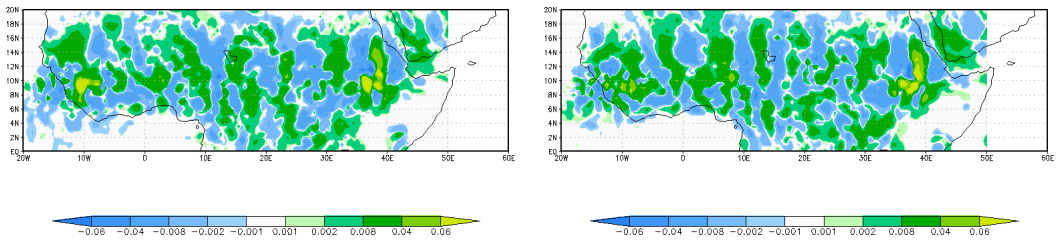

Fig. 3.17: Third EOFs for H-RAMS precipitation: ModSST (left) and HadSST (right).

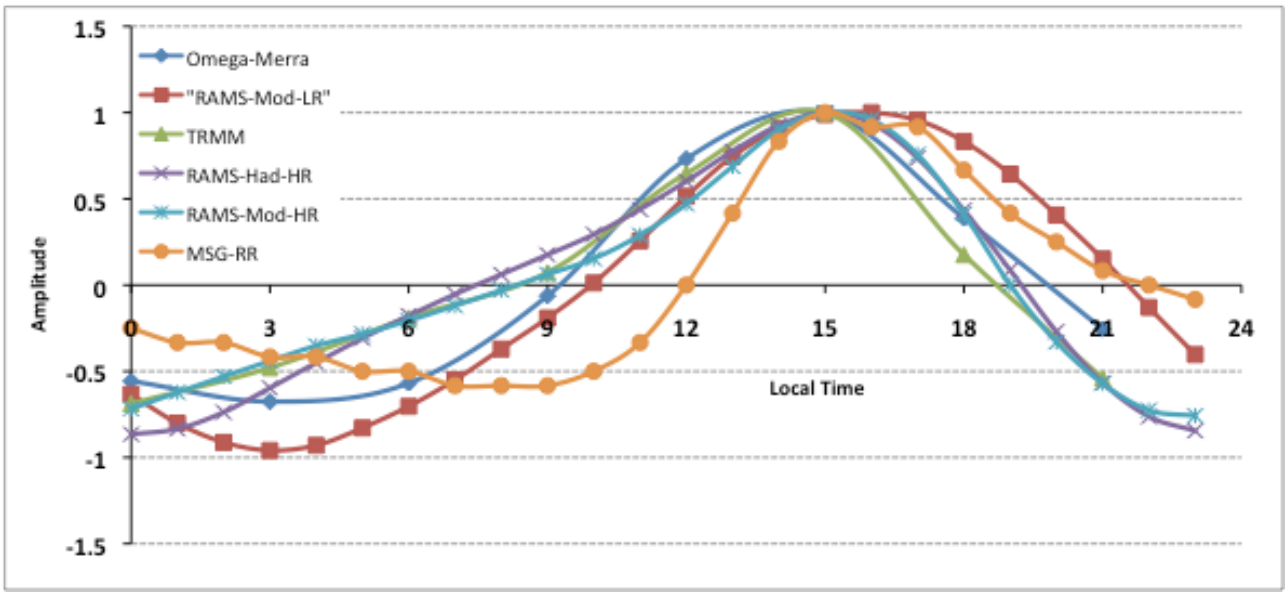

Fig. 3.18: First PCA loading time series for RAMS precipitation (ModSST-L-RAMS in red, ModSST-H-RAMS in light blue, HadSST-H-RAMS in violet), MERRA precipitation (blue), rainfall from TRMM (green) and MSG-Rainfall Rate (light brown).

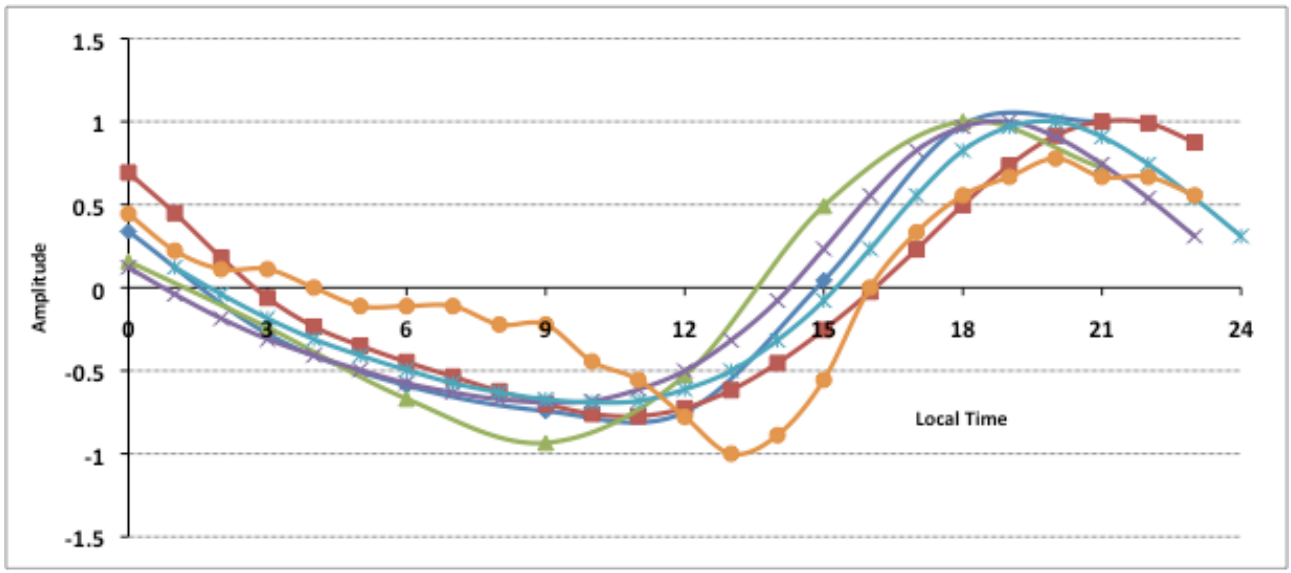

Fig. 3.19: Second PCA loading time series for RAMS precipitation (ModSST-L-RAMS in red, ModSST-H-RAMS in light blue, HadSST-H-RAMS in violet), MERRA precipitation (blue), rainfall from TRMM (green) and MSG-Rainfall Rate (light brown).

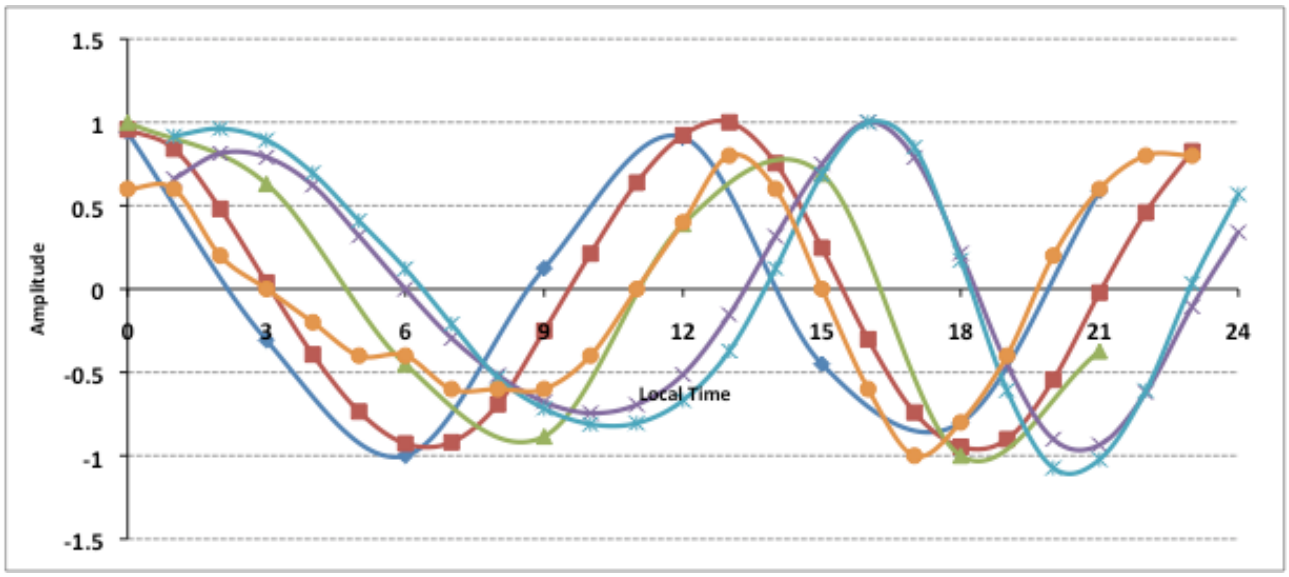

Fig. 3.20: Third PCA loading time series for RAMS precipitation (ModSST-L-RAMS in red, ModSST-H-RAMS in light blue, HadSST-H-RAMS in violet), MERRA precipitation (blue), rainfall from TRMM (green) and MSG-Rainfall Rate (light brown).

The loading time series represent the timing weight of the correspondent EOF. Thus, by using the PCA analysis the spatial and temporal variability could be analyzed separately to highlight different features from different simulation datasets. A summary of the explained variance by each single EOF for all the analyzed datasets is shown in Tab. 1. EOFs show a large dependence on the model horizontal resolution and a small dependence on the SST dataset used. As shown from Fig. 3.10 the

TRMM – precipitation EOFs has the well known bimodal patterns, which separate the first and second components with different timing. The third component takes into account the small scale features due both to sea-land border and mountain chain disturbances.

MSG rainfall estimate have a similar rainfall patterns (Fig. 3.11) with respect to TRMM EOFs: the 1st EOF takes into account the diurnal inland convective activity; the 2nd EOF describes the off shore and coastal precipitation, which is marginally present probably due to the limitation of the available dataset from 3° to 20°N. The 3rd EOF represents small scale features related to the mountain elevation. In this analysis the MSG rain rate original dataset (which has a 0.04° spatial resolution) has been downscaled to 1° of spatial resolution in order to reduce the total amount of data. Thus some heterogeneity is present when compared with the corresponding TRMM EOFs patterns.

MERRA convective signatures, extracted using the vertical velocity *omega* show similar patterns as the TRMM EOFs. In particular, the MERRA-EOF-1 is closer to the TRMM-EOF-1 on the Guinea coast and Sahel region while around 10°N MERRA shows an opposite signature. The second components of MERRA-EOF-2 and TRMM-EOF-2 are significantly similar revealing a good capability of reproducing that spatio-temporal variability. Larger differences where present in the last analyzed component: the MERRA-EOF-3 does not reproduce the TRMM variability probably due to the small resolution of the model configuration and its hydrostatic formulation.

RAMS spatial variability is shown in Fig. 3.13 and Fig. 3.14 for L-RAMS and H-RAMS, respectively, forced with ModSST. The L-RAMS shows broader areas where convection is active. In particular, the first two components seem to described all the inland convection and the active areas downstream the Ethiopian Plateau, but strong limitations appear as to the coastal convection, which is essentially missing. This is probably due to a resolution issue, since the convective systems active along the Guinea coast are sub grid dynamical features with respect to the L-RAMS mesh size. This hypothesis is supported by observing the 2nd and 3rd TRMM EOFs (Fig. 3.10), which show a narrow active band over the Guinea coast and a large active area over the Atlantic ocean. Both type of rainfall patterns are characterized by small convective systems that are not properly reproduced by the L-RAMS.

The H-RAMS, due to its higher spatial resolution reached a higher level reliability over land. The first two components, in Fig. 3.14, are close to the correspondent TRMM EOFs. In particular in land precipitation patterns are similar to those from TRMM. Several spot areas with an opposite anomaly are present downstream of major mountain chain. Again it represents a model resolution related feature related to low level instabilities induced by the interaction of the main easterly flow with mountain chains. It could increase the potential instability of the boundary layer, but this

triggering mechanism may be a numerical artifact. The third EOF takes into account the scattered convective activity due to small scale triggering mechanisms. Note that only the H-RAMS is able to reproduce such a scatter pattern, while large scale models, both MERRA and L-RAMS, do not capture this precipitation feature.

Finally, in Fig. 3.15, Fig. 3.16 and Fig. 3.17 a comparison of different SST forcing effects is shown. As mentioned above, the different SST dataset forcing has a major impact on the total amount of precipitation, while the impact is rather marginal on high frequency variability and in particular on the diurnal cycle. This can be interpreted as an effect of the well known role played by the SST temporal variability on the WAM, which is prominent on the intra – annual modulation of rainfall distribution, but plays a marginal role in the diurnal variability (Giannini et al., 2003). As a result, correspondent EOFs show similar rainfall active patterns. Such evidence is valid analyzing the model results at fixed resolution.

In order to highlight the temporal variability of each EOF pattern of modelling datasets, "*loading*" time series were computed and compared with correspondent series from TRMM (Fig. 3.18, Fig. 3.19 and Fig. 3.20). The MSG rainfall estimate dataset shows a prominent and sharp peak for the 1st EOF comparing to all the other time series (Fig. 3.18). This is probably due to the spatial downscaling that smooths down small signals maintaining only stronger convective signatures, which in turn concentrate the maximum variability extracted by the PCA. The 2nd MSG EOF is delayed of about 3 hours with respect to the TRMM 2nd EOF and this could be a result of differences between the retrieval algorithms used for the different products, but such point needs a deeper investigation. Even though all modelling datasets represent the diurnal cycle quite reasonably, only H-RAMS datasets stay close to the TRMM signatures (Fig. 3.18 and Fig. 3.19). Both late morning convective inhibition minimum and early afternoon convective peak are represented. Differences with TRMM are marginal. Large scale model datasets show similar time variations, but some discrepancies show up. In particular, there is a general increase of the convective inertial response, driven by the more inertial destabilization of the atmospheric boundary layer. As a consequence, convection is triggered later in time with respect to the TRMM signature, the loading time series related to the third EOFs of L-RAMS and MERRA leading the TRMM EOF, while H-RAMS being delayed with respect to the TRMM one. It is a small scale convective systems propagation issue, probably due to the interaction between soil and atmosphere, by means of an incorrect estimate of surface moisture supply coming from surface evaporation, or to an incorrect estimate of destabilization due to downdraft currents within convective systems, which are not represented at those spatial resolution. Finally in Fig. 3.20 3rd EOFs are shown. Main difference are related to the diurnal timing of loading values. TRMM and MSG are close one to the other,

while MERRA and L – RAMS anticipate rainfall signature while H-RAMS simulation show a marked delay. One more discrepancies seems to be strongly related to the horizontal resolution chosen and marginally related to the model numerical schemes used

3.5 Concluding remarks

The analysis presented in this chapter highlights several discussion remarks that are summarized as follows:

- ***Models with low spatial resolution*** (about 50 km of grid mesh size) represent only a portion of the convective signature both in space and in time. The spatial patterns are marked by the footprint of mountain chains and all the boundary layer instabilities are driven by such kind of interactions. Areas where convective activities is inhibited are present both over land and over ocean revealing a common limitation in representing small scale convective systems. Timing is generally delayed with respect to the TRMM signatures, even if a major variability, also in the case of the diurnal cycle, is caught. Delayed rainfall during late afternoon and early night is thus present as a numerical artifact.
- ***H-RAMS with high spatial resolution*** (about 30 km grid mesh size) represents quite well the rainfall spatial patterns and timing. Areas with inhibition of convective activity are still present but limited on a northern band around the 10°-12°N. SST forcing datasets don't have a large impact on diurnal cycle, but ModSST, with its 8-day time resolution represents the best choice.
- ***Qualitative representation of rainfall and convective systems*** propagation is thus well represented by all models, even though the described limitations characterized every choice in the grid mesh size. High resolution, of about 30 km, seems to perform better on every time scale, from diurnal to intra seasonal.
- ***Quantitative representation of rainfall amount*** is better represented by high resolution models. It should be highlighted that in this analysis the precise amount of precipitation associated to the convective systems is not the focal theme of this thesis, while occurrence of convection is well identified and represented. Such characteristics is common to all the analysed datasets in this work, also those coming from satellite estimates such as TRMM and MSG rainfall estimates.

4 Synchronization

4.1 Introduction

A large number of chaotic dynamical systems in nature show rhythmic oscillations when their coupling or their temporal morphology is analyzed (Winfree, 2001, Pikovsky et al., 2001).
Since seminal work on clock phase synchronization done by Christiaan Huygens in "*Horologium oscillatorium sive de motu pendularium*" (1673), such non linear effect of oscillators coupling has highlighted in many fields of science. Several theoretical studies in the 90's (Rosemblum et al, 1996, Pikovsky et al., 2001) expanded the concept related to the synchronization to more generic chaotic dynamical systems and Winfree (2001) extends those concepts to extended systems.
In the framework of dynamical systems theory the stable self-sustained oscillation of an autonomous dissipative system are represented, in the phase space, by its limit cycle that, in turn, is stable. When an external force, acting on the oscillation is introduced, the dynamics changes, and in general the limit cycle does not represent anymore a trajectory in the phase space. Despite this sensitivity, weak or small forces represent a special class of external forcing: in these cases the dynamical behaviour of autonomous dissipative systems could be described in a very universal way. To reach that is it useful to define, for the unforced systems, a phase and an amplitudes coordinate system. The phase represents a measure of motion along the limit cycle, which, by definition, is the direction where neither contraction nor expansion of phase volume occurs. Thus it corresponds to the direction of the zero – Lyapunov exponent (Aurell et al., 1997). Amplitude, which is locally transverse to the cycle, is the orthogonal portion of motion corresponding to the negative Lyapunov exponent. Thus, since no dissipation is present, the motion along the phase variable could be controlled already by a weak perturbation of the external force; a series of weak perturbations of phase will cumulate one to the other. On the other side, a weak perturbation of amplitude, since it is ruled by the negative Lyapunov exponent, will exponentially decay to the stable value (for a complete review see Pikovsky et al, 2000).
In this particular framework, by means of two weakly coupled chaotic oscillators, a measure of their mutual interaction can be expressed through a phase difference of oscillations. Furthermore since hypersurface of constant phase form a "foliation" (Anosov, 2001) of cycle neighbourhood, the

correct phase variable can be extracted using any other cyclic variable by means of a phase – like coordinate obtained through a wide class of transformations of original phase and amplitude.

This characteristic could be clearer taking into account isochrones trajectories. Since the phase of an oscillation can be define as the distance form a fixed point x_0 of a trajectory in the limit circle Υ it is possible to define a phase of oscillation even outside Υ, using the notion of isochrons. Now the phase is depending on space and, when it is possible to define a Poincare Map with the same recurrence period, then the phase space can be redrawn on a sub set of points belonging to different isochrons. Due to the existence of a foliation it is always possible to define a trajectory on the Poincare map and thus extract a phase – like variable.

In a more general view the analysis of fluctuation phase differences among records of different weakly coupled chaotic oscillators could reveal different levels of interaction.

Thus, the phase synchronization of coupled systems is defined as the appearance of certain relation between their phases, while the amplitudes can remain non-correlated. But synchronization is not a coincidence of phases or frequencies of the rhythmic processes! Two uncoupled periodic processes always have a constant frequency ratio, but they are not synchronized at all. Synchronization is a mutual adjustment of rhythms due to some kind of interaction or coupling. The presence of epochs, by means of periods when the instantaneous frequency ratio of non-stationary signals remains stable while the frequencies themselves vary, and the existence of several different epochs within one record count in favour of the conclusion that the observed phenomena are associated with the process of adjustment of rhythms of interacting systems.

Some methods were developed in order to measure fluctuation phase differences in biological systems (Winfree, 2001), population dynamics (Rosemblum et al., 1996; Winfree, 2001), atmospheric variability (Rybski et al, 2003; Maraun and Kurts, 2004), large scale atmospheric patterns and surface temperature over the Europe (Tatli, 2007), ENSO internal variability (Stein et al., 2010), Gulf Stream oscillation variability and NAO phases (Feliks et al., 2011) and Solar cycle and atmospheric variability in the Northern Hemisphere and NAO index (Palus and Novotna, 2011).

For a large number of chaotic systems it can be defined a phase variable $\phi_i(t)=\omega_i t$ for each oscillator and a generalized phase difference $\varphi_{n,m}(t) = n\phi_1(t) - m\phi_2(t)$ between chaotic system *1* and *2*. A stable or bounded phase difference has been reached when:

$$| \varphi_{n,m}(t) - \delta| < const$$

where δ is a finite phase shift and the condition holds even when $\phi_i(t)$, and thus $\varphi_{n,m}(t)$ fluctuates with time.

More general dynamical systems do include a significant noise component. If this noise signal is small and bounded itself, then the dynamical behaviour is close to the case where the noise component is zero. On the other side, when the noise is not bounded, then there is a non – zero probability of having big fluctuations and phase slips are present. To evaluate such kind of systems and related dynamical regimes a distribution analysis is needed to highlight epochs of phase locking. Thus it is introduced a more convenient quantity, the distribution ψ of φ, to highlight phase difference dynamics, especially when "real" system has been taken into account. It is analyzed the statistical distribution of φ in a spatio - temporal domain and measuring dispersion of values of φ *factorized by* 2π:

$$\psi_{n,m} = \varphi_{n,m}(t) mod(2\pi)$$

Thus phase synchronization analysis of two records of length N could be summarized in five sequential steps:

- In the first step, from the scalar signals $\tau_i(t)$, i=1,2, the complex Hilbert transformed signal $\xi_i(t) = \tau_i(t) + i\,\tau_{Hi}(t) = A_i(t)e^{i\phi_i(t)}$ where $\tau_{Hi}(t)$ is the Hilbert transform of $\tau_i(t)$ has been computed *(Gabor,1946)*.
- Then the phases of $\phi_i(t)$ signals is extracted.
- Next it is computed the cumulative phases such that every cycle, or fluctuation in differences, the phases $\phi_i(t)$ increase by 2π.
- Then it is quantify the difference of the phases $\varphi^{12}_{n,m}(t) = n\phi_1(t) - m\phi_2(t)$.
- Finally, it is analyzed the quantity: $\psi_{n,m} = \varphi_{n,m}(t) mod(2\pi)$ for different *n* and *m* values and analyzed it in order to extract the phase difference behaviour.

As an example when no phase synchronization is present the distribution of $\psi_{n,m}$ doesn't exhibit any peak, while in the opposite case a peak is present, revealing a prevalence in the phase difference value distribution.

When distribute system should be analyzed, as in this study, a more convenient measure of phase difference is used. It is the so-called Phase Synchronization Index (Rosenblum et al., 2001) that it will be extensively used in the rest of this Chapter. It is defines as a measure of the phase difference dispersion, averaged over a defined time period:

$$\gamma^{12}_{n,m} = \left|\left\langle \exp\left(i\varphi^{12}_{n,m}(t)\right)\right\rangle_t\right| = \sqrt{\left\langle \cos\varphi^{12}_{n,m}(t)\right\rangle_t^2 + \left\langle \sin\varphi^{12}_{n,m}(t)\right\rangle_t^2} \qquad \text{eq.1}$$

When a prevalent dynamical regime is present, the $\varphi_{n,m}$ values will be compact and coherent thus it is highlighted by Υ values far from *0* and close to *1*. When Υ is equal to *1* a perfect synchronisation is reached. The <...> operation, which stands for a computed average, is essentially subjective and performed in a spatio - temporal domain.

The synchronisation between two signals can be highlighted and then measured by a sequence of measures. The first step is computing the standard deviation σ of the instantaneous phase difference between the two time series,

$$\sigma^2 = \langle (d(t) - \langle d(t) \rangle)^2 \rangle \quad eq.\ 2$$

The standard deviation provides a measure of the phase difference dispersion in a statistical sense. In order to provide a general overview, it is useful spatially identify areas of potential synchronization. A second step is provided by the measure of correlation $cor(A_1, A_2)$ between the instantaneous signal amplitudes:

$$corr(A_1, A_2) = \frac{\langle A_1 A_2 \rangle}{\sqrt{\langle A_1 \rangle \langle A_2 \rangle}}$$

where $\langle \diamond \rangle$ denotes average over time. As previously highlighted, weak perturbation on the limit cycle can persist, without damping in system without noise, and smoothly decay in system with noise. But phase synchronization do not imply any changes in the signals amplitudes.

To classify different interacting systems according to their capability of synchronize their rhythms here some rules, following Osipov et al. (2003) and summarised in Feliks et al. (2010), in order to identify three types of synchronisation in chaotic time series, labelled as follows:

1) synchronisation of the frequencies alone: *frequency locking* (FL),

$$0.5 = \sigma_0 < \sigma < \infty;$$

2) synchronisation of the phases as well: *phase locking* (PL)

$$\sigma < \sigma_0 = 0.5;$$

3) complete synchronisation (CS), including both phases and amplitudes, so that:

$$\mathrm{corr}(A_1, A_2) \approx 1.$$

From the analysis of chaotic systems FL does not implies PL and, as described in Rosenblum et al., (1996). In general by increasing the coupling strength the synchronisation degree increases as well

from FL to PL and CS. Thus in the most simple degree is when σ is bounded, while the phase locking appears when such bound is small. In this case a narrow distribution of possible phase difference values is observed. The complete synchronization emerges when both phase difference is small and amplitude correlation, between signals, is close to 1.

The synchronisation transition and occurrence of epochs with a clear signature of phase locking is far to be unambiguous since the presence of noise can change the topology of foliation around the isochronous hypersurface. Thus selecting the Poincare secant, in order to extract the phase dynamic, is not obvious and direct even if the physical mechanism knowledge can identify some more convenient choices.

In the rest of this work it will be analysed only the phase locking mechanism among several indices summarizing the occurrence of convective precipitation in the WAM area and in the warm season and for the case of $m = n = 1$.

4.2 Definition of the physical system

As mentioned in the Abstract the aim of this work is to highlight an internal coherent mechanism in the framework of WAM and in particular its convective precipitation dynamical footprint, initialisation factors, propagation features on the diurnal time scale. Many authors have study these convective precipitation features as described in the introduction, but a few have taken into account internal high frequency rhythms of the monsoon. In order to analyse the spatio temporal behaviour and in particular the emergence of a phase locking appearance several remarks must be taken into account:

- It is analysed the occurrence of convective precipitation over the WAM area, during the warm season June – July – August, with respect to the convective boundary layer destabilization at local scale due to latent heat release via evaporation of soil moisture. It is a partial view of the occurrence of the mechanism, but according to several authors (Koster et al, 2004 and Taylor et al, 2011a) not only this component is responsible of a strong coupling between land and atmosphere in the water cycle, by more specific it is the spatial patterns of soil moisture which drive propagation of convective systems in the WAM area.
- In order to summarise al the other effects, in convection spatio temporal occurrence, and in particular in order to take into account the large scale dynamical factors, such as African easterly waves, atmospheric moisture supply from the Guinea Gulf, it is analysed the Vertical Integrated Moisture Transport (VIMT) vector which is described before in Chapter 2.

- The numerical modelling strategy described in the Chapter 3 has been applied in order to provide a coherent description of physical mechanisms. Since it is analysed only a qualitative description by means the occurrence of convective systems and no information on precipitation amount has been taking into account, natural biases on numerical models and related errors should be consistently limited.
- From a pure mathematical point of view the grid point description, provided by numerical models, is a natural way to "discretise" numerical analysis on that spatial scale (a specific grid mesh dimension: 50km and 30km for RAMS model, around 67km for MERRA dataset). Thus a natural assumption follows: each grid points are considered as a single realization of a non-linear dynamical system. Grid time series of indices are analysed separately, even if the spatial coherence, due to the large-scale dynamics is present. This assumption needs further analysis, but it is reasonable since the very high frequency variability analysis performed: 1 hour for RAMS model and 3 hours for MERRA dataset. To support this last assumption, in Melani et al., 2010, which is only partly reported in the Chapter 2, it is shown (Table.2) that for propagating convective systems displacement characteristics are: *mean duration = 14.1 hours* and *mean span = 751 km*. Thus in one hour these systems have a span of about 50km, which is of the same order of magnitude of grid mesh size for both RAMS and MERRA datasets. This means that for the high frequency variability analysed in term of synchronization convection indices even the fast moving system are localized in the area cover by a grid point or a few adjacent grid points.
- The only external forcing taken into account is the solar radiation, but it is analysed through its effects on latent heat release. In this sense latent heat, as unique external forcing, is bounded by the total amount of soil moisture of the active surface layer. This assumption guaranties a more confident choice of the transverse Poincare section to the limit cycle.
- The shown analysis on temporal occurrence of convective precipitation (Chapter 2) reveals a natural choice for timing and Poincare transverse section: the physical time axis and its diurnal cycle. This choice implies that also derivates of indices time series can be analysed in terms of emergence of synchronization.

4.3 Evidence of a synchronization footprint

In order to highlight possible mechanisms of synchronization correlation standard deviation and PSI between signals have been computed over the study area. Rainfall, VIMT, latent heat surface fluxes were selected as potential signatures of phase difference adjustment due to interaction. Each grid

point time series of the previous atmospheric fields, both from RAMS dataset and MERRA dataset, could be represented as a realization of a dynamical system trajectory.
Thus each of them is characterized by a phase dynamics, which can be extracted using the Hilbert transform as described previously. Standard deviation of phase difference is then computed for all grid point of the study domain for each single year period revealing patterns of possible synchronization activity.
Original data coming from different model simulations have been analyzed on a grid point base for the full period: warm season (JJA) from 2004 to 2008 included. For each signal grid point time series the first order time derivate has been computed and then transformed according to the Hilbert operator. Finally the unwrapped phase difference has been computed for each simulation time step. To measure the synchronization between signals the mean Phase Syncrhonization Index is used, defined in *eq. 1*. Thus simplicity only a selection of more significant graphs are shown in this Chapter.

4.3.1 Phase difference dispersion analysis

A first step for determining if a synchronization between two dynamical systems can emerge from the background variability is to measure the phase difference dispersion. Following the check list from Feliks et al., (2010) the phase difference variance has been computed and are shown in Fig. 4.1 and Fig. 4.2 for MERRA dataset while in Fig. 4.3 and Fig. 4.4 are shown results from the high resolution simulation of RAMS forced by the ModSST dataset (H-RAMS with ModSST). The MERRA global simulation shown a quite homogeneous phase difference variance fields for all the signals analyzed. Values ranged from 0.1 to 0.3 aver the entire WAM area. A remarkable level of 0.3 is present over the more convective active WAM area. Since values are bounded and well below of the reference threshold of 0.5, the phase difference dispersion can be identified as compatible with a phase locking synchronization.

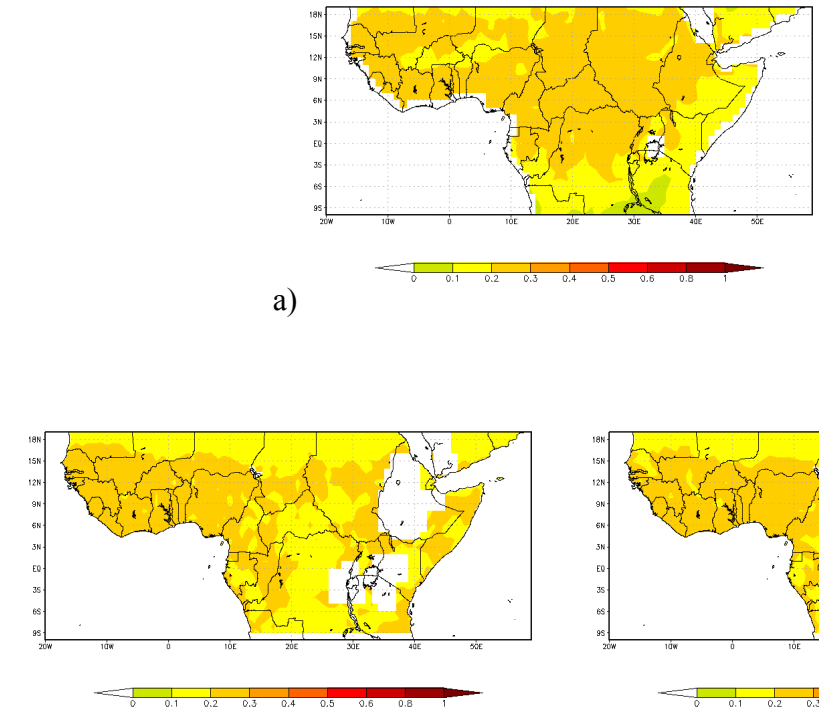

Fig. 4.1: Phase difference variance from MERRA dataset JJA 2004 – 2008 period: a) precipitation rate and latent heat flux; b) precipitation rate and vertical integrated moisture transport zonal component (vimtx); c) precipitation rate and vertical integrated moisture transport meridional component (vimty).

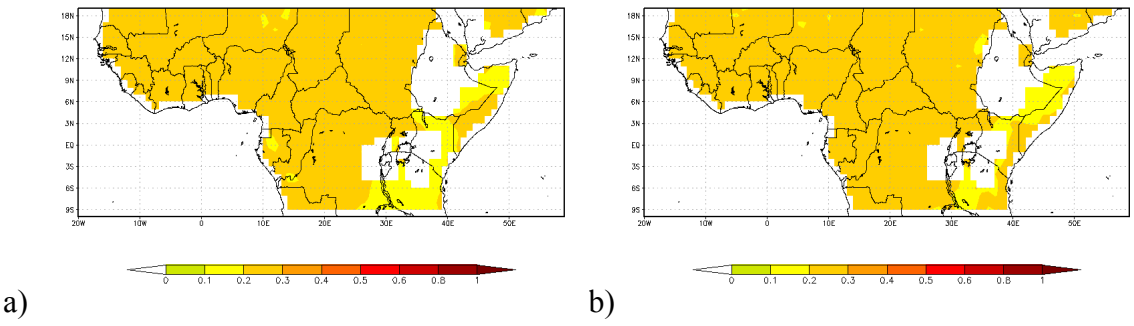

Fig. 4.2: Phase difference variance from MERRA dataset JJA 2004 – 2008 period: a) latent heat flux and vertical integrated moisture transport zonal component (vimtx); b) latent heat flux and vertical integrated moisture transport meridional component (vimty).

RAMS simulation results shown in Fig. 4.3 and Fig. 4.4 reveal a similar behaviour: a wide and homogeneous phase variance field with bounded value everywhere in the domain and well below the reference threshold of 0.5.

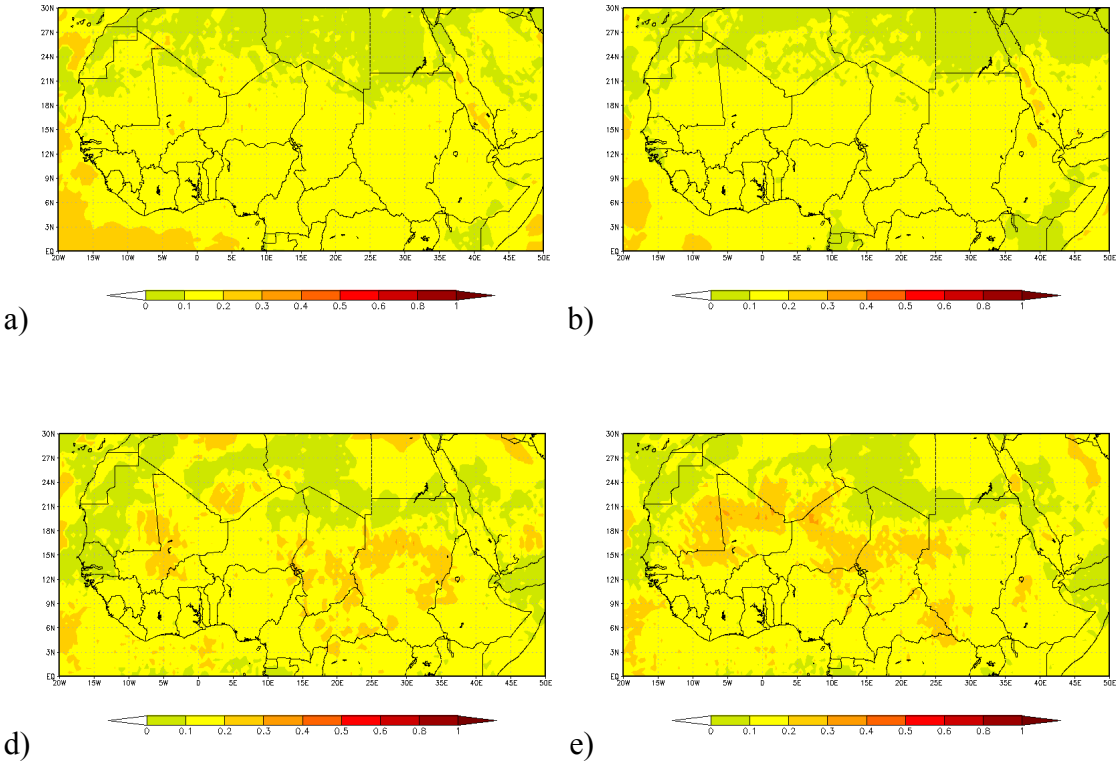

Fig. 4.3: Phase difference variance from H-RAMS (ModSST) dataset JJA 2004 – 2008 period: a) precipitation rate and latent heat flux; b) precipitation rate and sensible heat flux; c) precipitation rate and vertical integrated moisture transport zonal component (vimtx); d) precipitation rate and vertical integrated moisture transport meridional component (vimty).

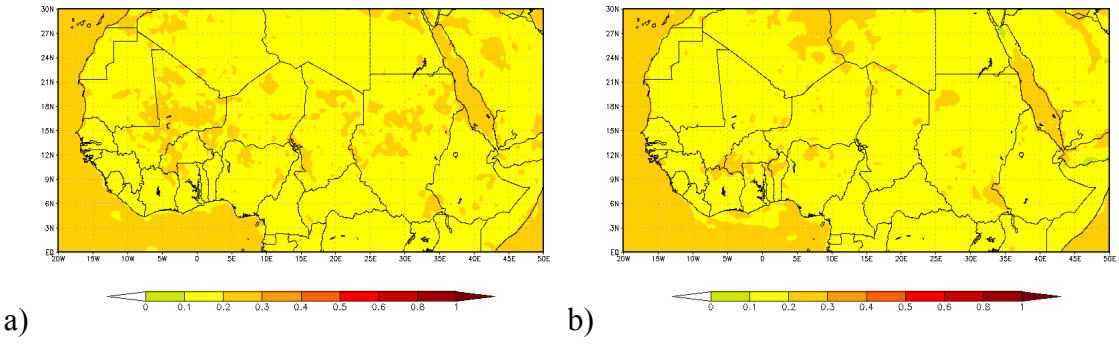

Fig. 4.4: Phase difference variance from H-RAMS (ModSST) dataset JJA 2004 – 2008 period: a) latent heat flux and vertical integrated moisture transport zonal component (vimtx); b) latent heat flux and vertical integrated moisture transport meridional component (vimty).

Availability of latent heat flux over the sea surface in RAMS provides a comparison of phase difference variance over land and ocean which are both homogeneous, but different in values, with some spot areas over land where σ is higher and similar to the ocean values. Furthermore there are

no differences between VIMT components revealing any particular preferred direction in the mechanism.

4.3.2 Phase difference correlation analysis

Phase difference correlation is deeply related to the interaction coupling strength between individual signals. As mention at the beginning of the present chapter higher values of correlation, in presence of synchronization, means the so called "complete" synchronization. In Fig. 4.5 and Fig. 4.6 correlation values for the MERRA global dataset. For the precipitation – latent heat pair, correlation values are close to zero along the Guinea Gulf and a wide belt inland. Outside this belt values are moderate in the range of 0.3 to 0.7 in the Sahelian region. While are almost close to zero for precipitation – VIMT (both x and y components) and latent heat – VIMT pairs. This confirms the natural interpretation that the latent heat release variability far from the coast is due the occurrence of rainfall as shown in Tremberth (1999) for the intensity of hydrological cycle and the so called "recycling" fraction in Africa during the JJA season (see fig. 6 and fig.8 in Trenberth, 1999).

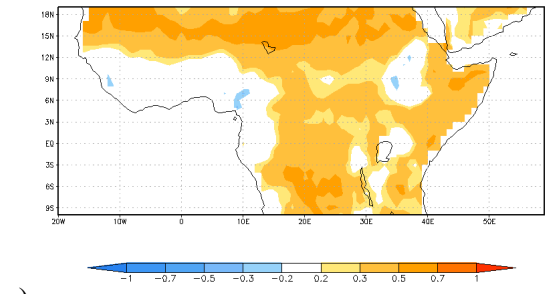

a)

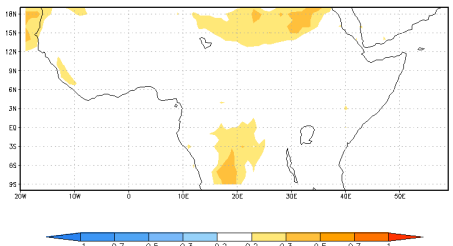

b)

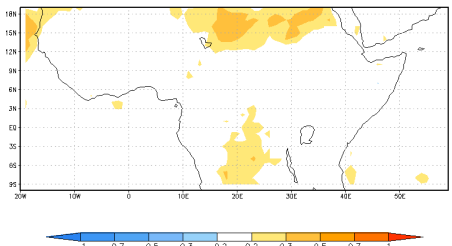

c)

Fig. 4.5: Amplitude correlation from MERRA dataset JJA 2004 – 2008 period: a) precipitation rate and latent heat flux; b) precipitation rate and vertical integrated moisture transport zonal component (vimtx); c) precipitation rate and vertical integrated moisture transport meridional component (vimty).

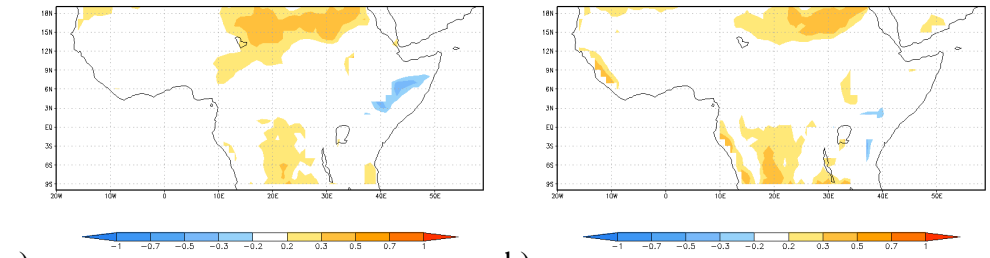

a) b)

Fig. 4.6: Amplitude correlation from MERRA dataset JJA 2004 – 2008 period: a) latent heat flux and vertical integrated moisture transport zonal component (vimtx); b) latent heat flux and vertical integrated moisture transport meridional component (vimty).

On the other side correlation strength between latent heat flux and VIMT components is very weak and similar to that for rainfall only in area far from Ocean as the southern part of Sudan and Egypt (Fig. 4.6).

A similar behaviour is found for the high resolution simulation from RAMS. Rainfall and latent heat shown a moderate to strong coupling in the Sahel and Central Africa (Fig. 4.7 a). Over the same area, but far from the Guinea Coast a moderate coupling is present between rainfall and VIMT (Fig. 4.7 c and d). It is a wider and stronger footprint with respect to the same coupling shown by the MERRA global dataset. This could be explained with the more detailed description of flux exchanges provided by RAMS model by means of a higher spatial resolution (both horizontal and vertical) and a more detailed land – atmosphere model (Walko et al, 2000). Probably the VIMT flux described by MERRA dataset, being more smoothed, is less influenced, by local modulation and thus reveals a weaker interaction.

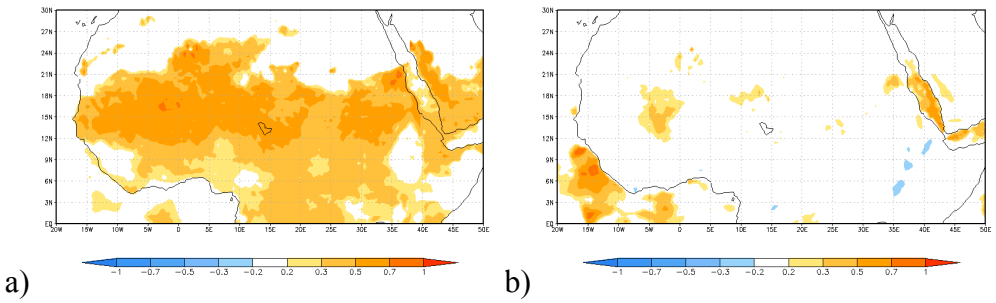

a) b)

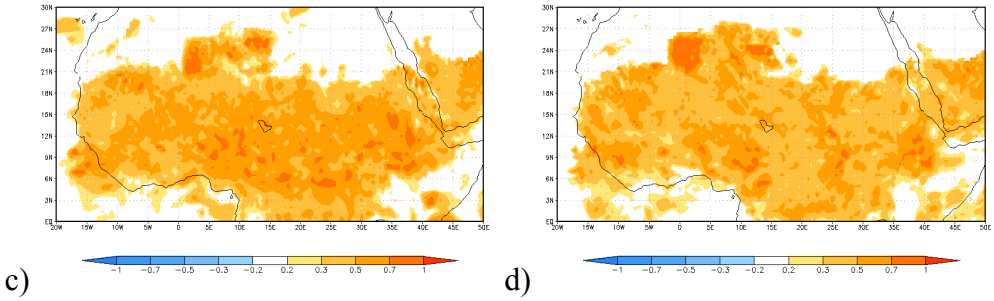

c) d)

Fig. 4.7: Amplitude correlation from H-RAMS (ModSST) dataset JJA 2004 – 2008 period: a) precipitation rate and latent heat flux; b) precipitation rate and sensible heat flux; c) precipitation rate and vertical integrated moisture transport zonal component (vimtx); d) precipitation rate and vertical integrated moisture transport meridional component (vimty).

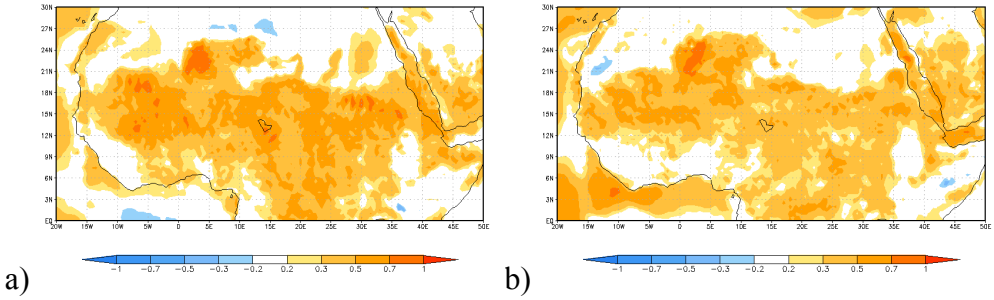

a) b)

Fig. 4.8: Amplitude correlation from H-RAMS (ModSST) dataset JJA 2004 – 2008 period: a) latent heat flux and vertical integrated moisture transport zonal component (vimtx); b) latent heat flux and vertical integrated moisture transport meridional component (vimty).

A special comment is needed fro the correlation pattern shown in Fig. 4.7b between precipitation and sensible heat flux. In particular it is evident how the areas over Guinea Gulf are more active and coupling is strong. This particular area has identified in Vizy and Cook (2001) as one of the more sensitive sea surface areas modulating monsoon rainfall in the Central Africa and West Africa.

4.3.3 Mean Phase Synchronization Index analysis

Highlighting the emergence of a coherent dynamics that could lead to a synchronization appearance is done by computing the mean PSI. For each fields pairs analyzed the phase difference is used to compute PSI averaged over a daily time window. This is a natural choice of time scale variability as supported by spectral analysis of precipitation (Chapter 2) and principal component analysis shown in Chapter 3. These time step values are finally averaging the mean PSI values for each grid points for the entire period available. Results for all fields pairs analysis are shown in Fig. 4.9 and Fig. 4.10 for MERRA dataset and in Fig. 4.11 and Fig. 4.12 for H-RAMS forced by ModSST. Synchronization between precipitation and latent heat flux is present and homogeneous on a wide area covering the Guinea coast Sahel belt Central Africa, Ethiopian Plateau and part of East African Horn Fig. 4.9(a). In this area values ranges from 0.45 to 0.9 maxima located in Sahel Central Africa Ethiopian Plateau and part of East African Horn. Compactness of mean PSI highest values, for example in the west Sahel region can be interpreted as a measure of spatio – temporal coherence and thus the internal coherence of dynamics linking latent heat and rainfall at local scale and for very high time frequency. Synchronization strength is weaker when precipitation filed is analyzed with respect to both components of VIMT (Fig. 4.9 b – c).

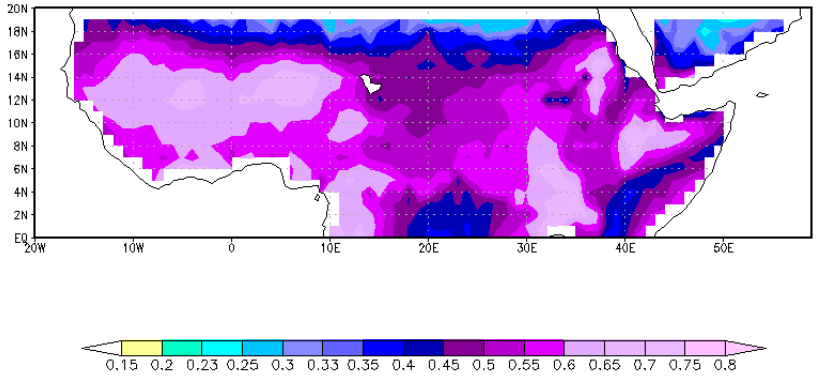

a)

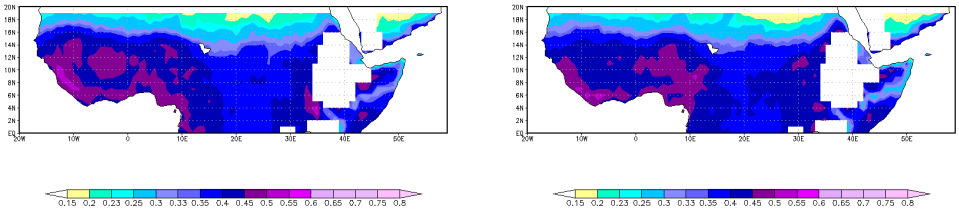

b) c)

Fig. 4.9: Mean PSI from MERRA dataset JJA 2004 – 2008 period: a) precipitation rate and latent heat flux; b) precipitation rate and vertical integrated moisture transport zonal component (vimtx); c) precipitation rate and vertical integrated moisture transport meridional component (vimty).

Mean PSI values are lower and the spatial distribution of maxima is concentrated on a narrow belt along the Guinea coast, with some more active areas over the west Africa: in Mali, Niger Mauritania. Patterns differ from meridional and zonal component of VIMT, being the latter stronger in Mali and weaken in Niger and Chad, while the opposite is true for the zonal component. Synchronization between latent heat flux and both component of VIMT is shown in Fig. 4.10. A wide area of values above the 0.5 threshold is present and pattern has a latitudinal structure. An area with minima is present in Central Africa, probably due to the presence of forests, which modulate solar radiation at the surface and then latent heat. There is a sharp drop of mean PSI around 20°North. This is the northern most latitudinal edge of VIMT transport. Thus the drop should be connected to the extremely reduction of transported moisture in the boundary layer and the intermittency of such flux.

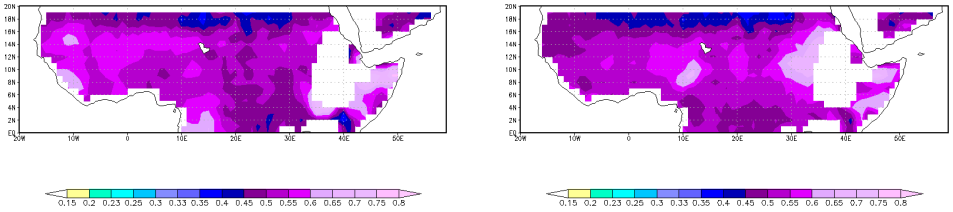

a) b)

Fig. 4.10: Mean PSI from MERRA dataset JJA 2004 – 2008 period: a) latent heat flux and vertical integrated moisture transport zonal component (vimtx); b) latent heat flux and vertical integrated moisture transport meridional component (vimty).

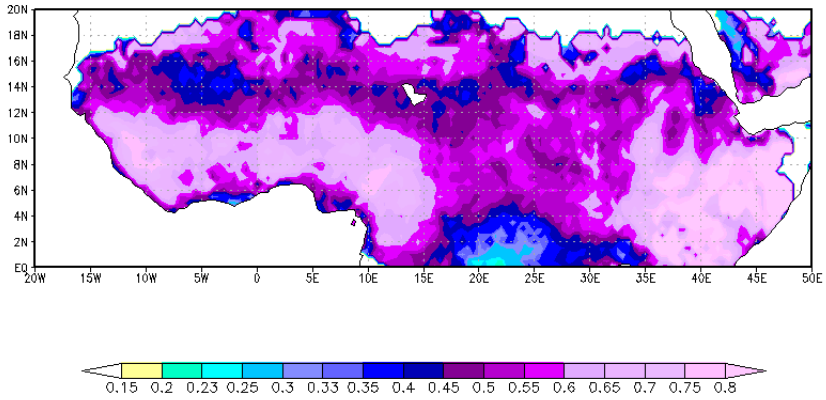

a)

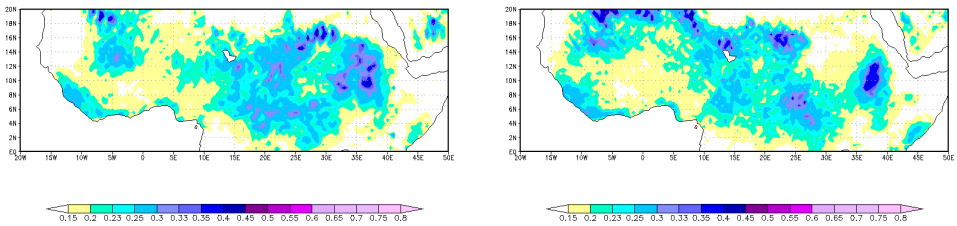

b) c)

Fig. 4.11: Mean PSI from H-RAMS (ModSST) dataset JJA 2004 – 2008 period: a) precipitation rate and latent heat flux; b) precipitation rate and vertical integrated moisture transport zonal component (vimtx); c) precipitation rate and vertical integrated moisture transport meridional component (vimty).

H-RAMS simulations provide a similar overview of synchronization with respect to the MERRA global datasets, but several sizeable differences are present. In Fig. 4.11 (a) mean PSI between precipitation and latent heat flux is shown. High values of mean PSI are present over a wide area

that is almost similar to the correspondent MERRA one. Within this pattern of synchronized dynamics, values are higher with respect to MERRA mean PSI with a narrow transition belt from moderate values to maximum values. Now the high values pattern is divided in two region by a narrow latitudinal trough around between 14°N and 15°N crossing, with some small heterogeneities, the entire African continent from Indian Ocean to Atlantic Ocean. Darfur mountain chain, located approximately around 25° E and 15°N seems to play a role in determining downstream to the prevalent easterly air flows a reduction of mean PSI values in the region between Chad, Niger and Mali. Mean PSI between precipitation and both components of VIMT is shown in Fig. 4.11 (b – c). As in MERRA simulations precipitation mean PSI values are smaller with respect to mean PSI values of latent heat. H-RAMS regional simulation provide a different view: VIMT meridional component moderate values of mean PSI are localized on a narrow belt along the Guinea coast, between 5°E and the Ethiopian plateau. A wide area of very small values is preset between Nigeria, Niger and Mali. It is something that MERRA simulations also shown, but less evident. Such discrepancy in the mean PSI values is likely linked to the coarser dynamical representation provided by MERRA model system, which smooth out boundaries of different region.

Probably surface wind pattern are responsible for a weaker development of synchronization, but this point needs a deeper and specific analysis.

Finally the mean PSI pattern computed from latent heat flux and VIMT components is show in Fig. 4.12. Once more the H-RAMS finer grid spacing provides a spatial pattern with a higher level of fine scale features. But analyzing broader areas many similarities came out from the comparison with MERRA global simulation. Broader areas in the West part of sub Saharan Africa, an elongated belt over the Sahel to 20°E, a broad area over the East Africa Horn due to the extremely moist flux coming from the Indian Ocean. But H – RAMS provides a dual belt latitudinal structure in West Africa for higher values. As for the mean PSI from precipitation and latent heat flux, there is a long belt starting from the Hoggar mountain chain to the Atlantic Ocean for the VIMT zonal component (Fig. 4.12 a). VIMT meridional component synchronization shows a belt inland in the West Africa of moderate values. The East Africa Horn shows very high mean PSI values again due to moisture rich air flow coming from Indian Ocean. There is an area in the northern east portion of the maps in Fig. 4.12 which shows values above 0.5. It is located between 20°E and 40°E and between 18°N and 20° (even if it extends further to the North, up to 21°N, not shown) which represents one of the final propagation path of moisture air coming from the Mediterranean Sea (Rowell 2003, Gaetani et al., 2010, Fontain et al., 2011).

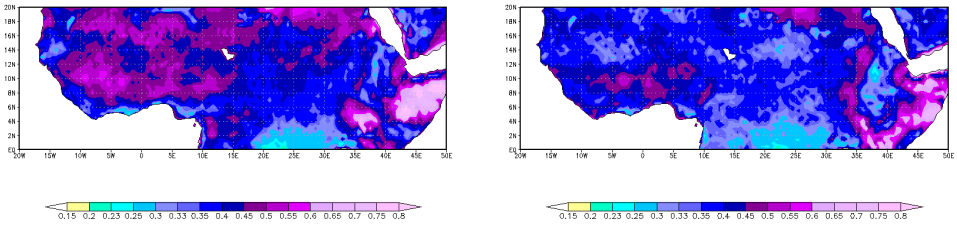

a) b)

Fig. 4.12: Mean PSI from H-RAMS (ModSST) dataset JJA 2004 – 2008 period: a) latent heat flux and vertical integrated moisture transport zonal component (vimtx); b) latent heat flux and vertical integrated moisture transport meridional component (vimty).

4.4 Long distance interaction synchronization between WAHL and WAM

4.4.1 The West African Heat Low pressure system - WAHL

One of the major dynamical components of the WAM system is represented by a semi – permanent pressure system generated and maintained by extremely high temperatures and low pressure over the western part of sub tropical Africa continent. It is referred to as the Saharan heat low or West Africa heat low (WAHL). Impacts of WAHL in the WAM dynamics are both in the lower part of troposphere and in the upper part. Near the surface WAHL eastern flank tents to increase the northern progression of ITCZ in Senegal, Mali and Niger (Parker et al. 2005c); while above the boundary layer it generates an anticyclonic circulation which is responsible in a strengthen and accelerating the African Easterly Jet (Thorncroft and Blackburn 1999). A number of recent papers provide new analysis of WAHL dynamics and specific features thanks to the AMMA project and a series of special observing periods experiments. In particular Lavaysse et al, (2009) analyzed its dynamical behaviour of WAHL and its seasonal evolution while Chauvin et al. (2010) highlighted its role as a "bridge" between the midlatitudes and WAM. WAHL shown two distinctive phases named *west* and *east*. These modes are due to the corresponding maximum (minimum) of temperature over Morocco – Mauritania and a minimum (maximum) temperature over Lybia – Sicilia. Such distinctive phases are preceded by large scale intra seasonal fluctuation in the North Atlantic and Europe sectors, while *west* phase is concomitant with enhanced precipitation in Darfur region (Chauvin et al., 2010). As shown in Lavaysse et al. (2009) the 850-hPa potential temperature field, being related to the thickness of boundary layer over Sahara was selected to represent the

WAHL. Taking an areal average between 10°W and 5°E and from 21°N to 27°N of potential temperature at 850hPa, from both MERRA and RAMS simulations, an index has been computed (Fig. 4.13) on a daily timescale. Then the 1-D index is analysed in relation to every domain grid points for MERRA and RAMS.

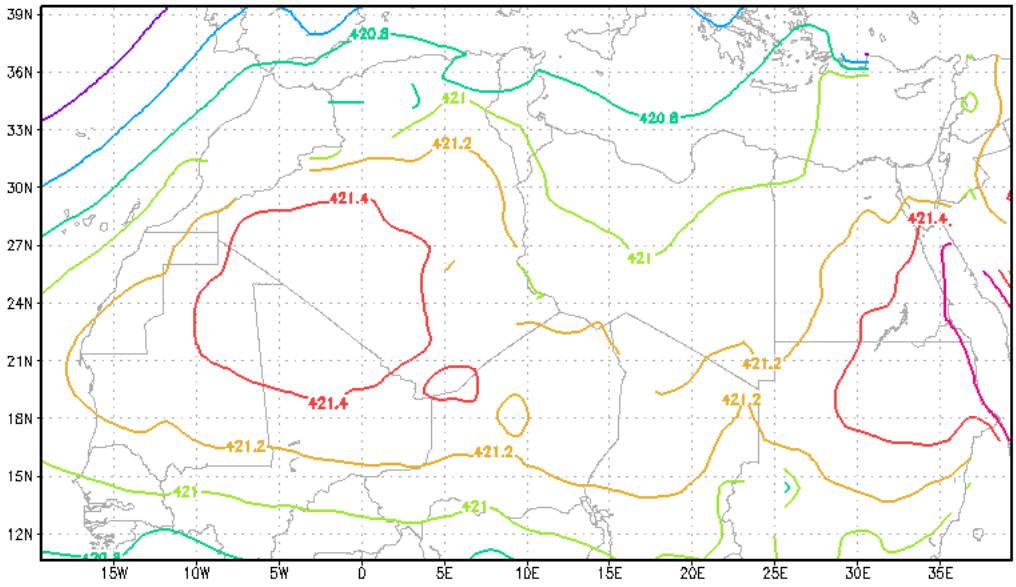

a)

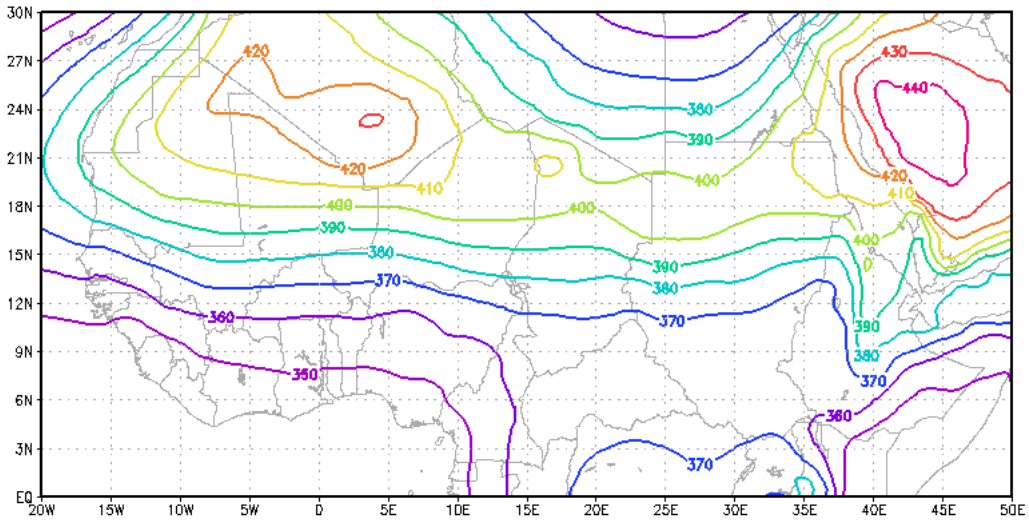

b)

Fig. 4.13: Potential temperature, at 850hPa, mean field from MERRA (a) and H - RAMS simulations: JJA 2004 - 2008

4.4.2 Interaction between WAM and WAHL measure by synchronization

Interaction between WAM and midlatitudes atmospheric variability is analyzed by means of emergence of sync between high frequency rainfall variability, latent heat flux and sensible heat flux and WAHL temporal variability described by the previously described index.

Impact of WAHL variability in the large scale atmospheric dynamics in summer on Europe and the North Atlantic sector, is deeply described in Lavaysse et al. (2009). In that study clearly emerges a possible role of WAHL as a "link" or an atmospheric bridge between North Atlantic sector and Europe in modulating WAHL phases on intraseasonal timescale. Thus it seems natural taking into account the WAHL variability using the approach proposed in this study: measure the sync emergence and its strength between physical mechanisms. Convective footprint is primary responsible of a synchronization emergence related to the WAHL variability. A convective occurrence increase of variance on a scale of 2-6 days, a convective outburst, is shown to precede AEWs developments downstream to specific areas such as Darfur mountains and Ethiopian highlands (Mekonnen at al., 2006, Fig.4b). As then described in Kiladis et al. (2006) and Thorncroft et al. (2008) convection in these areas, such as Darfur, plays a key role in triggering and modulating AEWs and thus rainfall distribution downstream of mountain ridges to the Atlantic coast.

Following the previous presentation scheme the mean PSI between computed variables is provided for different modelling datasets.

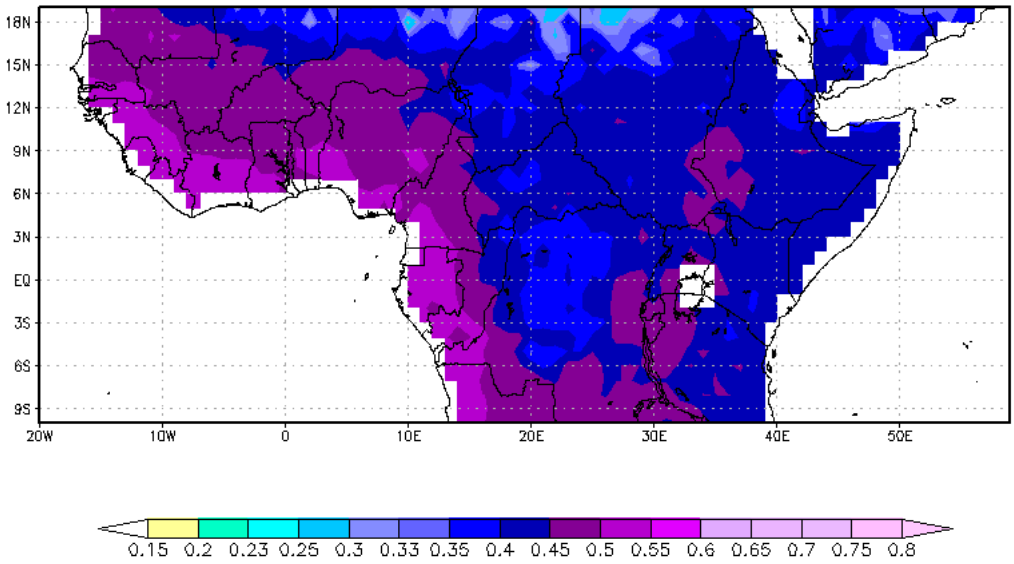

a)

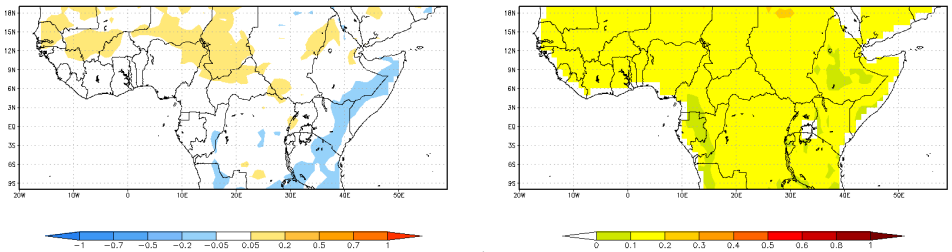

b) c)

Fig. 4.14: Synchronization footprint for MERRA dataset in JJA2004 – 2008 period for WAHL index and land latent heat flux: a) mean PSI values, b) phase difference variance, c) amplitude correlation.

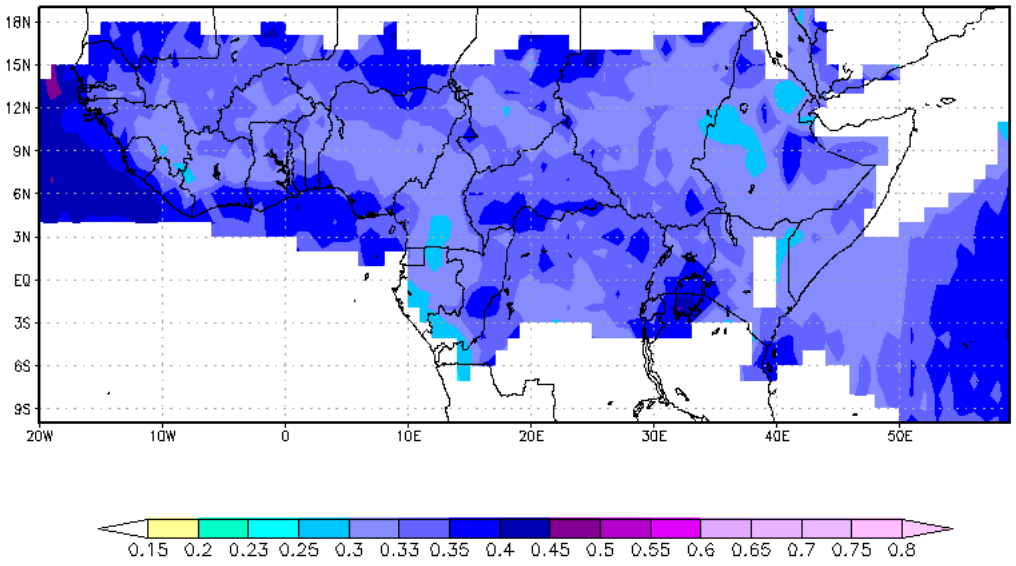

a)

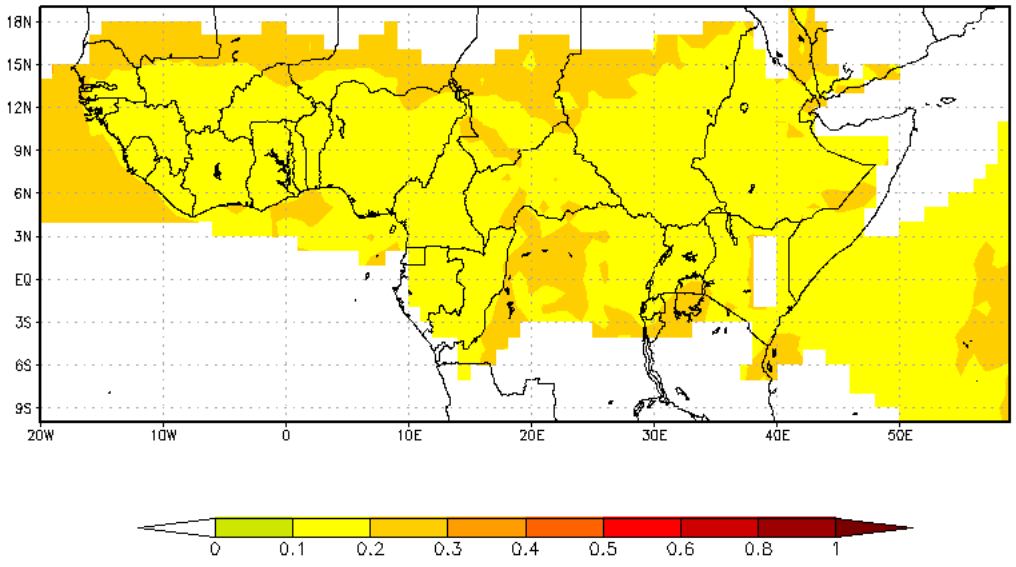

b)

Fig. 4.15: Synchronization footprint for MERRA dataset in JJA2004 – 2008 period for WAHL index and rainfall: a) mean PSI values, b) phase difference variance.

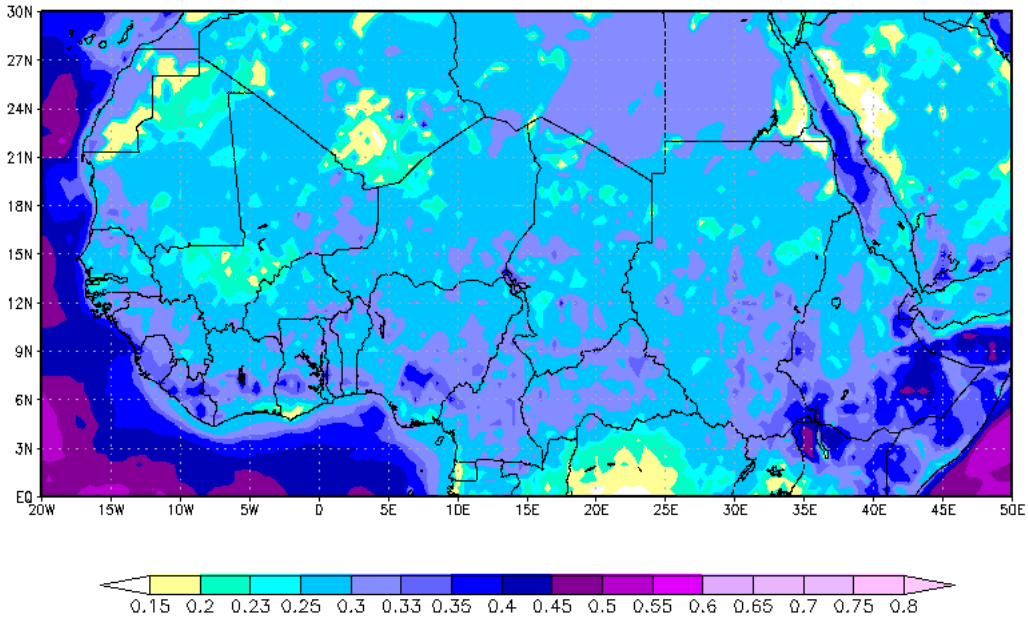

a)

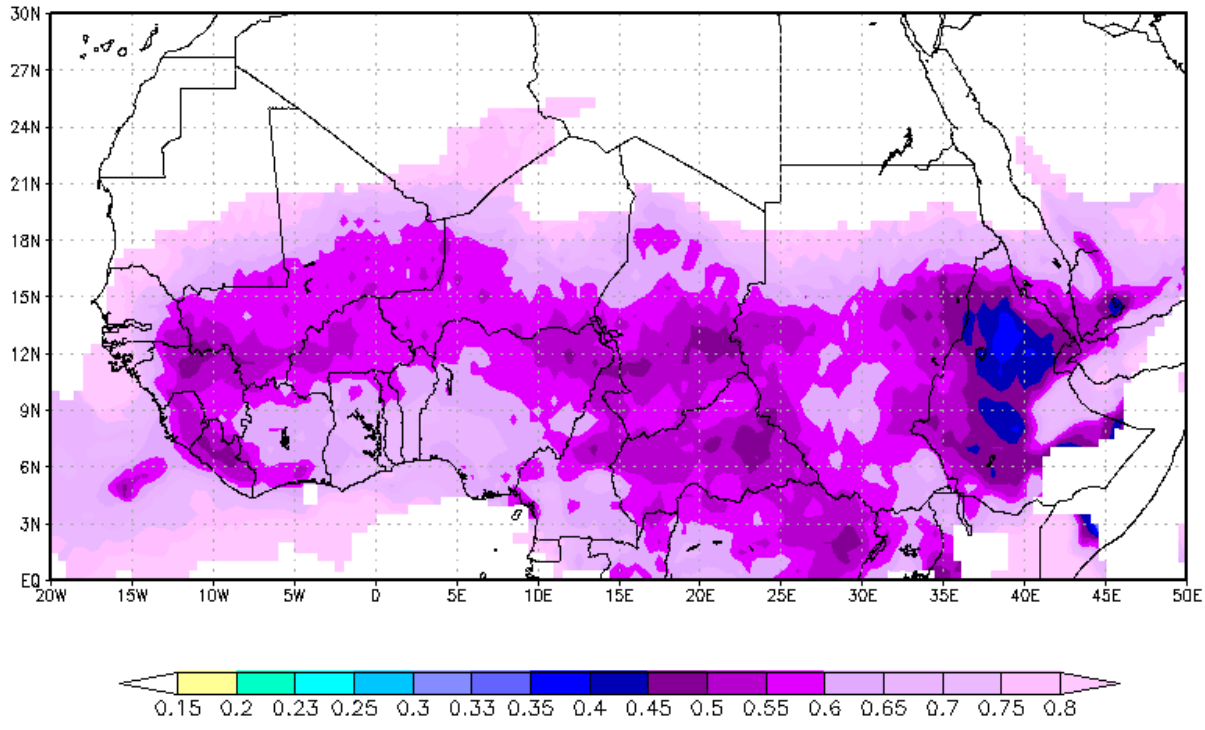

b)

Fig. 4.16: Mean PSI from H-RAMS (ModSST) fields values (JJA 2004 – 2008 period), computed against the WAHL index: a) latent heat flux; b) rainfall.

In MERRA dataset (Fig. 4.14 and Fig. 4.15) phase difference variances between WAHL and both latent heat flux and rainfall are bounded and correlation amplitude is weak. Rainfall correlation maps (Fig. 4.14 c) provides a pattern reveling a potential maxima ridge around 10°N. But since this amplitude is very weak this information should be taken carefully. Nevertheless it is similar to the pattern shown in Mekonnen et al., (2006) - Fig.4b where the variance of convective activity is represented. Mean PSI values show moderate sync signature a wide belt along the Guinea Gulf for latent heat flux (Fig. 4.14 a). A weaker signature is present for rainfall (Fig. 4.15 a), again along the coast but also inland over the Sahel area. Synchronization signature appears even if it seems due to convective boundary layer forcing instead of rainfall by itself. It should be noted that MERRA simulation system is not able to identify singular convective systems propagating westward, due to its low spatial resolution and simplified atmospheric dynamics representation with respect to regional numerical models.

Also in H-RAMS dataset phase difference variances between WAHL and both latent heat flux and rainfall are bounded and correlation amplitude is homogeneous and weak (about 0.2 homogeneously distributed on the domain, not shown here). Mean PSI maps show, respectively in Fig. 4.16 (a-b), a weak high values signature for latent heat flux and a strong signature for rainfall. Thus a phase locking signature is present and it is strong related to convective systems, while the latent heat flux, by means convective system triggering mechanism seems to have a weaker role in synchronization with WAHL. To highlight main features of synchronization, only grid points with an associated average seasonal precipitation above the 10mm have been drawn. There is a wide belt, from 3°N to 12°N Fig. 4.16 (b) where the rainfall footprint shows a synchronization signature with WAHL daily variability. This belt has some peaks located downstream mountain chains and along the Guinea coast. On the western side, this belt extents over the Atlantic Ocean. The footprint reveals a second belt located above 18°N in the sub Saharan region. Since the synchronization is related to occurrence of rainfall, no matter how frequent it happens. Even with the seasonal precipitation threshold imposed (10mm), this second high mean PSI values is related to the very rare precipitation systems that sometimes can be triggered downstream Hoggar mountains.

5 CONCLUDING REMARKS

As described in the Chapter 1, WAM rainfall diurnal cycle has been analyzed extensively in a series of papers trying to highlight its characteristics dynamical time scales, local and remote forcing and interactions with other physical mechanisms. One of its major features is a clear precipitation phase locking footprint during the active phased of the monsoon in the wet season. Soil moisture pattern has been identified to play a key role in the strong interaction between soil and atomosphere over the West Africa (Koster et al., 2004). In particular development and maintenance of convection systems, and their propagation, is found to be crucially linked to boundary layer convective instabilities modulated by soil moisture patterns (Taylor et al, 2011a,b). These evidences are now supported by modelling and observation study, but a "unified description" of the link between small scale and large scale dynamic behaviour still lacks. A gap thus exists between the dynamics of the single convective systems and the monsoon behaviour at sub - continental scale. The present study aims at providing a contribution to fill this gap by investigating African monsoon large scale convective dynamics and, in particular, some characteristics of the rainfall diurnal cycle through an exploration of the hypothesis behind the mechanisms of a monsoon phenomenon as an emergence of a collective dynamics of many propagating convective systems. Such hypothesis is based on the existence of an internal self – regulation mechanism among the various components. Should be noticed that in order to achieve a potential reliable representation of the whole physical monsoonal mechanism a series of needs must be addressed:

- a high spatio – temporal resolution quantitative analysis of convective occurrence over a wide region;
- a high spatio – temporal resolution quantitative and reliable representation of most of active physical mechanisms, including soil, vegetation, atmosphere and microphysical characteristics of clouds;
- a synchronous and possible long representations of above mentioned issues;
- a robust dynamical theory able to merge this large amount of information into a few representative elements.

To achieve these results a possible approach is represented by a multiple analysis shown here and based on remotely sensed rainfall dataset, and global and regional modeling data for a period of 5 June-July-August seasons: 2004 - 2008. Satellite rainfall data and convective occurrence variability were studied for assessing typical spatio – temporal signatures and characteristics with an emphasis

to the diurnal cycle footprint. Analysis on rainfall satellite estimation shown in Chapter 2 have been published, on Atmospheric Research journal, in Melani et al. (2010).

Numerical modeling reanalysis datasets were developed in order to provide that physical coherence needed and then to extract evidence of mutual interactions between the different components: soil dynamics, atmospheric variability, and convective occurrence footprint. Since every numerical system has a limited capability of representing the real world mechanisms, two completely different numerical representations of the WAM are analyzed: MERRA global model and RAMS datasets with different grid spacing, specifically developed for this thesis. This multiple representation should reduce possible purely numerical effects.
The reanalysis strategy developed in this study and its convection occurrence representation shown a good level reliability. In section 3.2 and 3.3 standard measures of quantitative precipitation evaluation was presented showing good performances of simulated rainfall patterns and time distributions. In the more restrictive framework of high frequency variability evaluation, shown in section 3.4, results shown, again, a good capability of models to catch spatio – temporal convection features such as: occurrence patterns and their related diurnal timing. Differences among model simulations and discrepancies with respect to remote sensed data and rainfall estimates were discussed. Major source of errors came out from the location of mountain chains and their impact on prevailing air flow easterly regimes. In RAMS the non-hydrostatic formulation of motion guarantees a more detail description of that interaction, thus increasing the correct location of convection in the domain with respect to MERRA dataset. RAMS precipitation amount is still poorly represented, but this limitation could be overcome trough a post calibration procedure if needed. Different grid resolutions in RAMS along with different SST datasets highlighted critical model limitations and possible solution to reduce them. As a result in the in the rest of this study only the best configuration with high spatial resolution and Modis-SST has been used. Thus regional strategy, using a high resolution regional model forced by global reanalysis and sea surface observed temperature were confirmed as an excellent tool for analysis as highlighted in Vigaud et al. (2009) and in Paerth et al. (2011) review papers.

Many authors have study convective precipitation features as described in the Introduction, but a few have taken into account internal high frequency rhythms of the WAM. In order to analyse the spatio temporal behaviour and in particular the emergence of a phase locking appearance several remarks must be taken into account:

- It is analysed the occurrence of convective precipitation over the WAM area, during the warm season June – July – August, with respect to the convective boundary layer destabilization at local scale due to latent heat release through evaporation of soil moisture;
- in order to represent the large scale dynamical factors, Vertical Integrated Moisture Transport has been analysed;
- each grid points are considered as a single realization of a non linear dynamical system. Grid time series of indices are analysed separately, even if the spatial coherence, due to the large scale dynamics is present;
- the only external forcing taken into account is the solar radiation, but it is analysed through its effects on latent heat release. In this sense latent heat, as unique external forcing, is bounded by the total amount of soil moisture of the active surface layer;

Thus to highlight a possible synchronization mechanism among different dynamical component of the WAM a "*Eulerian*" like approach has been applied: for each grid point interesting variable time series has been analyzed. Thus the description of motion is made in terms of the spatial coordinates only. Seasonal average of numerical indexes, like PSI, shown coherent patterns and potential occurrence of a specific dynamical feature like the synchronization between analyzed mechanisms.
Results from numerical model datasets thus highlight the evidence of synchronization between the destabilization of the convective boundary layer and rainfall occurrence due to the solar radiation forcing through the latent heat release. This fact can be considered as a basis of the spatio – temporal coherence, which, in turn, could be associated to the rainfall diurnal cycle. Thus, moisture provision, due to large scale and local latent heat flux, driven by solar radiation, synchronize with the convective rainfall occurrence footprint. This supports the conclusion that the studied interacting systems are associated with a process of mutual adjustment of rhythms. In particular the driving solar radiation variability provide a "natural" frequency for rainfall occurrence, but the emergence of a coherent rainfall pattern in sync with latent heat release flux increase our structural knowledge of WAM.
Latent heat flux from surface has a clear diurnal cycle link to the solar radiation but also linked to moisture availability in soil. Thus in addition to the natural oscillatory fluctuations, latent heat flux has an amplitude modulation linked to the antecedent precipitation. In turn, the increasing latent heat flux, increase the atmospheric instabilities increasing potential temperature in the atmospheric boundary layer, creating conditions favorable for convection. This dynamical features is a local scale features and contributes to the background moisture availability provided by large scale dynamic and described, for example by VIMT.

Within this context it could be very interesting expand, in a near future, this analysis to a "*Lagrangian*" like approach, following convective systems along their motion highlighting the importance of synchronization between latent heat flux and propagating convective systems. Such specific study could improve our knowledge of propagating convective systems not only over the Tropical Africa, but also in other areas, like Europe, where clear rainfall diurnal cycle where found in summer (Levizzani et al., 2010).

WAM internal coherence over tropics was studied in relation to the West African Heat Low pressure system, a sub tropical semi permanent atmospheric feature. It has a prominent role in the large scale summer variability over the Mediterranean area since it is acting as one of dynamic links between sub tropical and mid latitudes atmospheric variability (Lavaysse et al., 2009).
Results from the synchronization analysis confirm what shown in previously studies: WAM convective systems occurrence is shown to precede AEWs developments downstream to specific areas such as Darfur mountains and Ethiopian highlands (Mekonnen at al., 2006, Fig.4b). As then described in Kiladis et al. (2006) and Thorncroft et al. (2008) convection in these areas, such as Darfur, plays a key role in triggering and modulating AEWs and thus rainfall distribution downstream of mountain ridges to the Atlantic coast providing a mechanism for WAHL modulation and then a substantial mechanism to link tropical to midlatitudes variability over the Mediterranean basin and Europe in summer.

Synchronization in the WAM dynamical system arose from local interaction between latent heat release and rainfall as a result of the solar radiation forcing. But these elements, shown in this thesis, arose out from numerical modeling experiment. Thus a confirmation from direct observed data is needed and it will be done in the next future using new available observational data. Nevertheless some concluding remarks can be outlined as conclusion:

- Numerical models, no matters if global or regional, do exhibit a synchronization footprint in the boundary layer dynamics. In other words, high frequency variability in numerical schemes describing interactions between soil – vegetation – atmosphere, under specific conditions, are in sync. Once more it is evident how soil moisture initialization plays a crucial role in numerical model reliability both within a forecast and reanalysis frameworks.
- Synchronization analysis may be used as a filtering tool, able to highlight not only active mechanisms, but also their mutual interaction and periods, or epochs, when such interaction

is present. Furthermore as highlighted in Rybsky et al (2003), synchronization can highlight mutual interaction even when only weak coupling is present and other classic approaches of cross – correlation are strongly limited.

- Future analysis on synchronization of convection and surface fluxes in tropics and extratropics may provide a structural theoretical framework to identify local physical mechanisms responsible of emerging dynamical regimes like wet spells over specific areas.

REFERENCES

Ahijevych, D. A., Carbone, R. E., Tuttle, J. D., Trier, S. B., 2001. Radar data and climatological statistics associated with warm season precipitation episodes over the continental U.S. NCAR Tech. Note TN-448+STR., 81 pp. [available from NCAR, PO Box 3000, Boulder, CO 80307]

Alonge, C.J., K.I. Mohr, and W.K. Tao 2007, Numerical Studies of Wet versus Dry Soil Regimes in the West African Sahel. J. Hydrometeor., 8, 102–116.

Anosov, D.V. 2001, "Foliation", in Hazewinkel, Michiel, Encyclopedia of Mathematics, Springer, ISBN 978-1556080104

Arthur T. Winfree 2001. The Geometry of Biological Time. Springer-Verlag. ISBN 0-387-98992-7. (Second edition, first edition published 1980).

Aurell E., G Boffetta, A Crisanti, G Paladin and A Vulpiani 1997. "Predictability in the large: an extension of the concept of Lyapunov exponent". J. Phys. A: Math. Gen. 30 (1): 1–26. Bibcode 1997J

Avissar, R., Schmidt, T., 1998: An evaluation of the scale at which ground– surface heat flux patchiness affects the convective boundary layer using large-eddy simulations. J. of the Atmos Sci. 55, 2666–2689.

Brown, O. B., and P. J. Minnett, 1999 MODIS infrared sea surface temperature algorithm – Algorithm Theoretical Basis Document. Products: MOD28. ATBD Reference Number: ATBD-MOD-25.

Carbone, R. E., Tuttle, J. D., Ahijevych, D., Trier, S. B., 2002. Inferences of predictability associated with warm season precipitation episodes. J. Atmos. Sci. 59, 2033-2056.

Castro, C. L., W. Y. Y. Cheng, A. B. Beltran, C. H. Marshall Jr., R. A. Pielke Sr., and W. R. Cotton 2002, The incorporation of the Kain- Fritsch cumulus parameterization scheme in RAMS with a terrainadjusted trigger function, paper presented at Fifth RAMS Users and Related Applications Workshop, Santorini, Greece.

Castro, C. L., R. A. Pielke Sr., and G. Leoncini 2005, Dynamical downscaling: Assessment of value retained and added using the Regional Atmospheric Modeling System (RAMS), J. Geophys. Res., 110, D05108.

Chauvin, F., R. Roehrig, and J.-P. Lafore, 2010: Intraseasonal variability of the Saharan heat low and its link with midlatitudes. J. Climate, 23, 2544–2561.

Chen, F., Avissar, R., 1994 Impact of land– surface moisture variability on local shallow convective cumulus and precipitation in large-scale models. J. of Appl. Meteor. 33, 1382– 1401.

Chen, T.-C., van Loon, H., 1987. Interannual variation of the Tropical Easterly Jet. Mon. Wea. Rev. 115, 1739-1759.

Cook, K. H., 1999. Generation of the African Easterly Jet and its role in determining West African precipitation. J. Climate 12, 1165-1184.

Cook, K. H., and E. K. Vizy, 2006: Coupled model simulations of the West African monsoon system: 20th century simulations and 21st century predictions. J. Climate, 19, 3681-3703.

Dalu G.A., M. Gaetani, M. Baldi, 2009: A hydrological onset and withdrawal index for the West African monsoon. Theoretical and Applied Climatology, 96, 179-189, doi:10.1007/s00704-008-0022-8.

Dee, D. P., Uppala, S. M., Simmons, A. J., Berrisford, P., Poli, P., Kobayashi, S., Andrae, U., Balmaseda, M. A., Balsamo, G., Bauer, P., Bechtold, P., Beljaars, A. C. M., van de Berg, L., Bidlot, J., Bormann, N., Delsol, C., Dragani, R., Fuentes, M., Geer, A. J., Haimberger, L., Healy, S. B., Hersbach, H., Hólm, E. V., Isaksen, L., Kållberg, P., Köhler, M., Matricardi, M., McNally, A. P., Monge-Sanz, B. M., Morcrette, J.-J., Park, B.-K., Peubey, C., de Rosnay, P., Tavolato, C., Thépaut, J.-N. and Vitart, F., 2011, The ERA-Interim reanalysis: configuration and performance of the data assimilation system. Quarterly Journal of the Royal Meteorological Society, 137: 553–597. doi: 10.1002/qj.828 doi: http://dx.doi.org/10.1175/2008JAS2575.1

Diedhiou, A., Janicot, S., Viltard, A., de Felice, P., Laurent, H., 1999. Easterly wave regimes and associated convection over West Africa and tropical Atlantic: Results from the NCEP/NCAR and ECMWF reanalyses. Climate Dyn. 15, 795-822.

Douville, H., Conil, S., Tyteca, S., Voldoire, A., 2007. Soil moisture memory and West African monsoon predictability: Artefact or reality? Climate Dyn. 28, 723-742.

Druyan L, Fulakeza M, Lonergan P., 2006 Mesoscale analyses of West African summer climate: focus on wave disturbances. Clim Dyn 27:459–481. doi:10.1007/s00382-006-0141-9

Druyan L, Fulakeza M, Lonergan P., 2007 Spatial variability of regional model simulated June–September mean precipitation over West Africa. Geophys Res Lett 34:L18709.

Ebert, E. E., Janowiak, J., Kidd, C., 2007. Comparison of nea-real-time precipitation estimates from satellite observations and numerical models. Bull. Amer. Meteor. Soc. 88, 47-64.

Eltahir, E. A. B. and C. Gong, 1996. Dynamics of Wet and Dry Years in West Africa, Journal of Climate, 9(5): 1030-1042.

Fasullo J., Webster P.J., 2003 A hydrological definition of Indian monsoon onset and withdrawal. J Climate 16:3200–3211

Feliks, Yizhak, Michael Ghil, Andrew W. Robertson, 2010: Oscillatory Climate Modes in the Eastern Mediterranean and Their Synchronization with the North Atlantic Oscillation. J. Climate, 23, 4060–4079.doi: 10.1175/2010JCLI3181.1

Feliks, Yizhak, Michael Ghil, Andrew W. Robertson, 2011: The Atmospheric Circulation over the North Atlantic as Induced by the SST Field. J. Climate, 24, 522–542.

Ferraro, R. R., 1997. Special sensor microwave imager derived global rainfall estimates for climatological applications. J. Geophys. Res. 102 (D14), 16715-16735.

Ferraro, R. R., Marks, G. F., 1995. The development of SSM/I rain-rate retrieval algorithms using ground-based radar measurements. J. Atmos. Oceanic Technol. 12, 755–770.

Fontaine, B., and S. Janicot, 1996: Near-global SST variability associated with West African rainfall anomaly types. J. Climate,9, 2935–2940.

Fontaine B. and Philippon N. 2000 Seasonal evolution of boundary layer heat content in the West African monsoon from the NCEP/NCAR reanalysis (1968-1998). International Journal of Climatology : 20, 1777-1790.

Fontaine, B., M. Gaetani, A. Ullmann, and P. Roucou 2011, Time evolution of observed July–September sea surface temperature-Sahel climate teleconnection with removed quasi-global effect (1900–2008), J. Geophys. Res., 116, D04105, doi:10.1029/2010JD014843.

Futyan, J. M., Del Genio, A. D., 2007. Deep convective system evolution over Africa and the Tropical Atlantic. J. Climate 20, 5041-5060.

Gaetani, M., B. Fontaine, P. Roucou, and M. Baldi, 2010, Influence of the Mediterranean Sea on the West African Monsoon: Intraseasonal variability in numerical simulations, J. Geophys. Res., 115, D24115, doi:10.1029/2010JD014436.[AGU] Gielen, Eds., New York: North-Holland, 2001, pp. 279–321.

Gantner, L., and N. Kalthoff, 2009, Sensitivity of a modelled life cycle of a mesoscale convective system to soil conditions over West Africa, Q.J.R. Meteorol Soc, n/a.

Geerts, B., Dejene, T., 2005. Regional and diurnal variability of the vertical structure of precipitation systems in Africa based on spaceborne radar data. J. Climate 18, 893-916.

Giannini, A., R. Saravanan and P. Chang, 2003. Oceanic forcing of Sahel rainfall on interan- nual to interdecadal time scales. Science, 302, 1027-1030. Published online 9 October 2003. doi:10.1126/science.1089357

Golaz, J.-C. et al., 2001: A large-eddy simulation study of cumulus clouds over land and sensitivity to soil moisture. Atmos. Res. 59–60, 373–392.

Grist, J. P., Nicholson, S. E., 2001. A study of the dynamic factors influencing the rainfall variability in the West African Sahel. J. Climate 14, 1337-1359.

Hall, N. M. J., Kiladis, G. N., Thorncroft, C. D., 2006. Three-dimensional structure and dynamics of African Easterly Waves. Part II: Dynamical modes. Quart. J. Roy. Meteor. Soc. 63, 2231-2245.

Hodges, K. I., Thorncroft, C. D., 1997. Distribution and statistics of African mesoscale convective weather systems based on the ISCCP Meteosat imagery. Mon. Wea. Rev. 125, 2821-2837.

Hollinger, J. P., Peirce, J. L., Poe, G. A., 1990. SSM/I instrument evaluation. IEEE Trans. Geosci. Remote Sens. 28, 781-790.

Hossain, F., Huffman, G. J., 2008. Investigating error metrics for satellite rainfall data at hydrologically relevant scales. J. Hydrometeor. 9, 563-575.

Hsieh, J.-S., Cook, K. H., 2005. Generation of African Easterly Wave disturbances: Relationship to the African Easterly Jet. Mon. Wea. Rev. 133, 1311-1327.

Huffman, G.J., R.F. Adler, B. Rudolph, U. Schneider, and P. Keehn, 1995: Global Precipitation Estimates Based on a Technique for Combining Satellite-Based Estimates, Rain Gauge Analysis, and NWP Model Precipitation Information, J. Clim., 8, 1284-1295.

Huffman, G.J., R.F. Adler, P. Arkin, A. Chang, R. Ferraro, A. Gruber, J. Janowiak, A. McNab, B. Rudolph, and U. Schneider, 1997: The Global Precipitation Climatology Project (GPCP) Combined Precipitation Dataset, Bul. Amer. Meteor. Soc., 78, 5-20.

Huffman, G.J., R.F. Adler, D.T. Bolvin, G. Gu, E.J. Nelkin, K.P. Bowman, Y. Hong, E.F. Stocker, D.B. Wolff, 2007: The TRMM Multi-satellite Precipitation Analysis: Quasi-Global, Multi-Year, Combined-Sensor Precipitation Estimates at Fine Scale. J. Hydrometeor., 8(1), 38-55.

Jackson, B., Nicholson, S. E., Klotter, D., 2009. Mesoscale convective systems over Western Equatorial Africa and their relationship to large-scale circulation. Mon. Wea. Rev. 137, 1272-1294.

Janicot, S., Sultan, B., 2001. Intra-seasonal modulation of convection in the West African monsoon. Geophys. Res. Lett. 28, 523-526.

Janicot, S., Mounier, F., Hall, N. M. J., Leroux, S., Sultan, B., Kiladis, G. N., 2009. Dynamics of the West African Monsoon. Part IV: Analysis of 25–90-day variability of convection and the role of the Indian Monsoon. J. Climate 22, 1541-1565.

Kalnay, E. and Coauthors, 1996: The NCEP/NCAR Reanalysis 40-year Project. Bull. Amer. Meteor. Soc., 77, 437-471.

Kanamitsu R., W. Ebisuzaki, J. Woollen, S-K Yang, J.J. Hnilo, M. Fiorino, and G. L. Potter. 2002. NCEP-DEO AMIP-II Reanalysis (R-2): 1631-1643, Bul. of the Atmos. Met. Soc.

Kiladis, G. N., Thorncroft, C. D., Hall, N. M. J., 2006. Three-dimensional structure and dynamics of African easterly waves. Part I: Observations. J. Atmos. Sci. 63, 2212-2230.

Kirtman, B., Pirani, A., Eds., 2008. WCRP position paper on seasonal prediction. Report from the First WCRP Seasonal Prediction Workshop, Barcelona, Spain, 4-7 June, WCRP Informal Report No. 3/2008 ICPO Publication No. 127, 23 pp. [available at http://wcrp.wmo.int/documents/WCRP_SeasonalPrediction_PositionPaper_Feb2008.pdf]

Kohler M., N. Kalthoff, C. Kottmeier 2009, The impact of soil moisture modifications on CBL characteristics in West Africa: A case-study from the AMMA campaign, Q.J.R. Meteorol Soc, , DOI: 10.1002/qj.430.

Koster R.D, and Coauthors. 2004 Regions of strong coupling between soil moisture and precipitation. Science. 305, 1138–1140

Laing, A. G., Fritsch, J. M., 1993. Mesoscale convective complexes in Africa. Mon. Wea. Rev. 121, 2254-2263.

Laing, A. G., Carbone, R. E., Levizzani, V., 2004. Developing a warm season climatology of precipitating systems in Africa. Proc. 14th Int. Conf. on Clouds and Precipitation, Bologna, 18-23 July, 1806-1807.

Laing, A. G., Carbone, R. E., Levizzani, V., Tuttle, J. D., 2008. The propagation and diurnal cycles of deep convection in northern tropical Africa. Quart. J. Roy. Meteor. Soc. 134, 93-109.

Lavaysse, C., C. Flamant, S. Janicot, D. J. Parker, J.-P. Lafore, B. Sultan, and J. Pelon, 2009: Seasonal evolution of the West African heat low: A climatological perspective. Climate Dyn., 33, 313–330.

Lavender, S. L., Matthews, A. J., 2009. Response of the West African Monsoon to the Madden–Julian Oscillation. J. Climate 22, 4097-4116.

Lebel, T., Amani, A., 1999. Rainfall estimation in the Sahel: What is the ground truth? J. Appl. Meteor. 38, 555-568.

Leroux, M., 2001. Meteorology & climate of tropical Africa. Springer Praxis Books/ Environmental Sciences, 550 pp.

Leroux, S., Hall, N. M. J., 2009. On the relationship between African Easterly Waves and the African Easterly Jet. J. Atmos. Sci. 66, 2303-2316.

Levizzani, V., Pinelli, F., Pasqui, M., Melani, S., Laing, A. G., Carbone, R. E., 2010: A 10-year climatology of warm-season cloud patterns over Europe and the Mediterranean from Meteosat IR observations. Atmos. Res., this issue.

Levizzani, V., Schmetz, J., Lutz, H. J., Kerkmann, J., Alberoni, P. P., Cervino, M., 2001. Precipitation estimations from geostationary orbit and prospects for METEOSAT Second Generation. Meteorol. Appl. 8, 23-41.

Maraun, D., and J. Kurths, 2004: Cross wavelet analysis: Significance testing and pitfalls. Nonlinear Processes Geophys., 11, 505–514.

Mathon, V., Laurent, H., 2001. Life cycle of Sahelian mesoscale convective cloud systems. Quart. J. Roy. Meteor. Soc. 127, 377-406.

Mathon, V., Laurent, H., Lebel, T., 2002. Mesoscale convective system rainfall in the Sahel. J. Appl. Meteor. 41, 1081-1092.

McCollum, J. R., Krajewski, W. F., Ferraro, R. R., Ba, M. B., 2002. Evaluation of biases of satellite rainfall estimation algorithms over the continental United States. J. Appl. Meteor. 41, 1065-1080.

McGarry, M. M., Reed, R. J., 1978. Diurnal variations in convective activity and precipitation during phases II and III of GATE. Mon. Wea. Rev. 106, 101–113.

Mekonnen, A., C. D. Thorncroft, and A. Aiyyer, 2006: Analysis of convection and its association with African easterly waves. J. Climate, 19, 5405–5421.

Melani S., M. Pasqui, F. Guarnieri A. Antonini, A. Ortolani V. Levizzani, “Rainfall variability associated with the summer African monsoon: A satellite study”, acepted for publication in Atmos. Res., 2010.

Melani, S., Antonini, A., Pasqui, M., Ortolani, A., Levizzani, V., Ginnetti, R., 2008. A satellite and model study of rainfall associated with the West African Monsoon. Proc. 15th Int. Conf. on Clouds and Precipitation, CD-ROM. [available at http://cabernet.atmosfcu.unam.mx/ICCP-2008/abstracts/Program_on_line/Poster_08/Melani_extended.pdf]

Mellor, G. L. and T. Yamada, 1982: Developement of a turbulence closure model for geophysical fluid problems, Rev. Geophys. Space Phys., 20, 851-875.

Meneguzzo, F., Menduni, G., Maracchi, G.,Zipoli, G., Gozzini, B., Grifoni, D., Messeri, G.,Pasqui, M., Rossi, M., and C.J. Tremback, 2001: Explicit forecasting of precipitation: sensitivity of model RAMS to surface features, microphysics, convection, resolution. In: Mediterranean Storms. 3rd Plinius Conference 2001. Ed. by: R. Deidda, A. Mugnai, F. Siccardi. GNDCI Publ. N.2560, ISBN 88-8080-031-0, 79-84.

Meneguzzo, Pasqui, Menduni, Messeri, Gozzini, Grifoni, Rossi and Maracchi, 2003: "Sensitivity of meteorological high-resolution numerical simulations of the biggest floods occurred over the arno river basin, Italy, in the 20th century", Journal of Hydrology, in Press

Meyers, M. P., R. L. Walko, J. Y. Harrington, W. R. Cotton, 1997: New RAMS cloud microphysics parameterization. Part II: The two-moment scheme. Atmos. Res., 45, 3-39.

Miguez-Macho, G., G. L. Stenchikov, and A. Robock, 2005: Regional climate simulations over North America: Interaction of local processes with improved large-scale flow. J. Climate,18, 1227–1246.

Mohr, K. I., Thorncroft, C. D., 2006. Intense convective systems in West Africa and their relationship to the African easterly jet. Quart. J. Roy. Meteor. Soc. 132, 163–176.

Navarra A. and V. Simoncini, A Guide to Empirical Orthogonal Functions for Climate Data Analysis. 1st Edition., 2010, VI, 200 p. ISBN 978-90-481-3701-5.

Nguyen, H., Duvel, J.-P., 2008. Synoptic wave perturbations and convective systems over Equatorial Africa. J. Climate 21, 6372-6388.

Onogi, K., J. Tsutsui, H. Koide, M. Sakamoto, S. Kobayashi, H. Hatsushika, T. Matsumoto, N. Yamazaki, H. Kamahori, K. Takahashi, S. Kadokura, K. Wada, K. Kato, R. Oyama, T. Ose, N. Mannoji and R. Taira, 2007: The JRA-25 Reanalysis. J. Meteor. Soc. Japan, 85, 369-432.

Osipov, G. V., B. Hu, C. Zhou, M. V. Ivanchenko, and J. Kurths, 2003: Three types of transitions to phase synchronization in coupled chaotic oscillators. Phys. Rev. Lett., 91, 024101, doi:10.1103/PhysRevLett.91.024101.

Paeth, H., Hall, N. M., Gaertner, M. A., Alonso, M. D., Moumouni, S., Polcher, J., Ruti, P. M., Fink, A. H., Gosset, M., Lebel, T., Gaye, A. T., Rowell, D. P., Moufouma-Okia, W., Jacob, D., Rockel, B., Giorgi, F. and Rummukainen, M. 2011, Progress in regional downscaling of west African precipitation. Atmosph. Sci. Lett., 12: 75–82. doi: 10.1002/asl.306

Paluš, M. and Novotná, D.: 2011. Northern Hemisphere patterns of phase coherence between solar/geomagnetic activity and NCEP/NCAR and ERA40 near-surface air temperature in period 7–8 years oscillatory modes, Nonlin. Processes Geophys., 18, 251-260, doi:10.5194/npg-18-251-2011.

Parker, D. J., Thorncroft, C. D., Burton, R. R., Diongue-Niang, A., 2005a. Analysis of the African easterly jet, using aircraft observations from the JET2000 experiment. Quart. J. Roy. Meteor. Soc. 131, 1461–1482.

Parker, D. J., Burton, R. R., Diongue-Niang, A., Ellis, R. J., Felton, M., Taylor, C. M., Thorncroft, C. D., Bessemoulin, P., Tompkins, A. M., 2005b. The diurnal cycle of the West African monsoon circulation. Quart. J. Roy. Meteor. Soc. 131, 2839-2860.

Parker DJ, Thorncroft CD, Burton R, Diongue-Niang A., 2005c Analysis of the African easterly jet, using aircraft observations from the JET 2000 experiment. QJR Meteorol Soc 131:1461–1482

Pasqui et al. 2000: "Performances of the operational RAMS in a Mediterranean region as regards to quantitative precipitation forecasts. Sensitivity of precipitation and wind forecasts to the representation of the land cover". Proceedings of "4th RAMS Users Workshop", Cook College - Rutgers University. , 22-24 May 2000, New Jersey, USA.

Pasqui et al. 2002: "Historical severe floods prediction with model RAMS over central Italy". 5th RAMS Users Workshop", Santorini, Greece.

Pasqui M., Baldi M, Giuliani G., Gozzini B., Maracchi G. and Montagnani S., 2005. Operational Numerical Weather Prediction systems based on Linux cluster architectures, Nuovo Cimento, 28 C, N.2, DOI 10.1393/ncc/i2005-10183-4.

Pielke, R. A. & Coauthors, 1992: A comprehensive meteorological modelling system-RAMS. Meteor. Atmos. Phys., 49, 69– 91.

Pielke Sr., R.A., 2001: Influence of the spatial distribution of vegetation and soils on the prediction of cumulus convective rainfall. Reviews of Geophysics 39, 151–177.

Pikovsky A., M. Rosenblum, J. Kurths. Synchronization: A Universal Concept in Nonlinear Science, Cambridge University Press, Cambridge, 2001.

Pikovsky A.S., M.G. Rosenblum, and J. Kurths, 2000, Phase Synchronization in Regular and Chaotic Systems, Int. J. of Bifurcation and Chaos, 10, pp. 2291-2306.

Pytharoulis, I., Thorncroft, C. D., 1999. The low-level structure of African Easterly Waves in 1995. Mon. Wea. Rev. 127, 2266-2279.

Polcher J (1995) Sensitivity of tropical convection to land surface processes. J Atmos Sci 52:3143–3161

Rayner, N.A., Parker, D.E., Horton, E.B., Folland, C.K., Alexander, L.V, Rowell, D.P., Kent, E.C. and Kaplan, A., 2003: Globally complete analyses of sea surface temperature, sea ice and night marine air temperature, 1871-2000. J. Geophysical Research 108, 4407, doi:10.1029/2002JD002670

Reed, R. J., Norquist, D. C., Recker, E. E., 1977. The structure and properties of African wave disturbances as observed during Phase III of GATE. Mon. Wea. Rev. 105, 317-333.

Rienecker, Michele M., and Coauthors, 2011: MERRA: NASA's Modern-Era Retrospective Analysis for Research and Applications. J. Climate, 24, 3624–3648. doi:

Rosenblum M., A. Pikovsky, J. Kurths, and C. Schafer, P. Tass, 2001, "Phase synchronization: From theory to data analysis," Handbook of Biological Physics, vol. 4, Neuro-Informatics and Neural Modelling.

Rosenblum, M. G., A. S. Pikovsky, and J. Kurths, 1996: Phase synchronization of chaotic oscillators. Phys. Rev. Lett., 76, 1804–1807.

Rowell D. P., 2003: The Impact of Mediterranean SSTs on the Sahelian Rainfall Season. J. Climate, 16, 849–862.

Rowell, D. P, Milford, J. R., 1993. On the generation of African squall lines. J. Climate 6, 1181–1193.

Rybski D., S. Havlin, and A. Bunde, "Phase synchronization in temperature and precipitation records", Physica A, vol. 320, pp. 601- 610, 2003.

Sapiano, M. R. P., Arkin, P. A., 2009. An intercomparison and validation of high-resolution satellite precipitation estimates with 3-hourly gauge data. J. Hydrometeor. 10, 149-166.

Schmetz, J., Pili, P., Tjemkes, S., Just, D., Kerkmann, J., Rota, S., Ratier, A., 2002. An introduction to Meteosat Second Generation (MSG). Bull. Amer. Meteor. Soc. 83, 977-992.

Schumacher, C., Houze, R. A., 2006. Stratiform precipitation production over sub-Saharan Africa and the tropical East Atlantic as observed by TRMM. Quart. J. Roy. Meteor. Soc. 132, 2235-2255.

Sealy, A., Jenkins, G. S., Walford, S. C., 2003. Seasonal/regional comparisons of rain rates and rain characteristics in West Africa using TRMM observations. J. Geophys. Res. 108, D10, 4306, doi:4310.1029/2002JD002667.

Seo, H., Jochum, M., Murtugudde, R., Miller, A. J., Roads, J. O., 2008. Precipitation from African Easterly Waves in a coupled model of the Tropical Atlantic. J. Climate 21, 1417-1430.

Sijikumar S, Roucou P, Fontaine B 2006 Monsoon onset over Sudan-Sahel: similuation by the regional scale model MM5. Geophys Res Lett 33. doi:10.1029/2005GL024819

Soderman, D., F. Meneguzzo, B. Gozzini, D. Grifoni, G. Messeri, M. Rossi, S. Montagnani, M. Pasqui, A. Orlandi, A. Ortolani, E. Todini, G. Menduni, and V. Levizzani, 2003: Very high resolution precipitation forecasting on low cost high performance computer systems in support of hydrological modeling. Prepr. 17th Conf. on Hydrology, AMS, Long Beach.

Solomon, S., Qin, D., Manning, M., Chen, Z., Marquis, M., Averyt, K. B., Tignor, M., Miller, H. L., Eds., 2007. Climate change 2007: The physical science basis. Cambridge Univ. Press, Cambridge, 996 pp.

Stein, Karl, Niklas Schneider, Axel Timmermann, Fei-Fei Jin, 2010: Seasonal Synchronization of ENSO Events in a Linear Stochastic Model*. J. Climate, 23, 5629–5643.

Sultan, B., Janicot, S., 2003. The West African monsoon dynamics. Part II: The "preonset" and "onset" of the summer monsoon. J. Climate 16, 3407–3427.

Sultan, B., Janicot, S., Diedhiou, A., 2003. The West African monsoon dynamics. Part I: Documentation of intraseasonal variability. J. Climate 16, 3389–3406.

Tatli, H. 2007, Synchronization between the North Sea–Caspian pattern (NCP) and surface air temperatures in NCEP. Int. J. Climatol., 27: 1171–1187. doi: 10.1002/joc.1465

Taylor, C. M., and R. J. Ellis 2006, Satellite detection of soil moisture impacts on convection at the mesoscale, Geophys. Res. Lett., 33, L03404, doi:10.1029/2005GL025252.

Taylor, C. M., D. J. Parker, and P. P. Harris 2007, An observational case study of mesoscale atmospheric circulations induced by soil moisture, Geophys. Res. Lett., 34, L15801, doi:10.1029/2007GL030572.

Taylor CM, Gounou A, Guichard F, Harris PP, Ellis R, Couvreux F, Mg DK. 2011a. Frequency of Sahelian storm initiation enhanced over mesoscale soil moisture patterns. Nature Geosci. 4: 430–433.

Taylor CM, Parker DJ, Kalthoff N, Gaertner MA, Philippon N, Bastin S, Harris PP, Boone A, Guichard F, Agustí-Panareda A, Baldi M, Cerlini P, Descroix L, Douville H, Flamant C, Grandpeix JY, Polcher J. 2011b. New perspectives on land–atmosphere feedbacks from the African Monsoon Mulitdisciplinary Analysis (AMMA). Atmos. Sci. Lett. 12: 38–44.

Tetzlaff, G., Peters, M., 1988. A composite study of early summer squall lines and their environment over West Africa. Meteor. Atmos. Phys. 38, 153-163.

Thorncroft, C. D., Blackburn, M., 1999. Maintenance of the African easterly jet. Quart. J. Roy. Meteor. Soc. 125, 763-786.

Thorncroft, C. D., Hoskins, B. J., 1994a. An idealized study of African easterly waves. I: A linear view. Quart. J. Roy. Meteor. Soc. 120, 953-982.

Thorncroft, C. D., Hoskins, B. J., 1994b. An idealized study of African easterly waves. II: A nonlinear view. Quart. J. Roy. Meteor. Soc. 120, 983-1015.

Thorncroft, C. D., Hodges, K. I., 2001. African Easterly Wave variability and its relationship to Atlantic tropical cyclone activity. J. Climate 14, 1166-1179.

Thorncroft, Chris D., Nicholas M. J. Hall, George N. Kiladis, 2008: Three-Dimensional Structure and Dynamics of African Easterly Waves. Part III: Genesis. J. Atmos. Sci., 65, 3596–3607.

Trenberth, K. E., 1999. Atmospheric moisture recycling: Role of advection and local evaporation. J. Climate 12, 1368–1381.

Turk, F. J., Hawkins, J., Smith, E. A., Marzano, F. S., Mugnai, A., Levizzani, V., 2000a. Combining SSM/I, TRMM and infrared geostationary satellite data in a near-real time fashion for rapid precipitation updates: Advantages and limitations. Proc. 2000 EUMETSAT Meteorological Satellite Data Users' Conf., 452-459.

Turk, F. J., Rohaly, G., Hawkins, J., Smith, E. A., Marzano, F. S., Mugnai, A., Levizzani, V., 2000b. Meteorological applications of precipitation estimation from combined SSM/I, TRMM and geostationary satellite data. In: Microwave Radiometry and Remote Sensing of the Earth's Surface and Atmosphere, P. Pampaloni and S. Paloscia Eds., VSP Int. Sci. Publisher, Utrecht (The Netherlands), 353-363.

Turk, F. J., Sohn, B.-J., Oh, H.-J., Ebert, E. E., Levizzani, V., Smith, E. A., 2009. Validating a rapid-update satellite precipitation analysis across telescoping space and time scales. Meteor. Atmos. Phys. 105, 99-108.

Uppala, S. M., KÅllberg, P. W., Simmons, A. J., Andrae, U., Bechtold, V. D. C., Fiorino, M., Gibson, J. K., Haseler, J., Hernandez, A., Kelly, G. A., Li, X., Onogi, K., Saarinen, S., Sokka, N., Allan, R. P., Andersson, E., Arpe, K., Balmaseda, M. A., Beljaars, A. C. M., Berg, L. V. D., Bidlot, J., Bormann, N., Caires, S., Chevallier, F., Dethof, A., Dragosavac, M., Fisher, M., Fuentes, M., Hagemann, S., Hólm, E., Hoskins, B. J., Isaksen, L., Janssen, P. A. E. M., Jenne, R., Mcnally, A. P., Mahfouf, J.-F., Morcrette, J.-J., Rayner, N. A., Saunders, R. W., Simon, P., Sterl, A., Trenberth, K. E., Untch, A., Vasiljevic, D., Viterbo, P. and Woollen, J. 2005, The ERA-40 re-analysis. Quarterly Journal of the Royal Meteorological Society, 131: 2961–3012. doi: 10.1256/qj.04.176

Vigaud N, Roucou P, Fontaine B, Sijikumar S, Tyteca S 2011 WRF/ARPEGE-CLIMAT simulated trends over West Africa. Clim Dyn 35:925–944

Vivoni, E. R., Kinwai T., and D. J. Gochis 2009, Effects of Initial Soil Moisture on Rainfall Generation and Subsequent Hydrologic Response during the North American Monsoon, J Hydrometeorology, 10(3), 644. http://dx.doi.org/10.1175/2008JHM1069.1

Vizy, E. K., and K. H. Cook, 2001: Mechanisms by which Gulf of Guinea and eastern North Atlantic sea surface temperature anomalies can influence African rainfall. J. Climate, 14, doi: 10.1175/1520-0442, 795-821.

Vizy, E. K., and K. H. Cook, 2002: Development and application of a mesoscale climate model for the tropics: Influence of sea surface temperature anomalies on the West African monsoon. J. Geophys. Res. - Atmos., 107 (D3), 10.1029/2001JD000686.

Walko, R. L., W. R. Cotton, M. P. Meyers, and J.Y. Harrington, 1995: New RAMS cloud microphysics parameterization. Part I: The single-moment scheme. Atmos. Res., 38, 29–62.

Walko, R.L., L.E. Band, J. Baron, T.G.F. Kittel, R. Lammers, T.J. Lee, D. Ojima, R.A. Pielke, C. Taylor, C. Tague, C.J. Tremback, and P.L. Vidale, 2000: Coupled atmosphere-biophysics-hydrology models for environmental modeling. J. Appl. Meteor., 39, 931-944.

Wang, Bin, H.-J. Kim, K. Kikuchi, and A. Kitoh, 2011: Diagnostic metrics for evaluation of annual and diurnal cycles. Climate Dyn., 37, 5-6, 941-955, DOI: 10.1007/s00382-010-0877-0

Wang, C.-C., Chen, G. T.-J. , Carbone, R. E., 2004. A climatology of warm season cloud patterns over East Asia based on GMS infrared brightness temperature observations. Mon. Wea. Rev. 132, 1606-1629.

Wang, C.-C., Chen., G. T.-J., Carbone, R. E., 2005. Variability of warm-season cloud episodes over East Asia based on GMS infrared brightness temperature observations. Mon. Wea. Rev. 133, 1478-1500.

Wilks, D.S., 1995: Statistical methods in the atmospheric sciences: an introduction. Academic Press, 464 pp

Wu, M.-L. C., Reale, O., Schubert, S. D., Suarez, M. J., Koster, R. D., Pegion, P. J., 2009. African Easterly Jet: Structure and maintenance. J. Climate 22, 4459-4480.

Kikuchi, K., and B. Wang, 2008: Diurnal precipitation regimes in the global tropics. J. Climate, 21, 2680-2696. DOI: 10.1175/2007JCLI2051.1.